Towards Compact Photonic Devices in Highly Nonlinear Chalcogenide Microwires

Raja Ahmad

Department of Electrical & Computer Engineering
McGill University
Montreal, Canada

April 2014

A thesis submitted to McGill University in partial fulfillment of the requirements of the degree of Doctor of Philosophy.

Abstract

The future of fiber optic systems lies in the development of all fiber photonic devices that are compact, power efficient, and can provide novel functionalities. Here, we propose and demonstrate the realization of such photonic devices using chalcogenide microwires. The devices include Bragg gratings, wavelength converters, broadband amplifiers and lasers. The devices' operation relies on the ultrahigh nonlinear optical gain (>5 orders of magnitude larger than in silica fibers) and the high photosensitivity of chalcogenide microwires. The resulting photonic devices are a few centimeters in length, a few micrometers in diameter, and operate at record-low optical power levels (i.e., in the order of a few hundreds of micro Watts). In addition, chalcogenide glasses are transparent over an ultrabroad wavelength range (1-10 microns in wavelength), making these devices capable of operation in the mid-infrared wavelength region. Such photonic devices have been realized for the first time in such a compact and power efficient geometry, and are thus leading candidates for replacing their electronic counterparts. The devices are applied with a polymer coating to add physical strength and for protection against any environmental damage. Owing to their compactness, power efficiency and ultra broadband operation window, these novel photonic devices carry great commercial and research value for a wide range of fields, including biomedicine, instrumentation and mid-infrared spectroscopy.

Sommaire

L'avenir des systèmes par fibre optique réside dans le développement de dispositifs photoniques compact, à faible consommation dénergie et ajoutant de nouvelles fonctionnalits. Cette thèse propose et démontre la réalisation de tels dispositifs photoniques à base de microfils faits de chalcogénure. Les dispositifs réalisés comprennent des réseaux de Bragg, des convertisseurs de longueur d'onde, des amplificateurs à large bande et des lasers. Le fonctionnement de ces dispositifs repose sur le gain optique non linéaire ultra-élevé (jusquà >5 ordres de grandeur plus élevé que dans les fibres de silice) et la photosensibilité élevée du chalcogénure. Les dispositifs photoniques obtenus sont longs de quelques centimètres, de quelques microns de diamètre, et fonctionnent à des niveaux de puissance optique exceptionnellement bas (de l'ordre de quelques centaines de micro Watts). De plus, les verres de chalcogénures sont transparents sur une gamme de longueurs d'onde ultra-large (1-10 microns de longueur d'onde) compatible avec l'infrarouge moyen. Les dispositifs sont recouverts dun revtement de polymère pour ajouter la résistance mécanique et la protection contre les dommages environnementaux. En raison de leur compacité, leur efficacité énergétique et leur bande de fonctionnement ultra-large, ces dispositifs photoniques novateurs ajoutent une grande valeur commerciale et de recherche dans plusieurs domaines, notamment la biomédecine, l'instrumentation et la spectroscopie dans l'infrarouge moyen.

Acknowledgments

My deepest gratitude goes to the *Almighty* for creating me a human being and bestowing me with the physical and mental abilities to carry out the research for this thesis.

I would like to express my sincere gratitude to my thesis advisor Prof. *Martin Rochette* for all the guidance and support he has provided throughout the course of my Ph.D. research. I credit his teaching and supervision for almost all the knowledge about nonlinear optics that I have to this point. In particular, I extremely enjoyed and learned a lot while working in lab with him during the first year of my graduate studies. The encouragement and freedom that I received from him were crucial for developing the research skills. I will always be grateful to him for hiring me as a graduate student and for allowing me the opportunity to perform research in the fascinating field of nonlinear optics. I am also grateful for his and his wife's hospitality in France. I feel blessed to have such a friendly, welcoming, skilled, and frank mentor and supervisor.

I thank all the professors, including Profs. *Lawrence R. Chen, Jon Webb, Suzanne Lacroix* and *Nicolas Godbout* who were, at one point or the other, part of my thesis committee. I am particularly grateful to Prof. *Chen* who, despite his very busy schedule, was always available for answering questions, whether related or unrelated to his courses.

I am grateful to all the Professors in the photonics systems group at McGill University. I am grateful to Prof. *Liboiron-Ladouceur* for sharing space in her lab for more than a year. I am grateful to Profs. *David Plant* and *Andrew Kirk* for sharing the equipments and facilities that were crucial for my Ph.D. research.

I am grateful to Dr. *Thibaut Sylvestre* and all the researchers in his Nonlinear Optics Group at Universite de Franche-Comte, France for welcoming me to their group. I thoroughly enjoyed my stay in their group and came to know many good people, including Drs. *Jean-Charles Beugnot, Gil Fanjoux, Hervé Maillotte, Eric Lantz, Fabrice Devaux* and *Thomas Godin*, who I greatly value as colleagues and friends.

I am grateful to the Natural Sciences and Engineering Research Council of Canada (*NSERC*) for financial support of this research, and to *CorActive High-Tech, inc.*, and Mr. *Stephane Chatigny* for providing the Erbium-Ytterbium doped fiber amplifier and the chalcogenide glass fibers for carrying out the research described in this thesis.

I am grateful to all those who shared the office facilities with me at McGill University. I will miss the discussions with *M. Imran Cheema* about everything ! I had the privilege to develop close friendship with Prof. *Victor Torres-Company* who inspired (and still inspires) me, both as a researcher and as a human being. I enjoyed listening to the very enthusiastic Dr. *Philip Roche* about his research and cricket games. I thank all the students and postdoc fellows in the Photonics group, whom I interacted with during my Ph.D. studies.

I am also grateful to the other members of the photonics group at McGill University, including *Bhavin Shastri, Pegah Seddighian, Mina Spasojevic* (particular help in preparing the thesis in LaTeX), *Sandrine Filion-Cote* (french translation of the thesis abstract), *Jonathan Buset*, *Xian Xu, Dragos Cotruta* and *Venkat Veerasubramanian*.

I am also grateful to the administrative staff at McGill University, including *Christopher Rolston, Carrie Serban, Maru Basanez, Michel (Mike) Medeiros, Connie Greco* and *Caroline Brown*. A big thanks goes to *Don Pavlasek* and *Ali Belmebarki* in the mechanical workshop who have a great contribution in carrying out the work presented in this thesis.

During my stay in Montreal, I had the opportunity to make some very good friends. In particular, I greatly value the friendship with *M. Imran Cheema, Abdul Aziz Khan, Victor Torres-Company, Chams Baker* (already miss the long walks and the great time spent with him), *Alain Boudreau, Yassine Amaiche, Ahmad A. Hayat, Eslam Elesawy, Alaa Al-kadri, Hammad U. Khan, Lizhu Li, S. Haroon Gardezi, Mustafa Khalid, Erfan Amjad, Hazem Elsayed* and *Abdullah Farooqi*. I am also grateful to the great colleagues and friends in our group, including *HongQuan Yue, Kai Sun, Thibault North, Ali SalehiOmran, Amado V-Benitez, Sameer Arabasi, Francis Vanier, Martin Gorjan, Noor* and *Damian Marek*.

I am also very grateful to Dr. *M. Asif Yasin*, Prof. *Yasin A. Raja*, Dr. *Nadeem Lehrasab* and Dr. *Azeem Sarwar*, who encouraged and helped me to pursue graduate studies.

I am also grateful to my sister-like-aunt *Farri*, and her husband *Musawwir Raja*, for being so caring and friendly throughout my life, and for the great food that she cooked whenever I visited her in Toronto.

Finally, the biggest thanks goes to my parents, *Raja Riaz Ahmad* and *Nayyer Riaz* whose continued support, guidance and encouragement made the Ph.D. journey much more pleasant and easier than it could have actually been ! I am also much grateful to my sister, *Rakhshindah* and her husband *Viqas* (for their hospitality in France), my brothers, *Raja M. Qasim* and *Raja Ibrahim Ahmad*, and my sister-in-law, *Madiha*. I do not have words to express my gratitude to my parents and siblings; I feel blessed to have them as my best friends, with whom I can share almost anything.

Raja Ahmad

Contents

List of Figures

List of Tables

List of Acronyms

AMP	Amplifier
ASE	Accumulated Spontaneous Emission
ATT	Attenuator
BBS	Broadband Source
BPF	Band Pass Filter
CIR	Circulator
CMOS	Complementary MetalOxideSemiconductor
CW	Continuous Wave
DFB	Distributed Feedback Structure
DUT	Device Under Test
DWDM	Dense Wavelength Division Multiplexing
EDFA	Erbium Doped Fibre Amplifier
FBG	Fiber Bragg Grating
FC	Fiber coupler
FWM	Four-Wave Mixing
DFWM	Degenerate Four-wave Mixing
HNLF	Highly Nonlinear Fiber
OPO	Optical parametric oscillator
OSA	Optical Spectrum Analyzer
ODL	Optical Delay Line
PC	Polarization controller
PM	Power Meter
PMMA	Poly-methyl meth-acrylate
SC	Supercontinuum

SMF	Single-Mode (silica) Fiber
SPM	Self Phase Modulation
SHG	Second Harmonic Generation
THG	Third Harmonic Generation
TPA	Two Photon Absorption
WDM	Wavelength Division Multiplexing
XPM	Cross Phase Modulation

Chapter 1

Introduction

1.1 Background

Photonic devices are the optics counterparts of electronic devices where the photons, instead of electrons, are manipulated to achieve desired functionalities. The photonic devices can be broadly categorized into four major types, that is, for the (1) generation (2) manipulation (3) transmission and (4) detection of light. Photonic devices are attractive due to the low loss and high transmission speed of photons and thus, allow data transmission over long distances and information processing at faster rates and over large bandwidths. In addition, such devices offer novel and highly flexible operations and are widely expected to replace, in future, the existing electronic devices. This, however, demands continued efforts from researchers to explore different materials and techniques for improving the functionality of existing photonic devices, and for realizing novel devices.

1.2 Nonlinear optics for photonic devices

When sufficiently high intensity light travels through a medium, the optical properties of the medium are modified and the response of the medium becomes a nonlinear function of the optical field intensity. The polarization induced in the medium in response to the travelling optical field can be expressed as a Taylor series expansion, written as [1]

$$\mathbf{P} = \varepsilon_0 \left(\chi^{(1)} \cdot \mathbf{E} + \chi^{(2)} : \mathbf{EE} + \chi^{(3)} \vdots \mathbf{EEE} + \cdots \right) \tag{1.1}$$

where ε_0 is the free space permittivity, and $\chi^{(j)}(j = 1, 2, \ldots)$ is the j-th order susceptibility of the medium under consideration. The complex linear susceptibility $\chi^{(1)}$ is responsible only for attenuation and slowing down of the optical signal, via the linear absorption coefficient α and the linear refractive index n of the medium. The 2nd order susceptibility $\chi^{(2)}$ is available in quadratic nonlinear media, which are mainly in the form of crystals or bulk materials, and is responsible for such nonlinear effects as second harmonic generation and sum/difference frequency generation [1].

The $\chi^{(3)}$ nonlinearity is available in centrosymmetric media like amorphous glasses and semiconductors. Most of these materials can be easily drawn into fiber or planar waveguides. Although, the nonlinearity of $\chi^{(3)}$ materials is several orders of magnitude lower than that of $\chi^{(2)}$ nonlinear materials, the ability of $\chi^{(3)}$ materials to be drawn into long length waveguides results in an exponential increase in the effective nonlinear interaction. This makes the $\chi^{(3)}$ nonlinear materials a preferred choice for photonics applications, where compactness and low power consumption are the desired features of the devices. Another important motivation for using the $\chi^{(3)}$ nonlinear materials is the availability of a wide range of useful nonlinear optical phenomena, including the Kerr and the four wave mixing effects. Kerr effect leads to effects like self and cross phase modulation which result directly from the intensity dependence of the refractive index. The four wave mixing on the other hand, involves the simultaneous interaction of medium with four photons, and leads to a variety of frequency conversion processes. These $\chi^{(3)}$ nonlinear processes provide opportunities for realizing a variety of photonic devices for generating light at new frequencies as well as for manipulating light.

The $\chi^{(3)}$ processes discussed above are termed elastic or parametric in that the total energy of the interacting fields remains conserved and the state of the system remains stationary. There are however inelastic nonlinear processes, like Raman and Brillouin scattering, in which energy is exchanged between the fields and the medium. This energy exchange can take place back and forth between the medium and the optical field depending on the initial state of the medium. The Raman scattering, which is more relevant in the context of this thesis, is associated with the excitation of optical phonons or vibrational modes of molecules/atoms of the medium. The energy transfer from the field to the medium is usually the dominant process and results in the lowering of photon energy or frequency. This appears in the form of emission of an additional optical field that is longer in wavelength with respect to the input field, by an amount defined by the excited phonon energy. The Raman (and Brillouin) scattering therefore, result in the frequency conversion of the input light, and find applications for developing devices aimed at the generation, the amplification and the control of properties (like speed) of light, as well as for developing spectroscopic tools for studying the fundamental properties of the medium.

1.3 Chalcogenide microwires for compact and power-efficient photonic devices

Ever since the development of silica glass optical fibers, researchers have been working towards the development of photonic devices and a variety of photonic devices have been demonstrated, including lasers, amplifiers, wavelength converters, regenerators and switches, to name a few. The low nonlinear coefficient of silica glass however renders such devices impractical requiring (1) tens of meters to kilometers of silica fibers, and (2) tens of watts to kilowatts of pump power, thus losing the properties of compactness and power efficiency.

Over the past decade, researchers have explored different nonlinear materials to achieve the goals of compactness and power efficiency. Arsenic triselenide (As_2Se_3) chalcogenide glass is a material with nonlinear coefficient that is nearly 1000× larger than that of silica glass [2]. Furthermore, the As_2Se_3 glass can be easily drawn into long length fiber waveguides [3], has high photosensitivity [4] and is transparent over an ultra broadband wavelength transmission range of $\lambda \sim 1{-}10\mu m$ [3]. These features make As_2Se_3 chalcogenide glass, a leading candidate for realizing novel, compact and power efficient photonic devices.

It is known that the strength of most of the useful nonlinear processes in optical glasses increases exponentially with the product of the relevant gain coefficient (usually a characteristic of the medium), the interaction length of the medium L_{eff} and the intensity of the optical pump $I = P_{pump}/A_{eff}$ [1]. Therefore, compactness and power efficiency of the nonlinear photonic devices can be further improved by reducing the effective mode area A_{eff} of the propagating optical field.

As_2Se_3 microwires, where the diameter of the fiber is reduced down to sub wavelength scale, provide an excellent platform to achieve compact and power efficient photonic devices. By heating and stretching the As_2Se_3 optical fibers, chalcogenide microwires can be easily prepared, resulting in an enhancement of the waveguide nonlinear coefficient [1] by ∼150× with respect to the single mode As_2Se_3 fiber, and thus by ∼1,50,000× with respect to a single mode silica fiber. A detailed comparison of the performance of leading waveguide media for nonlinear photonics, including the highly nonlinear silica and bismuth glass fibers,

As_2S_3 and silicon waveguides, and As_2Se_3 microwires, is provided in Chapter 3. As will be explained, the As_2Se_3 microwires outperform any other medium in regards to nonlinear photonics as it exhibits a figure-of-merit − a quantity defined to compare different nonlinear media − that is 1−3 orders of magnitude larger than the above mentioned nonlinear media. Such microwires, therefore, offer an ideal platform for the development of compact and next generation photonic devices, operating at sub-watt power levels.

1.4 Main contribution

Before undertaking this research, very little or no experimental information was available about the performance of PMMA-cladding chalcogenide glass microwires. From scaling arguments, it was expected that PMMA-cladding chalcogenide glass microwires would offer a high waveguide nonlinearity coefficient; however, there was no information on how the enhanced optical nonlinearity affects the performance of such microwires when the reduced power-handling capacity of such small diameter microwires is taken into account and also, whether or not, the resulting devices are able to operate at the power levels required for observing nonlinear optical effects. By performing the experiments, we were able to identify the optimum geometries of the microwire devices for different applications, and were also able to find the optimum optical sources to be used for those experiments. These experimental details are included in each chapter of the thesis. Finally, the discovery of photosensitivity of As_2Se_3 chalcogenide glass at the telecommunication wavelengths light was completely unexpected.

The main contributions of the thesis are summarized as follows. These contributions have been disseminated in the form of journal papers and have been presented at various conferences. First, the task of fabricating Bragg gratings based optical band reject filters in As_2Se_3 chalcogenide microwires is undertaken, and two different techniques are employed to do so. Second, the nonlinear process of parametric four-wave mixing in As_2Se_3 microwires is studied and the observed parametric gain is trapped in an optical fiber based resonant cavity to realize an optical parametric oscillator. Third, we utilize the Raman gain in As_2Se_3 microwires to realize Raman lasers in two different cavity configurations, that is in (1) loop cavity, and (2) Fabry-Perot cavity configurations. Finally, we combine the Bragg grating filters as laser cavity integrated mirrors to realize a device that simultaneously acts as a Raman and parametric laser, frequency/wavelength converter and an amplifier and supercontinuum source.

1.5 Outline of thesis

The thesis is organized as follows:

- Chapter 2 describes our work on fabricating Bragg grating filters in chalcogenide microwires. The chapter starts with describing the motivation and the basic principle of operation of Bragg gratings in As_2Se_3 microwires. This is followed by the detailed description of fabricating the As_2Se_3 microwire Bragg gratings using a He-Ne laser (λ =633nm) operated free-space interferometer. The microwire is placed at the plane of interference, and the Bragg gratings are referred to as being externally written. In the latter part of the chapter, the technique for internal fabrication of Bragg gratings in the As_2Se_3 microwires is described. This process involves the use of a telecommunications band laser source (λ =1550nm), utilizing the photosensitivity of chalcogenide glass at near-infrared wavelengths to create refractive index modulation for realizing the Bragg gratings.

- Chapter 3 describes our work on developing a parametric wavelength converter and an oscillator based on the chalcogenide microwires. The chapter starts with the basic introduction to the parametric four-wave mixing process and a theoretical study of its availability in the As_2Se_3 microwires, taking into account the engineered chromatic dispersion in microwires. This is followed by the experimental results and discussion about the ultra-broadband and high efficiency four-wave mixing in the As_2Se_3 microwires. Finally, we propose and demonstrate that the available parametric gain in As_2Se_3 microwires can be used to realize a chalcogenide optical parametric oscillator. This is achieved by using the As_2Se_3 dispersion engineered microwire, to achieve phase matching and thus high a efficiency, broadband parametric gain, that in turn is stored in a resonant fiber loop cavity to operate the optical parametric oscillator.

- Chapter 4 describes our work on developing chalcogenide microwires based Raman lasers. The chapter starts with a brief introduction to the Raman scattering process and its importance in the context of As_2Se_3 microwire based photonic devices. This is followed by the detailed description of two types of microwire Raman lasers that we realize in different cavity configurations. One cavity is a fiber loop-type, similar to the one used in case of parametric oscillator, while the second cavity is a Fabry-Perot type, in which the Fresnal and/or mirror reflections at the two ends of the microwire are used to complete the laser cavity.

- Chapter 5 describes a novel photonic device where we utilize both the Raman and the parametric gains in the As_2Se_3 dispersion engineered microwire to realize the simultaneous operation of a Raman-parametric laser, wavelength converter, and amplifier and supercontinuum generator. In this work, we combine our work on microwire Bragg gratings, controlled dispersion in microwires for phase matching for the parametric process, and Raman gain in microwires, to demonstrate a compact and high efficiency, all chalcogenide microwire laser and wavelength converter and an ultra-broadband optical amplifier and supercontinuum source.

- Chapter 6 concludes the thesis and suggests a few avenues for future research on chalcogenide microwires, in the context of compact and efficient photonic devices.

1.6 List of contributions

Relevant journal publications

- R. Ahmad and M. Rochette, All chalcogenide Raman parametric laser, wavelength converter, and amplifier in a single microwire, submitted to IEEE J. Sel. Top. Quant. Electron. (2013).
  Contributions:
  R. Ahmad : Performed experiment and prepared manuscript.
  M. Rochette : Prepared manuscript and supervised the project.

- R. Ahmad and M. Rochette, Raman lasing in a chalcogenide microwire-based FabryPerot cavity, Opt. Lett. 37, 4549-4551 (2012).
  Contributions:
  R. Ahmad : Performed experiment and prepared manuscript.
  M. Rochette : Prepared manuscript and supervised the project.

- R. Ahmad and M. Rochette, Chalcogenide microwire based Raman laser, Appl. Phys. Lett. 101, 101110 (2012).

Contributions:
R. Ahmad : Performed experiment and prepared manuscript.
M. Rochette : Prepared manuscript and supervised the project.

- R. Ahmad and M. Rochette, Chalcogenide optical parametric oscillator, Opt. Express 20, 10095-10099 (2012).
  Contributions:
  R. Ahmad : Performed experiment and prepared manuscript.
  M. Rochette : Prepared manuscript and supervised the project.

- R. Ahmad and M. Rochette, High Efficiency and ultra-broadband optical parametric four wave mixing in chalcogenide-PMMA hybrid microwires, Opt. Express 20, 9572-9580 (2012).
  Contributions:
  R. Ahmad : Performed experiment and prepared manuscript.
  M. Rochette : Prepared manuscript and supervised the project.

- R. Ahmad and M. Rochette, Photosensitivity at 1550 nm and Bragg grating inscription in As_2Se_3 chalcogenide microwires, Appl. Phys. Lett. 99, 061109 (2011).
  Contributions:
  R. Ahmad : Performed experiment and prepared manuscript.
  M. Rochette : Prepared manuscript and supervised the project.

- R. Ahmad, M. Rochette, and C. Baker, Fabrication of Bragg gratings in sub wavelength diameter As_2Se_3 chalcogenide wires, Opt. Lett. 36, 2886-2888 (2011).
  Contributions:
  R. Ahmad : Performed experiment and prepared manuscript.
  M. Rochette : Prepared manuscript and supervised the project.
  C. Baker : Performed experiment and prepared manuscript.

Other journal publications

- T. Godin, Y. Combes, R. Ahmad, M. Rochette, T. Sylvestre, and J. M. Dudley, Normal dispersion modulation instability in an As_2Se_3 chalcogenide hybrid microwire, *submitted to* Opt. Lett. (2013).

- J-C. Beugnot, R. Ahmad, M. Rochette, V. Laude, H. Maillotte and T. Sylvestre, Reduction and control of stimulated Brillouin scattering in polymer-coated chalcogenide optical microwires, *accepted at* Opt. Lett. (2013).

- A. V-Bentez, R. Ahmad, T. North, M. Gorjan, J. H-Cordero and M. Rochette, All-optical broadband-variable optical attenuator based on an As_2Se_3 microwire, IEEE Photon. Technol. Lett. 25, 697-700 (2013).

- C. Baker, R. Ahmad, and M. Rochette, Simultaneous measurement of the core diameter and the numerical aperture in dual-mode step-index optical fibers, J. Lightwave. Technol. 29, 3834-3837 (2011).

- M. Rochette, C. Baker, R. Ahmad, and A. Al Kadry, Chalcogenide microwires and their applications, Photons Technical Review 9(2), 35-38 (2011).

- M. Rochette, C. Baker, and R. Ahmad, All optical PMD monitor for communication systems at 40 Gb/s and Beyond, Opt. Lett. 35, 3703 3705 (2010).

- R. Ahmad, S. Chatigny, and M. Rochette, Broadband amplification of high power 40 Gb/s channels using multimode Er-Yb doped fiber, Opt. Express 18, 19983-19993 (2010).

- A. Pasquazi, R. Ahmad, M. Rochette, M.R.E. Lamont, B.E. Little, S.T. Chu, R. Morandotti, and D.J. Moss, All-optical wavelength conversion in an integrated ring resonator, Opt. Express 18, 3858-3863 (2010).

Relevant conference publications

- R. Ahmad and M. Rochette, Chalcogenide microwires based Raman lasers, CLEO, OSA Technical Digest (online) (Optical Society of America), paper CF1E6 (2013).
  Contributions:
  R. Ahmad : Performed experiment and prepared manuscript.
  M. Rochette : Prepared manuscript and supervised the project.

- R. Ahmad, C. Baker and M. Rochette, Demonstration of chalcogenide optical parametric oscillator, Nonlinear Photonics, OSA Technical Digest (online) (Optical Society of America), post-deadline paper JW4D.3 (2012).

Contributions:
R. Ahmad : Performed experiment and prepared manuscript.
C. Baker : Prepared manuscript.
M. Rochette : Prepared manuscript and supervised the project.

- R. Ahmad and M. Rochette, Photosensitivity at 1550 nm and Bragg grating inscription in As_2Se_3 microwires for sensing applications, Specialty Optical Fibers, OSA Technical Digest (CD) (Optical Society of America), post-deadline paper SOWE1 (2011).
Contributions:
R. Ahmad : Performed experiment and prepared manuscript.
M. Rochette : Prepared manuscript and supervised the project.

- R. Ahmad and M. Rochette, Bragg grating in sub-wavelength chalcogenide wires, Specialty Optical Fibers, OSA Technical Digest (CD) (Optical Society of America), paper SOTuB4 (2011).
Contributions:
R. Ahmad : Performed experiment and prepared manuscript.
M. Rochette : Prepared manuscript and supervised the project.

Other conference publications

- J. C. Beugnot, R. Ahmad, M. Rochette, V. Laude, H. Maillotte and T. Sylvestre, Stimulated Brillouin Scattering in Chalcogenide-PMMA Hybrid Microwires, Workshop on Specialty Optical Fibers and their Applications, (Optical Society of America, 2013), paper F2.13 (2013).

- A. V-Bentez, R. Ahmad J. H-Cordero and M. Rochette, Photoinduced birefringence in an azopolymer-coated microwire, Photonics North, Proc. SPIE vol. 8007 80070E, 255-EaDw-53 (2012).

- A. V-Bentez, R. Ahmad J. H-Cordero and M. Rochette, Controlled generation of free-carriers to induce broadband attenuation in As_2Se_3 microwires, Photonics North, Proc. SPIE vol. 8007 80070E, 255-3R1K-53 (2012).

- R. Ahmad, M. Rochette and S. Chatigny, Spectrally Wide and High-Power Er-Yb Fiber Amplifier for 40 Gb/s Telecommunications Applications, CLEO, OSA Technical

Digest (CD) (Optical Society of America), paper CWI2 (2010).

- A. Pasquazi, R. Ahmad, M. Rochette, M. Lamont, B. E. Little, S. T. Chu, R. Morandotti and D. J. Moss, All Optical Wavelength Conversion in an Integrated Ring Resonator, CLEO, OSA Technical Digest (CD) (Optical Society of America), paper CThN2 (2010).

- R. Ahmad, S. Chatigny and M. Rochette, Spectrally Flat and High-Power Er-Yb Amplifier for Telecommunications Applications, IEEE LEOS Annual Meeting Conference Proceedings, pp.777-778 (2009).

Chapter 2

Bragg gratings in chalcogenide microwires

[1]In this chapter, we describe our work on the inscription of Bragg gratings in chalcogenide (As_2Se_3) microwires. We have employed two different techniques for the gratings inscription. One technique allows the external inscription with a visible light interferometer, while the other technique allows internal inscription using a near-infrared wavelength laser. In the rest of this chapter, we provide a brief motivation for realizing Bragg gratings in As_2Se_3 microwires, followed by the experimental details on each of the techniques employed. The inscription of Bragg gratings in chalcogenide microwires enables the fabrication of new devices with applications in nonlinear optics, telecommunications and sensing in the near-to-mid-infrared regions of wavelength.

2.1 Externally written Bragg gratings

2.1.1 Introduction

Over the last two decades, fiber Bragg gratings (FBGs) have emerged as one of the most widely used fiber optic devices. As linear devices, FBGs are used for sensing in various fields ranging from bio-chemical systems to mechanical ones [5,6]. FBGs have also received consid-

[1]The content of this chapter has been subjected to publication in (1) R. Ahmad, M. Rochette, and C. Baker, Fabrication of Bragg gratings in sub wavelength diameter As_2Se_3 chalcogenide wires, Opt. Lett. 36, 2886-2888 (2011), and (2) R. Ahmad and M. Rochette, Photosensitivity at 1550 nm and Bragg grating inscription in As_2Se_3 chalcogenide microwires, Appl. Phys. Lett. 99, 061109 (2011).

erable scientific interest in nonlinear applications [7, 8] and have been utilized for all-optical switching [9, 10], pulse-shaping [11], enhancement of super continuum generation [12] and for slowing down the speed of light [13]. However, the minimum peak power required to observe nonlinear effects in silica FBGs is in the order of 1kW. The use of sub-wavelength diameter fibers or microwires, where the mode intensity is greatly increased and a considerable fraction of the mode power is present in the evanescent field outside the microwire, not only reduces the optical power to observe nonlinear effects in FBGs, but also enhances the sensitivity to the outside. The photo-inscription of Bragg gratings in silica microwires is however difficult to achieve because the photosensitive core of the silica fiber vanishes upon tapering to such small diameters, which renders the wire insensitive to photo-inscription. Alternate techniques, such as using femtosecond laser radiation [14], focused ion beam milling [15], metal deposition [16], plasma etch postprocessing [17], and post-fabrication photosensitivity enhancement [18], have been utilized in the past to fabricate Bragg gratings in cylindrical waveguides with diameters ranging from a few microns to tens of microns. However, these techniques are technologically challenging and often lead to surface damages. As of today, the photo-inscription of Bragg gratings in sub-wavelength diameter microwires is desirable, but has not been achieved so far.

As_2Se_3 chalcogenide glass is known to be highly photosensitive, it has a nonlinear coefficient that is ∼930 times larger than that of silica glass [2] and it is transparent in the 1-10µm wavelength window [3]. As a result, the combination of microwire fabrication, the use of As_2Se_3 glass and the photo-inscription of FBGs is a promising approach for linear and nonlinear applications in the near-to-mid infrared region of wavelengths. Further, our group has reported the fabrication of hybrid microwires made from an As_2Se_3 fiber surrounded by a protective PMMA coating [19] and observed a high waveguide nonlinear coefficient of $\gamma = 133\text{W}^{-1}\text{−m}^{-1}$. This is 5 orders of magnitude enhancement in γ value with respect to a standard single mode fiber made from silica glass. The PMMA coating provides mechanical strength for normal handling of the microwire and allows controlling the level of evanescent interaction with the surrounding environment. In this work, we report the first inscription of Bragg gratings in chalcogenide microwires. This is also the first time that Bragg gratings are being reported in any optical fiber waveguide with sub-wavelength diameter. The transmission spectrum evolution as a function of time, both during and after the holographic exposure, is recorded and analyzed. A theoretical fit with the coupled mode theory is provided to reveal the grating parameters. Also, we observe that the refractive index of

As_2Se_3 microwires decreases upon exposure to 633nm light. The details of the experiment are provided below.

2.1.2 Theory and Experiment

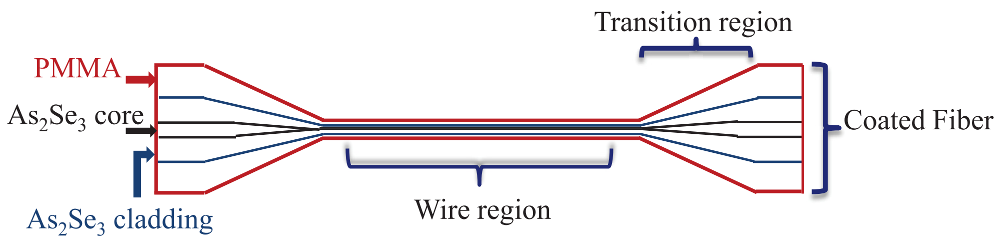

Figure 2.1 A schematic depicting the various parts of a typical hybrid microwire.

The chalcogenide fiber used for the experiment is provided by CorActive High-Tech inc. The fiber has a core/cladding diameter of 7/170 µm and a numerical aperture of 0.2. The fiber is coated with a protective layer of PMMA which is transparent to the photo-inscription wavelength of $\lambda_w = 633$nm (absorption coefficient $= 5.7 \times 10^{-4}$cm^{-1} [20]). The fiber is butt-coupled to a standard single mode fiber made of silica glass and the two fibers are bonded permanently with UV epoxy. A hybrid As_2Se_3/PMMA microwire is then fabricated from an adiabatic tapering process as described in [19]. Figure 2.1 provides a schematic of a typical microwire. After tapering, the diameter and length of the As_2Se_3 wire region is 1µm and 3cm, respectively. The grating fabrication setup consists of a modified Mach-Zehnder type interferometer, as shown in Figure 2.2(a). A He-Ne laser source (Spectra Physics, Model 106-1) at a wavelength of $\lambda_w = 633$nm provides the holographic photo-inscription pattern. The absorption coefficient of As_2Se_3 at this wavelength is 1.5×10^4cm^{-1} [21, 22]. This high absorption coefficient at the writing wavelength allows for a quick grating fabrication process. The output of the He-Ne laser source is split into two coherent beams that interfere at the inner surface of a glass prism and their angle ϑ, as shown in Figure 2.2(b), with respect to the prism surface is adjusted to achieve Bragg gratings with a first order resonance wavelength in the telecommunications C/L-band. The Bragg wavelength λ_{Bragg} is controlled by the period Λ of the holographic pattern, which depends on the angle 2φ between the two interfering beams inside the prism, as given below,

$$\lambda_{Bragg} = 2n_{eff}\Lambda \tag{2.1}$$

$$\Lambda = \frac{\lambda_w}{2\sin\varphi}, \tag{2.2}$$

where n_{eff} is the effective index of the propagating mode. The internal angle φ is in turn defined by the external angle ϑ, and the two angles in the case of a right-angled prism are related as follows,

$$n_p \sin(\varphi - 45^\circ) = \sin(\vartheta) \tag{2.3}$$

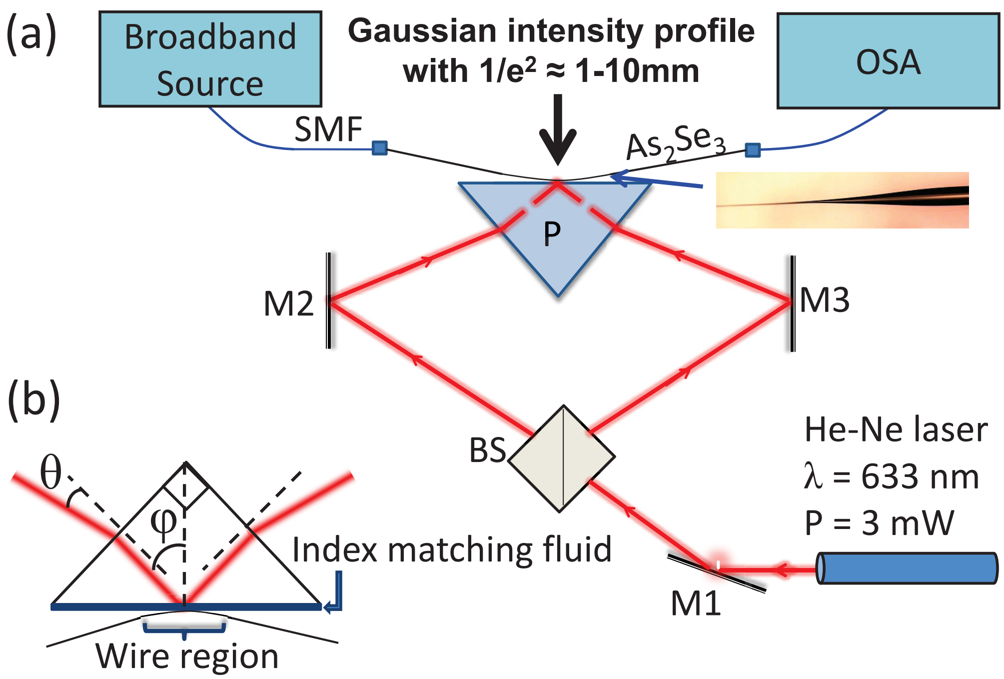

Figure 2.2 Experimental setup for the Bragg grating photo-inscription and *in-situ* monitoring of the process. SMF: single mode fiber, P: prism, OSA: optical spectrum analyzer, M1,M2, and M3: reflecting mirrors, BS: beam-splitter. (b) Detailed schematic of the prism where the microwire is placed during the grating growth, with the various angles defined in text, being labeled here.

For a 1µm diameter microwire with $n_{eff} = 2.68$, the grating period Λ equal to 0.265µm, and hence the angle ϑ equal to 1° is required to achieve the Bragg wavelength around 1.55µm. The microwire is placed over the external surface of the prism with an index matching fluid, as depicted in Figure 2.2(b), filling the gap between the prism and the microwire in order to maximize the transmission at the prism interface. The interfering beams are expanded using a focusing lens in each arm of the interferometer. The interference pattern has a Gaussian intensity profile with an adjustable $1/e^2$ full width of $1-10$mm and a total writing power of 3mW. The polarization of the two beams is identical and perpendicular with respect to the microwire axis in order to maximize the interference pattern contrast. The setup allows an *in-situ* monitoring of the grating growth process, with a broadband signal sent through the grating and observed on an optical spectrum analyzer.

2.1.3 Results and Discussion

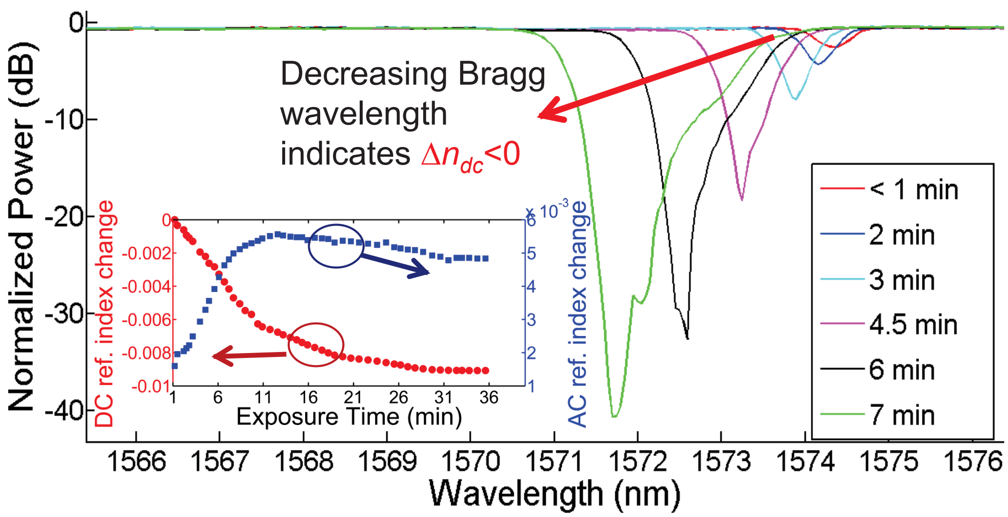

Figure 2.3 Transmissivity of the Bragg grating as a function of time during photo-exposure, illustrating the grating growth dynamics. (Inset) Evolution of AC and DC refractive index change during the photo-exposure is also shown.

Figure 2.3 shows the growth dynamics of the Bragg grating during the photo-exposure. The grating length in this case is 8mm and the interference pattern is apodized. A reversible and wavelength independent transmission loss of 0.5dB occurs during the process of photo-exposition, which can be observed from the spectra in Figure 2.3. A dip in the transmission spectrum appears at $\lambda = 1574.4$nm, and reaches -8dB in less than 3 minutes of exposure and eventually, -40dB after 7 minutes of exposure. Two observations can be made during this process: (1) the Bragg wavelength shifts towards shorter wavelengths, and (2) the width of the Bragg resonance increases. The first observation reveals that the refractive index of As_2Se_3 glass decreases upon the photo-exposure. This is supported by the appearance of grating apodization representative spectral features next to the longer wavelength edge of

Bragg resonance (which are more clear in Figure 2.4). Note that the previous studies on As_2Se_3 thin films have in contrast, reported an increase in refractive index upon exposure to 633nm light [23],Robinson03OL, which suggests that the refractive index change depends on the waveguide structure or the composition of the chalcogenide glass. A similar trend in the photoinduced index change in As_2Se_3 fiber was observed in an earlier report [24], but without any quantitative data. The second observation during the photo-exposure reveals an increase in AC refractive index of the grating. These two observations lead us to quanitfy the changes in DC and AC refractive indices of the grating i.e., Δn_{DC}(t), using the Eq.2.4 given below, and the Δn_{AC}(t), by fitting the grating spectra (not all being included in the figure) with the coupled mode theory. For a quick approximation of the Δn_{AC}(t), one can also use the Eq.2.5, provided below, although the values plotted in the inset of Figure 2.3 are those obtained from a fit with the coupled mode theory.

$$\Delta n_{DC}(t) = n_0 \frac{\lambda_{B,current}(t) - \lambda_{B,initial}}{\lambda_{B,initial}} \tag{2.4}$$

$$\Delta n_{AC}(t) = n_0 \frac{\Delta\lambda_{B,current}(t)}{\lambda_{B,initial}} \tag{2.5}$$

where, n_0 (= 2.68) is the effective index of the microwire, calculated using the beam propagation method; $\lambda_{B,current}$(t) and $\lambda_{B,initial}$, in Eq.2.4 are the current and initial Bragg wavelengths respectively; and the variable $\lambda_{B,current}$(t), in Eq.2.5 is the width of the current Bragg resonance. The temporal evolution of Δn_{DC}(t) and Δn_{AC}(t) is shown as inset in Figure 2.3. An AC refractive index change as high as 6.0$\times$ 10^{-3} is observed and a DC refractive index change of 10^{-2} is observed. The AC refractive index increases to a maximum value after $\sim$10 minutes of photo-exposure, and then decreases. This follows from a decrease in modulation depth of the holographic pattern. In fact, during the photo-exposure of the microwire, when the refractive index at the maxima of interference pattern decreases and eventually begins to saturate, the refractive index at the minima keeps decreasing at the same rate, thereby decreasing the modulation depth or the index contrast. This can be verified from Figure 2.3 (inset), where it is shown that the Δn_{AC}(t) starts dropping at the same time when the slope of Δn_{DC}(t) decreases, which indicates the onset of saturation. We find that the DC refractive index continues to decrease even up to 4 hours of photo-exposure, although, the rate of change of Δn_{DC}(t) becomes very small after the first 30 minutes of exposure.

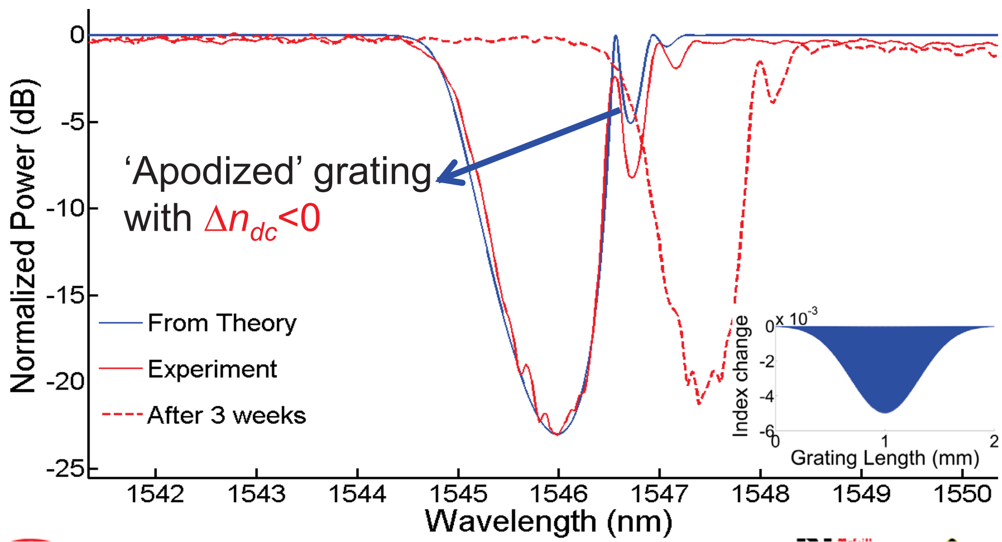

Figure 2.4 Transmission spectrum of a 1mm long Bragg grating (red curve), and a theoretical fit of transmission spectrum with coupled mode theory (blue curve). Also, shown is the transmission spectrum of the grating after 3 weeks of exposure to ambient light. (Inset) Grating index profile used for the simulation, assuming the grating to be apodized following a gaussian profile.

Figure 2.4 shows the spectrum of another grating, that is $\sim$ 1mm in length. A fit of the measured spectrum with coupled mode theory reveals a photoinduced refractive index change of Δn_{AC} =2.5×10^{-3}, which corresponds to a grating strength κL of 5.1 - κ being the coupling coefficient given by $\pi\eta\Delta n_{AC}/\lambda_{B,current}(t)$, with $\eta = 0.97$ being the fraction of the energy propagating in the microwire and L being the grating length. The presence of spectral features only on the longer wavelength side of the Bragg resonance shows that the grating is apodized. We also studied the aging of the grating at room temperature and observed a shift of Bragg wavelength by 1.5nm towards the longer wavelengths, after 3 weeks of aging. The spectrum of the grating, as shown in Figure 2.4, experiences no drastic degradation, which shows that the grating is quite stable in lab environment.

2.1.4 Summary

In conclusion, we have fabricated the first Bragg gratings in chalcogenide (As_2Se_3) sub-wavelength microwires. The transmission spectrum shows a -8dB dip at $\lambda = 1574$nm within 3 minutes of exposure with a 3mW laser interference pattern at a wavelength of 633nm. The Bragg grating dip shifts to 1571.5nm after 30 minutes, while growing to -40dB. The observation of the transmission spectrum profile during exposure and subsequent 3 weeks of annealing reveal that the refractive index of As_2Se_3 decreases under exposition to 633nm light and the grating strength remains stable. This device will find applications in sensing and nonlinear devices and for mid-infrared light processing.

2.2 Photosensitivity of As_2Se_3 glass at telcommunication wavelengths and internally written Bragg gratings

2.2.1 Introduction

Prior to the work presented in this section, light at a wavelength corresponding to a photon energy (E_v) equal or close to the bandgap ($E_v = 1.9$eV or $\lambda = 650$nm) of the As_2Se_3 glass had always been used to induce refractive index modulation and thus realize the Bragg gratings. The photosensitivity in As_2S_3 glass had been studied and reported for low photon energy with respect to the bandgap energy i.e., at a wavelength of 1550nm [25, 26], yet there was no report on the photosensitivity of As_2Se_3 in this wavelength range. In this section, we present the experimental observation of As_2Se_3 photosensitivity at telecommunication wavelength range of ∼1550nm. We use the photosensitivity to internally-write Bragg gratings in the As_2Se_3 microwires following Hill's approach [27]. The grating formation is monitored during the photo-exposure to reveal the time evolution of the induced refractive index change. This allows quantifying the intensity and time thresholds for inducing a significant change in the refractive index of As_2Se_3 with a telecommunication band laser. The tunability of the fabricated Bragg gratings with applied longitudinal strain is also measured.

2.2.2 Photosensitivity characterization and Bragg grating fabrication

Microwires with a waist diameter of 1µm and a length of 4cm were prepared from index-guiding As_2Se_3 fibers, again using the process detailed in [19]. Figure 2.5 shows the all-fiber interferometric setup used to photo-induce the Bragg gratings with laser sources at a wavelength of 1550nm. Two distinct approaches were used to write the Bragg gratings. In the first approach (A), the output of a continuous-wave (CW) laser was carved into pulses of 1ns in duration and a repetition rate of 131.072kHz. The modulation was provided from two cascaded intensity modulators driven by a pulse pattern generator. The modulated signal had an extinction ratio of 40dB. The large extinction ratio is important for keeping a low

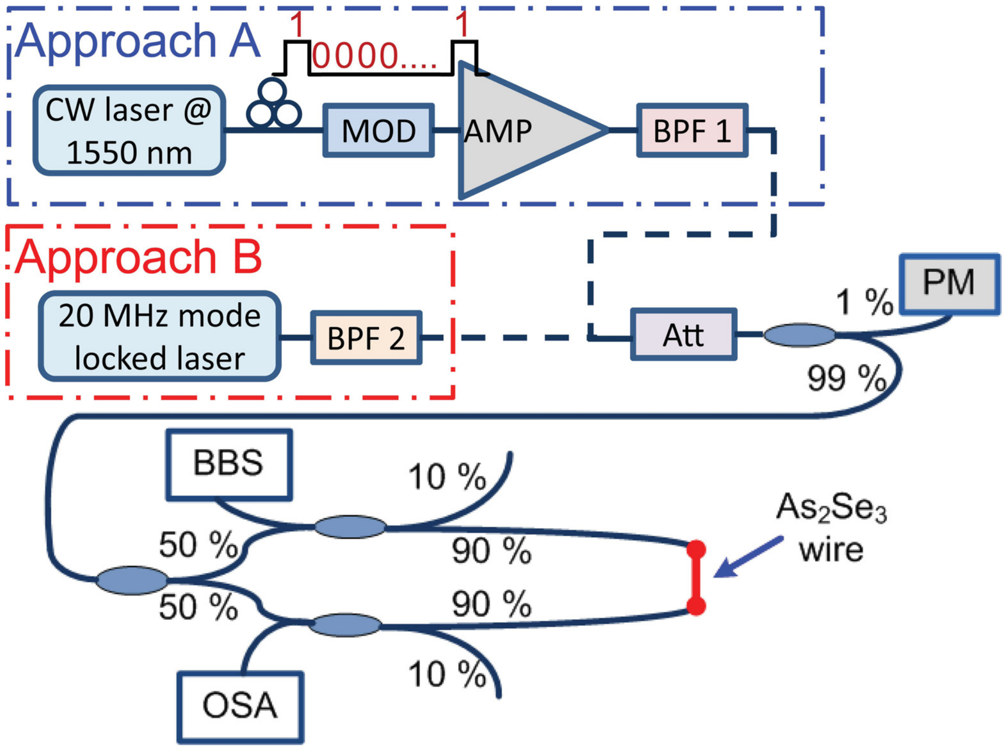

Figure 2.5 Experimental setup of approaches A and B to photo-induce a Bragg grating, Mod: Modulator, AMP: Amplifier, BPF: Bandpass filter, Att: Attenuator, BBS: Broadband optical source, OSA: Optical spectrum analyzer.

average power while maintaining a relatively high peak power, so as to minimize the thermal effects due to absorption in the chalcogenide glass. After modulation, the peak power of the pulses was increased above the photosensitivity threshold using an erbium doped fiber amplifier (EDFA). An optical bandpass filter (BPF 1) was used to eliminate the amplified spontaneous emission (ASE) noise added from the EDFA. In a second approach (B), the output of a mode-locked laser with femtosecond pulses and a repetition rate of 20 MHz was passed through a ∼0.25nm bandpass filter (BPF 2), which led to pulses with a full-width at half-maximum of ∼22ps. In both scenarios (A) and (B), the pulsed signal was sent through an optical attenuator followed by a 99 : 1 fiber coupler, with the 1% signal sent to a power meter while the 99% signal was sent to a 50 : 50 fiber coupler. The attenuator and 99 : 1 coupler assembly allowed monitoring and controlling the amount of power sent into the grating fabrication part of the setup. The two output ports of the 50 : 50 coupler were then connected to each end of the microwire. The optical signals interfered inside the

As_2Se_3 microwire, thereby creating a standing wave pattern and photo-inducing a periodic modulation of the refractive index, with a period equal to half the signal wavelength. This resulted in the formation of a Bragg grating inside the uniform waist region of the microwire. The Bragg grating was formed only in the uniform waist region because the mode intensity was considerably enhanced and thus exceeded the threshold value earlier, as compared to that in the transition and/or unstretched region of the microwire [28]. In order to observe the evolution of the grating, a 90 : 10 coupler was inserted at each end of the microwire, and the transmission of a broadband signal through the microwire was observed on an optical spectrum analyzer (OSA). Figure 2.6(a) and (b) show the spectra for the gratings formed by using the pulsed signal generated by using the approaches A and B, respectively. The inset in Figure 2.6(a) shows the 1ns square signal trace on the oscilloscope and the inset of Figure 2.6(b) contains the autocorrelation trace of the 22ps Gaussian pulses.

Figure 2.7 shows the time evolution of a typical Bragg grating. A transmission dip appeared at the input signal wavelength after ∼5 minutes of time exposure and reached -6dB after 10 minutes of time exposure. After this, there was a rapid decrease in the transmission dip as it reached less than -30dB within the next 3 minutes. Beyond this time, the exact level of the transmission dip was masked by the noise floor of the OSA and thus, could not be resolved accurately. We could, however, observe the increase in width of the grating resonance which allowed the calculation of the refractive index change, by fitting the spectrum with coupled mode theory. Importantly, the shift in Bragg wavelength towards the longer wavelengths during the process of grating formation revealed that the refractive index of As_2Se_3 glass increases upon exposure to 1550nm light. This contrasts with our previous findings with the photo-inducing wavelength of 633nm, where the refractive index was instead observed to decrease upon photo-exposure [28]. This implies that qualitatively different underlying physical phenomena are responsible for the refractive index change due to the exposure of chalcogenide glass to photons of different energies. The exact nature of these phenomena is, however, not yet completely identified and is still a matter of debate [29, 30].

We also performed experiments to determine the intensity and time thresholds required to induce a significant refractive index change. In the first set of experiments, we exposed each microwire sample with a different input intensity for a period of 20 minutes and observed the induced refractive index change. From Figure 2.8(a), three regions of the intensity range can be identified. At $<10\text{MW/cm}^2$ (region I), there was no grating formation, even

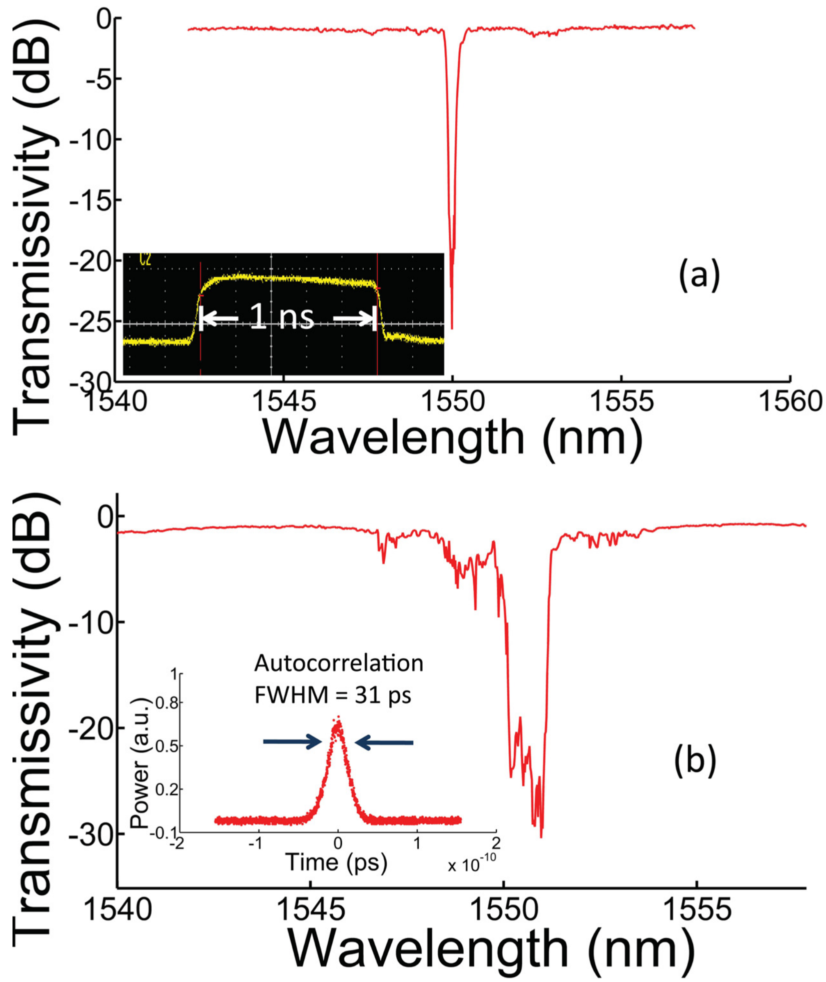

Figure 2.6 (a) Normalized transmission spectrum of a Bragg grating in microwire, written with 1ns square pulses. (Inset) The pulse shape as observed on an oscilloscope (b) Normalized transmission spectrum of a Bragg grating written with ~22ps Gaussian pulses. (Inset) Autocorrelation trace of the pulse.

after >90 minutes of photo-exposure (not in figure). Take note that the intensity provided is the sum of the pulse intensities circulating in both directions in the microwire. For the sum intensity values in the range of 10-225MW/cm^2 (region II), the induced refractive index change followed a linear increasing function. The threshold intensity was 333MW/cm^2 - or effectively 666MW/cm^2, which is the intensity of the standing wave−beyond which the increase in refractive index change was strongly enhanced (region III). The threshold intensity was defined as the point where the linear interpolation curves in the regions II and III intersect. We also characterized the time threshold for the formation of a Bragg grating.

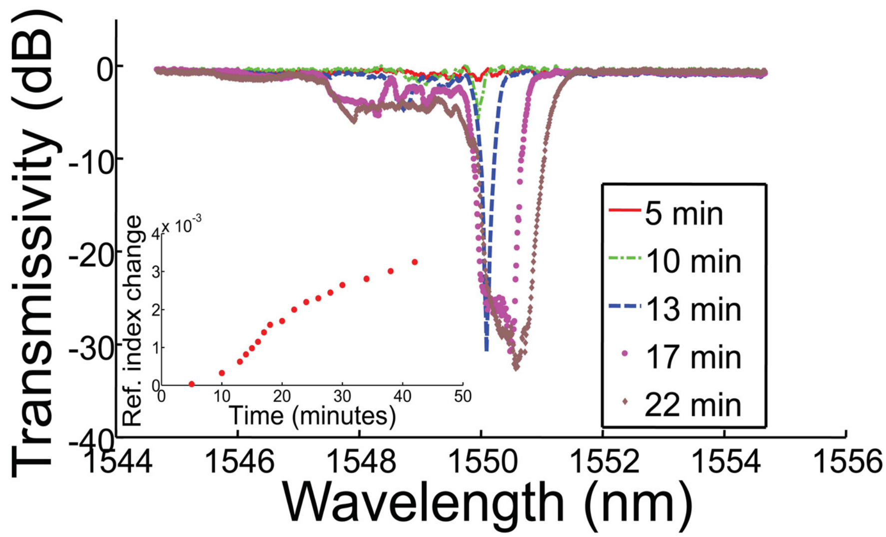

Figure 2.7 Transmission spectra of a Bragg grating as a function of time during photo-exposure. (Inset) Evolution of the AC refractive index change during the photo-exposure is also shown.

This was accomplished by monitoring the grating evolution over time with a fixed input intensity. For a input intensity sum equal to 425MW/cm^2, we measured a time threshold of 8.2 minutes, again estimated from the intersection of the linear interpolation curves in the two regions of time scale. A time threshold is associated to a given intensity value and changes upon varying the intensity. An important observation is that a time threshold was attained only when the intensity value lied in the region III of FigurePhotosensitivity thresholds(a), otherwise the refractive index change increased linearly up to a certain amount time and then remained constant. This was observed by exposing a sample with sum intensity value 52MW/cm^2 [in region II of Figure 2.8(a)] for the time duration even longer than 2 hours. The evolution of the refractive index change is shown as inset in the Figure 2.8(b).

2.2.3 Bragg grating performance as a strain sensor

Finally, the shift in Bragg wavelength due to the applied longitudinal strain ϵ was quantified. A Bragg grating was written in a 1μm diameter wire using the approach A, as discussed above. The total length of the uniform section of the microwire was 6cm. The microwire remained attached on the motorized translation stages during the entire experiment, from the process of heating and stretching the chalcogenide fiber into a wire, as well as stretching the Bragg grating after photo-inscription. The fiber was attached at both ends with a strong

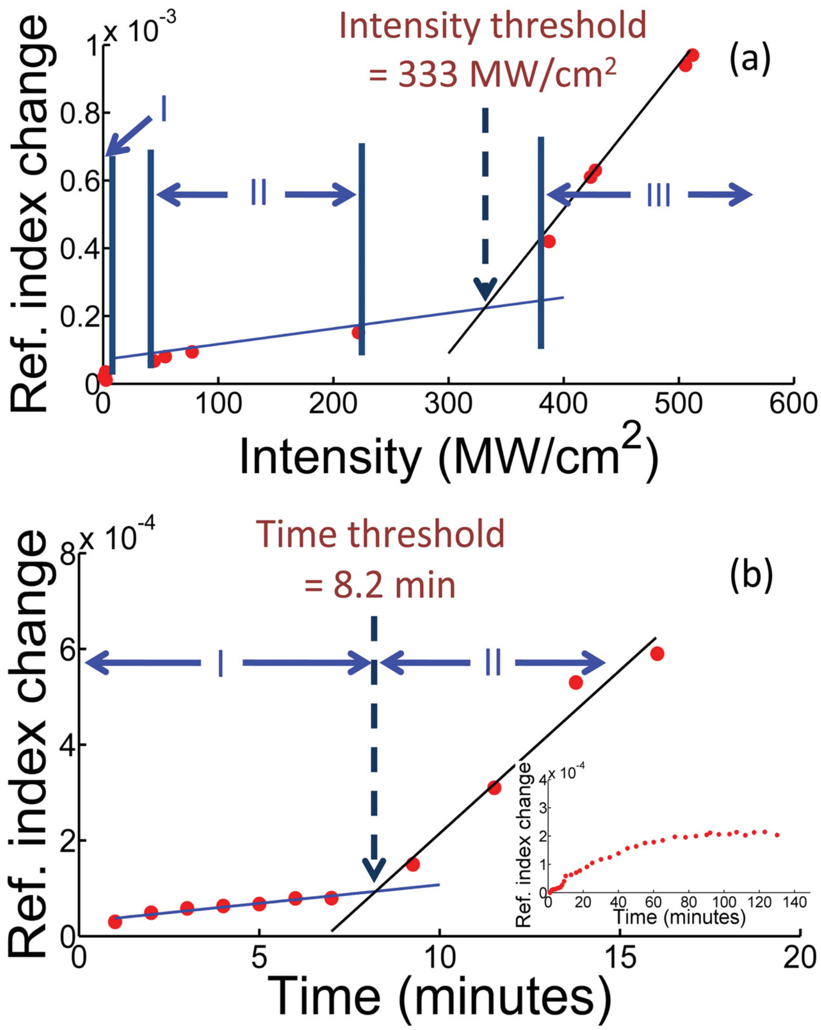

Figure 2.8 (a) Induced refractive index change as a function of input intensity for an exposure time of 20 minutes. Different intensity regions are labeled from I to III. (b) Induced refractive index change as a function of time for an input intensity sum of 425MW/cm^2. The time scale is labeled in regions I and II on either side of the time threshold. (Inset) Induced refractive index change as a function of time for an input intensity sum of 52MW/cm^2.

clamping system maintained with screws and ensured that no slipping could occur during the experiment. One end of the microwire was pulled slowly while the corresponding shift in Bragg wavelength was recorded. Figure 2.9 shows that the Bragg wavelength shifts as a function of applied strain, fitting with a linear function with a correlation coefficient of R^2 =0.9998. A sensitivity of 1.3pm/$\mu\epsilon$ is obtained from the linear fit, which agrees reasonably

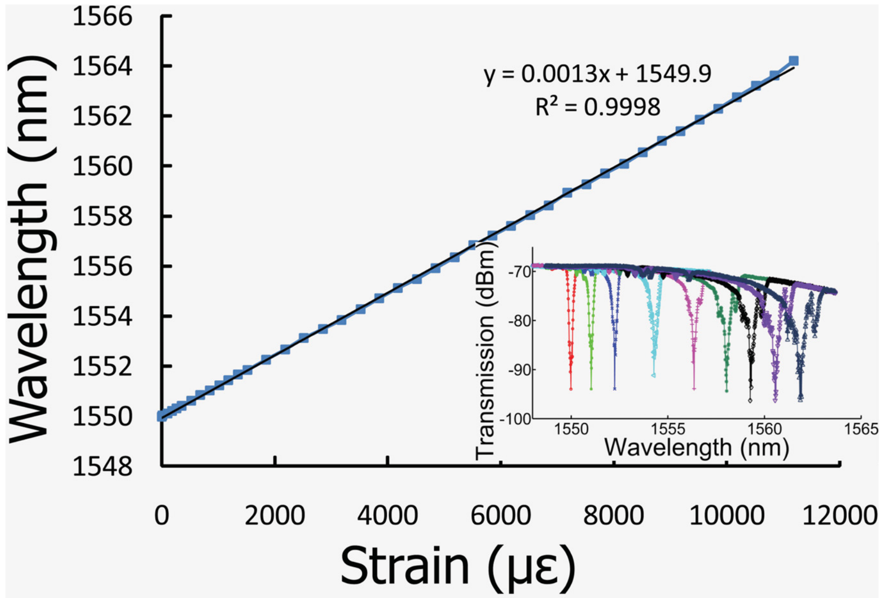

Figure 2.9 Strain measurement of a Bragg grating in an As_2Se_3 microwire. (Inset) Bragg grating transmission spectra for various strain values is shown as well.

well with the theoretical calculations [31,32]. Wavelength shift measurements over a spectral range of 1550-1564nm are provided in Figure 2.9, with the spectra provided as inset in the figure. Wavelength shift measurement was however limited by the spectral width of the broadband ASE source used for the characterization. The microwire could be stretched over a length of 1.6mm – corresponding to a strain value of $2.7 \times 10^4 \mu\epsilon$ –which shows that the microwires are remarkably strong and extensible. In comparison, a maximum strain of $10^4 \mu\epsilon$ can be applied to silica fiber Bragg gratings before the fiber breaks or its response becomes nonlinear [33]. By extrapolating the linear fit in Figure 2.9, this strain value corresponds to a wavelength shift of 54nm. We therefore, conclude that the grating can potentially be tuned over a wide wavelength range of 1550-1604nm.

2.2.4 Summary

In conclusion, we have characterized the photosensitivity in As_2Se_3 at a wavelength of 1550nm. We utilized this photosensitivity to make Bragg gratings in As_2Se_3 microwires and determined the intensity and time thresholds of the photosensitivity process. Finally, Bragg gratings written in the hybrid microwires can experience a strain of $2.7 \times 10^4 \mu\epsilon$, corresponding to a wavelength tunability range from 1550nm up to 1604nm.

Chapter 3

Parametric four wave mixing and oscillation in chalcogenide microwires

[1]In this chapter, we present our work on the study of four wave mixing or parametric wavelength conversion and oscillation in the As_2Se_3-PMMA hybrid microwires. The first part of the chapter includes the theoretical and experimental description of the parametric four-wave mixing in the microwires, while the second part describes our experiments on the realization of parametric oscillator using the available parametric gain in the microwires.

3.1 Parametric four-wave mixing

3.1.1 Introduction

The recent development of devices based on novel nonlinear materials like chalcogenides (ChGs), silicon (Si) and other semi-conductors has revolutionized the field of nonlinear photonics [4, 34, 35]. Among the nonlinear effects observed in these materials, four-wave mixing (FWM) is the process that finds the most applications including wavelength conversion [36], optical regeneration [37, 38], optical delay [39], time-domain demultiplexing [40], temporal cloaking [41] and negative refraction [42]. Of particular interest is the degenerate form of FWM (DFWM) in which two photons provided by a pump wave convert into a Stokes and an

[1]The content of this chapter has been subjected to publication in (1) R. Ahmad and M. Rochette, High Efficiency and ultra-broadband optical parametric four wave mixing in chalcogenide-PMMA hybrid microwires, Opt. Express 20, 9572-9580 (2012), and (2) R. Ahmad and M. Rochette, Chalcogenide optical parametric oscillator, Opt. Express 20, 10095-10099 (2012).

anti-Stokes photon. This leads to the simultaneous process of converting a signal from Stokes (or anti-Stokes) wavelength to the anti-Stokes (or Stokes) wavelength, and the amplification of the input signal. In the best DFWM conditions, the newly generated signal -called the idler- not only represents a wavelength-converted version of the input signal but it can even be more powerful than the original input signal. Although FWM has been observed in several media including chalcogenides [43–46], silicon [47,48], bismuth [49] and silica [50–52], there is a continued quest for devices that realize efficient and broadband FWM while offering compactness, low-power consumption and compatibility with optical fibers at low insertion loss. Among the commonly used nonlinear materials, As_2Se_3 chalcogenide glass boasts the highest nonlinear refractive index coefficient $n_2 = 2.3 \times 10^{-13}$cm^2/W [53], that is nearly 1000× that of silica, 20× that of Bi_2O_3, 4× that of As_2S_3, and 3× that of Si [53–55].

Despite the large value of n_2 in As_2Se_3, the material exhibits high normal chromatic dispersion in the 1,550nm wavelength band which, as explained below, prevents FWM in bulk medium or in large core optical fibers with low refractive index contrast cladding. This can however be remedied by stretching the As_2Se_3 fibers into microwires for which the anomalous waveguide dispersion overcomes the normal material dispersion. Such microwires also exhibit large values of waveguide nonlinear coefficient $\gamma(= n_2\omega_P/c\mathrm{A}_{eff}$, ω_P being the pump angular frequency, c being the speed of light and A_{eff} being the effective mode area in the microwire), which lowers the required power threshold for nonlinear processes. The highest reported value of γ in such microwires is more than 5 orders of magnitude larger than in silica fibers [19]. DFWM has been observed in As_2S_3 (air-clad) microwires but the process had improper phase-matching and led to low conversion efficiency (∼20dB) and narrow FWM gain bandwidth [43]. Incidentally, FWM has never been observed in microwires made of the most nonlinear chalcogenide glass, As_2Se_3.

In this work, we utilize the poly methyl-meth-acrylate (PMMA) coated As_2Se_3 microwires to attain phase-matching and generate the most efficient and broadband DFWM ever reported in such compact and power efficient devices. The PMMA cladding, in addition to optimizing the optical performance, imparts microwires remarkable physical strength [56], which otherwise are extremely fragile. Experiments were performed with wires of various core wire diameters to observe DFWM conversion efficiency as high as 21dB and a 12dB wavelength conversion range in extend of 190nm, limited by the tunability range of available probe lasers. The large nonlinearity, the reduced chromatic dispersion from PMMA cladding and the long effective length due to low absorption loss α <1dB/m of the hybrid microwires make them the most power efficient FWM devices, providing net broadband gain at peak pump powers as low as 70mW.

3.1.2 Theory

In theory, the efficiency of DFWM process depends on phase-matching conditions given by [1]

$$\Delta k = 2\gamma P_P - \Delta k_L \tag{3.1}$$

where P_P is the peak pump power, Δk_L is the linear phase-mismatch that is chromatic dispersion dependent and is approximated by

$$\Delta k_L = -\beta_2(\Delta\omega)^2 - \frac{1}{12}\beta_4(\Delta\omega)^4 \tag{3.2}$$

where β_i is the i-th order dispersion coefficient and $\Delta\omega$ is the angular frequency mismatch between the Stokes and anti-Stokes signals. It is well known that only the even order dispersion coefficients contribute to the phase mismatch because of the symmetry in FWM processes [1]. The DFWM gain coefficient g is then given by [1,57]

$$g = \sqrt{(\gamma P_p)^2 - (\Delta k/2)^2} = \sqrt{\gamma P_P \Delta k_L - (\Delta k_L/2)^2} \tag{3.3}$$

In the case where the pump depletion is neglected as it transfers energy to the Stokes and anti-Stokes signals, the peak conversion efficiency G_i of the idler wave is given by

$$G_i = P_{I,out}/P_{S,in} = (\gamma P_P/g)^2 \sinh^2(gL_{eff}) \tag{3.4}$$

where $P_{I,out}$ is the peak idler power at the output, $P_{S,in}$ is the input signal power and L_{eff} is the interaction length. From Eq.3.3, the gain is maximized when Δk =0. This illustrates that in order to observe any DFWM gain, the linear dispersive phase-mismatch Δk_L must lie within the range $0\Delta k_L 4\gamma P_P$, where the upper limit is adjusted by the pump induced nonlinear phase shift. Although the influence of β_4 is expected to be much smaller than that of β_2, it becomes the dominant dispersion term when the pump lies close to zero-dispersion wavelength (ZDW), where $\beta_2 \sim 0$. Indeed, the DFWM is optimal both in terms of efficiency and bandwidth when the pump lies at the ZDW [1]. According to Eqs.**??** and ref. [1] however, both efficiency and bandwidth are reduced when β_4 is large and/or positive at the ZDW. Therefore, in order to get $g > 0$ over a broad bandwidth, in addition to $\beta_2 \sim 0$, the value of β_4 must be small and negative so that the Δk approaches 0 with a small input pump power ($P_P > 0$). Figures 3.1 (a), (b) show the values of β_2 and β_4 in As_2Se_3 microwires surrounded by air or by a PMMA cladding, with a pump laser at λ_P =1,536nm. The β_2 and β_4 values are derived from the waveguide effective index n_{eff} which was numerically calculated from the charactersitic mode equation [58] using the refractive index parameters of As_2Se_3 provided in ref. [2] and those of PMMA in ref. [59].

Figures 3.1 (a), (b) show that in both situations whether the microwire is coated with air or PMMA, the β_2 profiles have two points where the chromatic dispersion is zero. Those are identified as ZDD_1 and ZDD_2 in order of decreasing wire diameter. Coating the As_2Se_3 microwire with PMMA (refractive index ~1.467 at λ =1,536nm) influences the values of β_2 and β_4 towards better phase-matching condition and more efficient broadband DFWM gain with respect to the uncoated case. Comparing the β_4 value at larger zero disperion diameters ($ZDD_{1,Airclad}$ = 1.17µm and $ZDD_{1,PMMAclad}$ = 1.013µm), it is found to increase from $\beta_{4,Airclad} = -6.9 \times 10^{-6}$ps^4/m to $\beta_{4,Airclad} = 3.4 \times 10^{-6}$ps^4/m by the application of a PMMA cladding rather than air. In addition, between the two ZDDs the value of β_2 -which is the dominant dispersion term in this range- advantageously reduces by up to one order of magnitude with the addition of the PMMA cladding. Finally, it is observed in Figure 3.1(c) that the value of γ -calculated following the procedure ref. [60]- increases from 76W^{-1}-m^{-1} (at $ZDD_{1,Airclad}$) to 98W^{-1}-m^{-1} (at $ZDD_{1,PMMAclad}$) from the addition of the PMMA cladding. This amounts to a total reduction in required pump power by 4.1dB for compensating the linear phase mismatch when the pump lies at ZDD 1 and up to 10dB when it lies between the two ZDDs the range where the dispersion is anomalous. The PMMA cladding improves not only the DFWM efficiency of the device but it also lowers the power consumption.

3.1.3 Experiment Design and Results

The hybrid As_2Se_3-PMMA microwires are fabricated following the procedure described in Ref. [19]. The length of the initial As_2Se_3-PMMA sample was kept short (< 5.5cm) to preserve a negligibly small DFWM gain compared to that in the 10cm long uniform microwire section. The microwires pigtailed to standard silica fibers (smf-28) have a total insertion loss of <4dB. This includes a loss of ~0.8dB due to the Fresnel reflection of 0.4dB on each end of the microwire, an As_2Se_3 and PMMA absorption loss of <1dB (depending on the

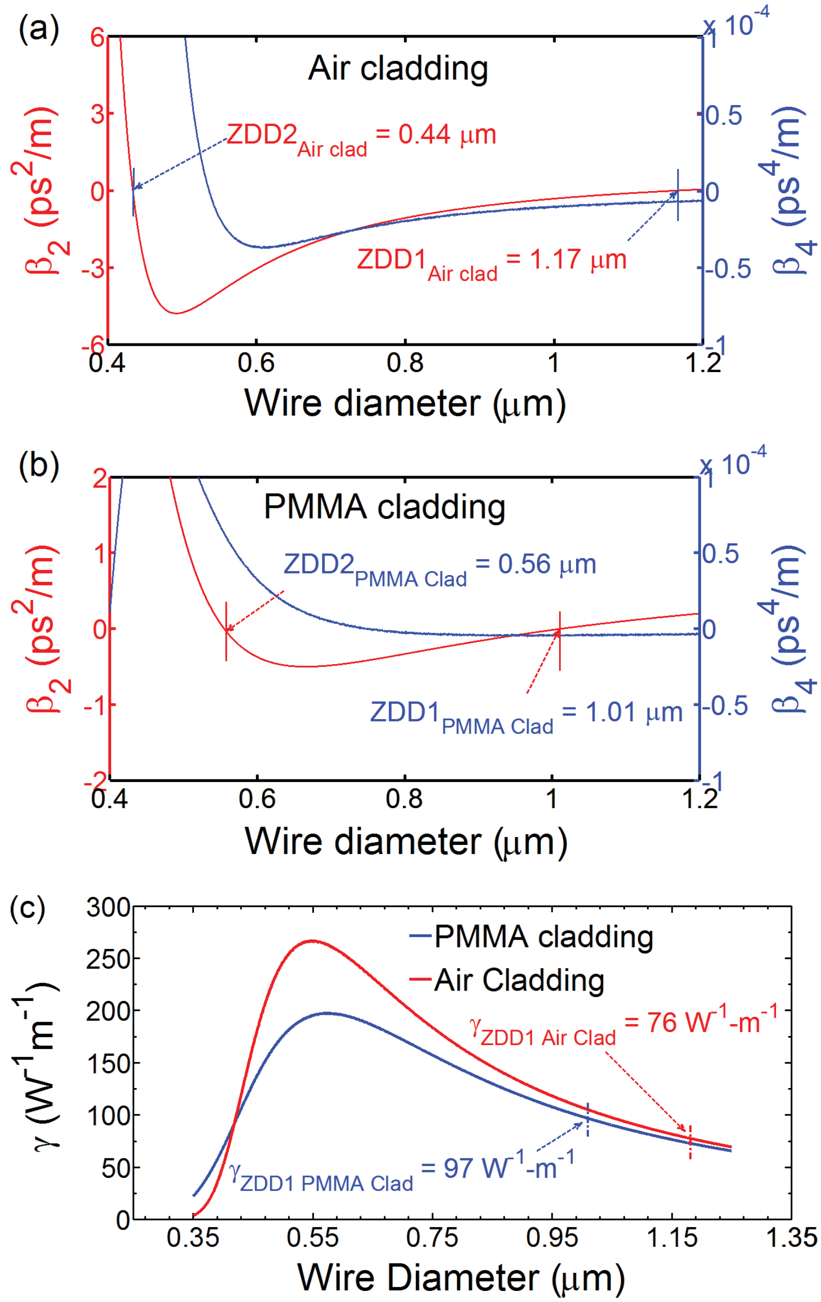

Figure 3.1 Dispersion and Nonlinearity curves. Calculated values of second (β_2) and fourth (β_4) order dispersion profiles at λ_P =1536nm, and the waveguide nonlinear coefficient (γ) as a function of As_2Se_3 wire diameter for the cases of air and PMMA cladding.

mode distribution in the As_2Se_3 core and the PMMA cladding that varies with the fiber core diameter), and the remaining loss is attributed to the mode mismatch between the microwire and the single mode silica fiber at the two ends of the device. This loss is reasonably low compared to that for the comparable waveguide structures [44, 47, 48], although even lower insertion loss could be achieved by a proper design for a minimum mode mismatch. It is noted that the microwires support higher order fiber modes if the As_2Se_3 core diameter is greater than $\sim$ 0.6µm. However, by observing the modal profile at the output end using a camera and observing the mode interference patterns using an OSA, the input coupling was optimized towards the fundamental mode [61].

The experimental measurement of DFWM in As_2Se_3-PMMA microwires is performed as follows: A pulsed pump laser centered at a wavelength of λ_P =1,536nm and a co-polarized tunable continuous-wave laser signal were injected into the microwire. The pump laser generated transform limited pulses with a full width at half maximum (FWHM) duration of 5ns and a repetition rate of 3.3kHz (duty cylce $\sim$ -48dB). The resulting DFWM was observed at the microwire output using an optical spectrum analyzer (OSA). Figure 3.2 (a) shows the spectra in response to a peak pump power P_P =0.3W and an average signal power $P_{S,in}$ =10.5dBm at the input of a 1.01µm diameter microwire. Two tunable laser sources with complementary wavelength coverage were used to characterize the idler wavelength conversion efficiency G_i on either side of λ_P. The two laser sources used for the DFWM measurements had different noise floor level that is evident from the correspondingly generated idler spectra. The combined tuning range of the cw lasers was 1,460-1,650nm and a corresponding idler was generated in the range 1,621-1,437nm. It was observed that the pump remained undepleted in the process since the output pump power remained unchanged when the signal was turned on/off. In order to perform wavelength conversion efficiency measurements, the peak idler power $P_{I,out}$ at the output was derived from the average output idler power and the duty cycle of the pump laser. Using the $P_{I,out}$ and the input signal power $P_{S,in}$, the conversion efficiency was then calculated from the Eq.3.4 provided above. The conversion efficiency measurements were performed with microwires of core diameters spreading in the range 0.58-1.05µm that enabled covering the entire anomalous region between the two ZDDs. Figure 3.2 (b)-(g) show the experimental results and corresponding simulations for those microwires. As shown in Figure 3.2 (c), for a core diameter of 1.01µm which approximately superimposes ZDD 1 and the pump wavelength, the value of G_i reaches up to 10dB and remains 2dB for a signal tuning range of 190nm. The efficiency is expected

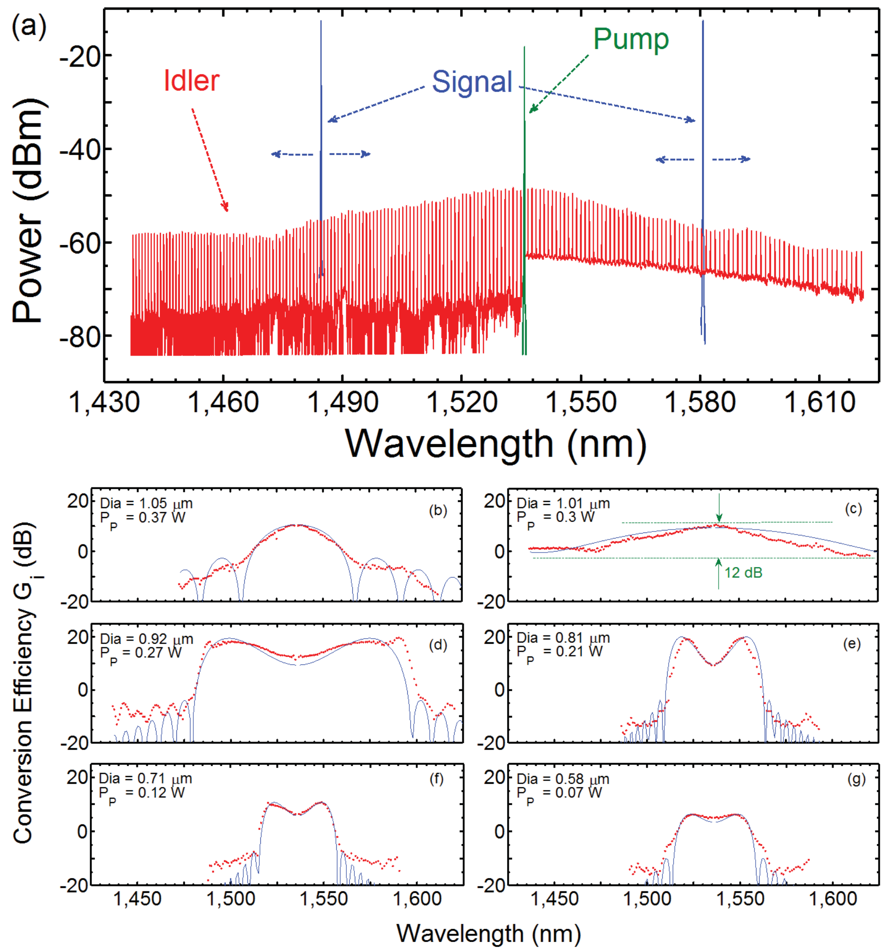

Figure 3.2 DFWM output spectra and idler wavelength conversion efficiencies. (a) Optical spectra of the pump, signal and the generated idler corresponding to the signal tuned in the wavelength range 1460-1650nm. The As_2Se_3 wire diameter was 1.01µm, P_P = 0.3W, $P_{S,in}$ = -10.5dBm and the microwire length was 10cm. Only two sampled signal wavelengths are shown for clarity whereas one sample of idler spectrum per nm is given. (b)-(g) Idler conversion efficiencies spectra for a range of As_2Se_3 microwire diameters and a fixed length of 10cm. The diameter value and the peak pump power used in the experiments are included as inset in each figure. Red (dotted) curves represent the experimental data, with the simulation fit denoted by the blue (continuous) lines.

to get even more flat with an increase in input pump power [1, 57]. The measured DFWM bandwidth is limited by the tuning range of the probe signal. Moreover, engineering of β_2 by the PMMA cladding allowed for a wide range of wire diameters, a broadband ($\geq$ 50nm) and efficient DFWM wavelength conversion (up to 21dB efficiency) from a low peak power pump (70-370mW). From a fabrication point of view, this adds tolerance by the DFWM process to a target microwire diameter. And from an application point of view, the bandwidth and gain of the DFWM device compare well with those of commercial fiber amplifiers doped with erbium and/or ytterbium [62]. In each of the conversion efficiency spectra, the impact of Raman scattering is also observed, appearing in the form of gain (loss) at a Stokes (anti-Stokes) wavelength shift of 7THz or ∼53nm at 1,550nm with respect to the pump wavelength.

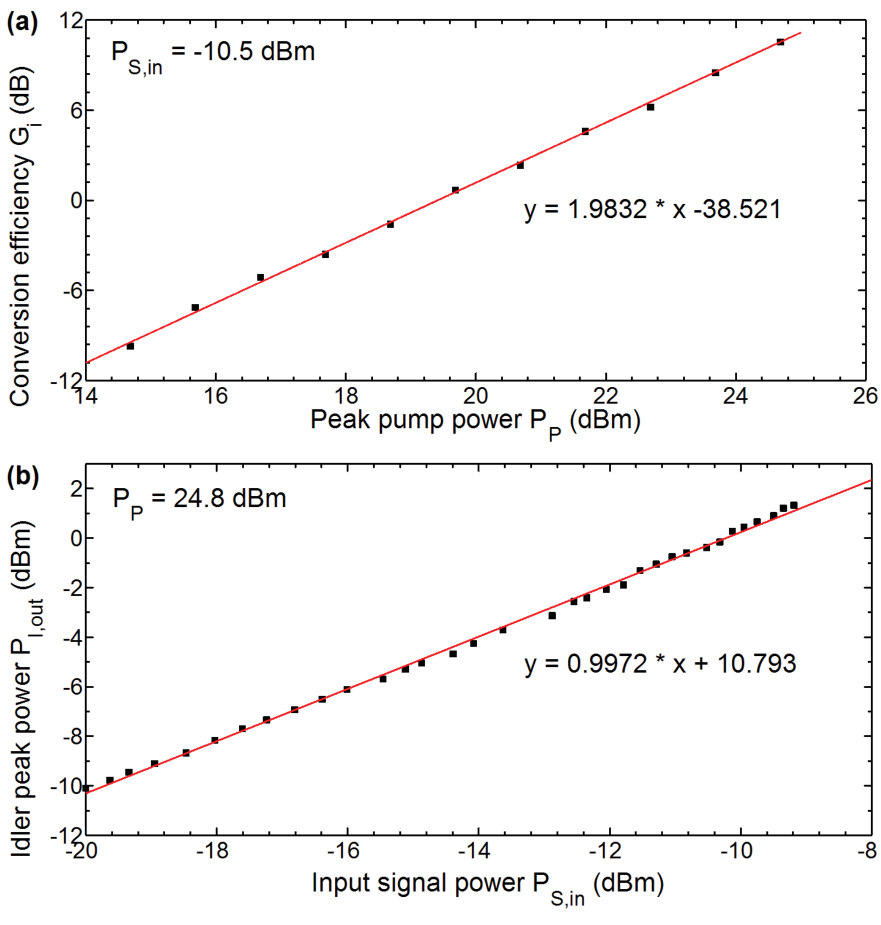

Figure 3.3 DFWM device performance characteristics. (a) Measured idler conversion efficiency plotted as a function of the peak input pump power for a microwire with 1.01µm diameter. (b) Measured idler peak power plotted as a function of input signal power for the same microwire.

Figure 3.3 (a) depicts the idler conversion efficiency of the DFWM process in a microwire with 1.01µm core diameter. The input signal power and the wavelength were maintained at -10.5dBm and 1,540.8nm, respectively. The plot shows an almost quadratic dependence (slope = 1.98) of the conversion efficiency on peak pump power which corresponds to theory. There is no sign of saturation due to multiphoton absorption up to 0.3W of input peak pump power which corresponds to the peak intensity of 37MW-cm^{-2}. The slight deviation of the slopes of idler conversion efficiency with the input pump power is expected to be leading from the departure from exact phase matching condition at a given wavelength when the pump power is increased, as stated quantitatively by the Eqs. (3) and (4). Figure 3.3(b) shows the dependence of the idler (peak) output power on the input signal power for a fixed (peak) pump power of 0.3W. In this case, the idler output power increases linearly (slope = 0.99) with the input signal power which again confirms the theoretical prediction. Since there is no sign of saturation, the conversion efficiency is expected to increase further from raising the input pump power. Likewise, the wavelength conversion efficiency can be enhanced further by employing longer microwires.

Table 3.1 Comparison of highly nonlinear fibers made from silica and bismuth, waveguide made from As_2S_3 chalcogenide and silicon and the microwires made from As_2Se_3.

Waveguide type	Waveguide nonlinear coefficient γ (W^{-1}-m^{-1})	Loss α (dB/m)	Maximum effective length L_{eff} (m)	Nonlinear figure of merit (FOM) γL_{eff} (W^{-1})
Highly nonlinear (HNL) silica fiber	0.021	10^{-3}	21715	91.20
Bismuth oxide (Bi_2O_3) fiber [63]	1.36	0.8	5.42	7.38
As_2S_3 waveguide [64]	9.9	60	0.072	0.72
Silicon waveguide [65]	150	400	0.011	1.63
As_2Se_3 microwire [This work]	97 (at ZDD 1) 187 (at ZDD 2)	<1 <1	4.343 4.343	421.27 812.14

We finally perform a detailed theoretical comparison of the FWM performance of various optical materials including silica, bismuth, silicon, and chalcogenides (As_2S_3 and As_2Se_3). The Table. 3.1 shows the values of nonlinear coefficient γ, propagation loss α and the calculated maximum effective lengths for DFWM devices made from different nonlinear optical materials including highly nonlinear (HNL) silica and bismuth fibers, As_2S_3 and Si waveg-

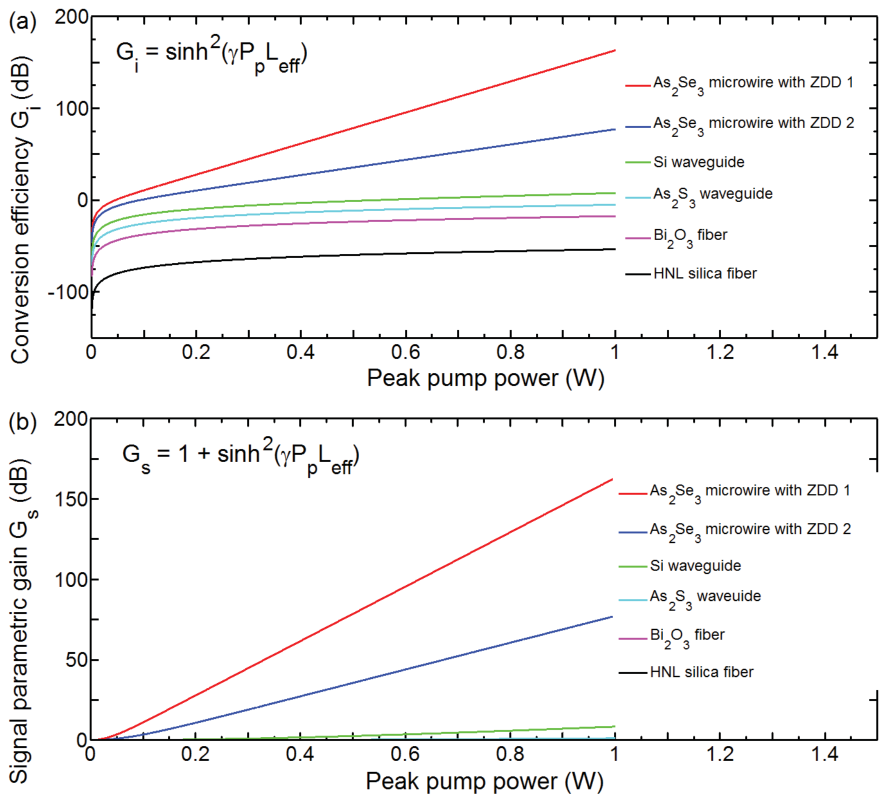

Figure 3.4 Calculated (a) idler conversion efficiency and (b) signal gain for phase matched DFWM process in 10cm long chalcogenides (As_2Se_3, As_2S_3), silicon, bismuth and silica fibers/waveguides. The low propagation loss with a high nonlinear coefficient in As_2Se_3 microwires allows the maximum conversion efficiency/signal gain in a compact scheme. The parameters used in these simulations are provided in the Table. 3.1.

uides and As_2Se_3 microwires. The large γ and low α values in As_2Se_3 microwires (and hence longer L_{eff}) leads to a much higher idler conversion efficiency G_i (and parametric gain G_S) from the DFWM process, assuming a zero phase-mismatch ($\Delta k = 0$). The values of G_i and G_S are plotted in Figures 3.4 (a), (b) for 10cm long (fiber or planar) waveguides made from silica, bismuth, silicon and chalcogenides, under the assumption of perfect phase matching. This figure shows that As_2Se_3, because of lower absorption loss and high nonlinearity, is the best choice for realizing compact, power efficient FWM related devices.

3.1.4 Summary

In summary, the addition of a PMMA cladding to an As_2Se_3 microwire advantageously enabled engineering the waveguide dispersion towards an optimization of DFWM process. This dispersion engineering accompanied by an enhanced nonlinear coefficient γ of the microwire ($\sim 10^5 \times$ that of silica fibers) led to an efficient and broadband DFWM in 10cm long microwires at peak power levels as low as 70mW. The next step is the introduction of resonant feedback [28] to realize a compact and low-threshold all-chalcogenide parametric oscillator, which will be a first distributed feedback (DFB) parametric oscillator in $\chi^{(3)}$ medium. Such a compact and efficient device will find a wide-range of applications in telecommunication systems, mid-infrared spectroscopy and free-space communications [66].

3.2 Chalcogenide optical parametric oscillator

3.2.1 Introduction

When a sufficiently high intensity optical pump propagates through medium, the nonlinear optical processes in the form of energy-matter interaction lead to the radiation of additional optical waves which appear at frequencies different from that of the original pump source. As mentioned in the previous section, parametric processes belong to a class of nonlinear processes which originate from the phase-matching between different optical frequency waves. The phase-matching between the pump and noise photons (available in the medium at all frequencies) can lead to the efficient waves interaction and stimulate parametric amplification of the phase-matched frequencies. When the parametrically amplified signal is trapped in a resonant cavity and experiences a gain that exceeds total cavity losses in a roundtrip, its intensity grows exponentially with the pump power and the resulting device is termed as an optical parametric oscillator (OPO).

OPOs are attractive owing to their tunability over a broad frequency range that cannot be easily covered with conventional laser sources. Moreover, the OPOs, if allowed to oscillate simultaneously at the signal and the idler frequencies, present a source of strongly correlated photon pairs that can be used for applications related to quantum communication, quantum cryptography and quantum computing. OPOs have been realized in different nonlinear materials, based on both the second order $\chi^{(2)}$ and the third order $\chi^{(3)}$ susceptibility, and in a variety of device structures and configurations. The OPOs based on $\chi^{(2)}$ nonlinear materials including $LiNbO_3$, KTP, BiB_3O_6, MgO:sPPLT [67–71] can offer high power operation with a wide wavelength tunability, but are bulky, susceptible to misalignment, and can only oscillate at wavelengths longer than that of the pump laser. On the other hand, $\chi^{(3)}$ based OPOs have been realized in conventional and microstructured optical fibers (MOFs), planar waveguides and microresonators made from various materials including silica and silicon [72–81]. However, the high power requirements and long nonlinear interaction lengths required for conventional silica fiber based OPOs render them impractical. The OPOs based on integrated or microresonator devices on the other hand, are attractive in terms of compactness but are not compatible with the existing fiber technology. Furthermore the microresonator based OPOs suffer from longer response times, from hundreds of picoseconds to hundreds of nanoseconds, and are thus restricted to low bandwidth applications, while the silicon based OPOs are restricted to beyond 2µm wavelengths owing to large two-photon absorption and free carrier generation in the telecommunications bands [75]. The MOF-OPOs on one hand are attractive for their fiber compatibility and their well controlled dispersion profile−that is critical for nonlinear parametric processes−but have only been realized using silica glass that itself suffers from relatively weak nonlinearity.

We present an OPO based on an As_2Se_3 microwire coated with poly methyl-meth-acrylate (PMMA) cladding. The PMMA cladding in addition to providing physical strength to the thin microwire [56], serves to optimize phase-matching conditions towards efficient and broadband parametric gain, as described in the previous section [82]. The OPO oscillates simultaneously at two wavelengths: at a Stokes and anti-Stokes wavelength shifts of +53nm and -50nm respectively from the pump laser. The large nonlinearity, the reduced chromatic dispersion from a PMMA cladding and the long effective length (due to the low absorption loss α <1dB/m) of As_2Se_3 hybrid microwires allows the OPO to oscillate at a low peak pump power threshold of 21.6dBm (pulse energy = 3.15pJ) and with a total conversion efficiency of $> 19\%$.

3.2.2 Experimental Results and Discussion

The hybrid As_2Se_3-PMMA microwire is prepared following the procedure detailed in Ref. [19, 82]. The microwire has an As_2Se_3 core diameter of 1.01µm and is 10cm long, with a total insertion loss of 5dB. This includes a loss of ∼0.8dB due to the Fresnel reflection of 0.4dB on each end of the microwire, an As_2Se_3 and PMMA absorption loss of <1dB, and the

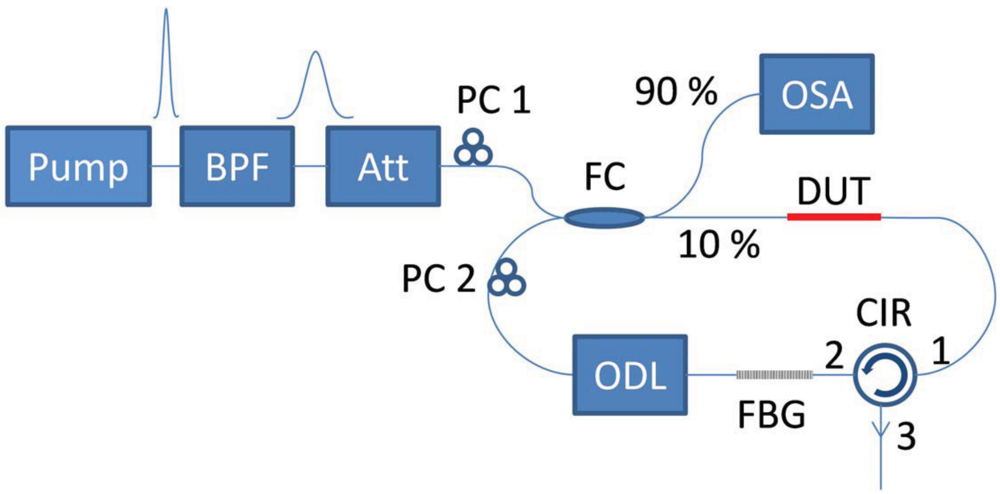

Figure 3.5 Experimental setup for the OPO operation. BPF: band pass filter; Att: optical attenuator; PC: fiber polarization controller; FC: fiber coupler; OSA: optical spectrum analyzer; DUT: device under test; CIR: optical circulator; FBG: silica fiber bragg grating; ODL: optical (tunable) delay line.

remaining loss is attributed to the mode mismatch between the microwire and the single mode silica fiber at both ends of the microwire. Figure 3.5 shows the experimental setup for the OPO operation. A mode-locked laser emitting pulses of full width at half maximum (FWHM) duration of ∼450fs, with a repetition rate of 20MHz and spectrally centered at around λ =1551nm, is used as the pump laser. The pump is filtered spectrally with a ∼0.25nm bandpass filter (BPF) centered at 1552nm to lengthen pulses to a FWHM duration ∼22ps [56]. The resulting pump pulses are then delivered to the microwire via the 10% output port of a 90/10 fiber coupler (FC). This results in the optical parametric amplification on both sides of the pump wavelength in an almost symmetric manner, determined precisely by the dispersion profile of the microwire. In order to realize OPO, the parametric gain obtained is fed back to the microwire via the second input port of the FC, thus completing the laser cavity. The residual pump pulse is filtered out from the fed back signal using a fiber Bragg grating resonant at the pump wavelength combined with an optical fiber circulator (CIR). This avoids any unfavourable interference of the incoming pump pulse with the preceding residual one. A fiber coupled tunable optical delay line (ODL) is introduced for a precise control of the cavity length so that the amplified Stokes and anti-Stokes signals that resonate in the loop cavity are precisely synchronized with the incoming pump pulse. It is noted that the dispersive walk off effect can be ignored since the walk off length of ∼2.2m [1], resulting from the wavelength separation between the pump and the Stokes/anti-Stokes signals is considerably longer than the length of the parametric gain medium i.e., the 10cm long microwire. Finally, a fiber polarization controller is inserted in the cavity to align the polarization state of the two amplified signals with that of the incoming pump pulse. The operation of the OPO is observed on an optical spectrum analyzer (OSA) connected to the 90% output port of the fiber coupler.

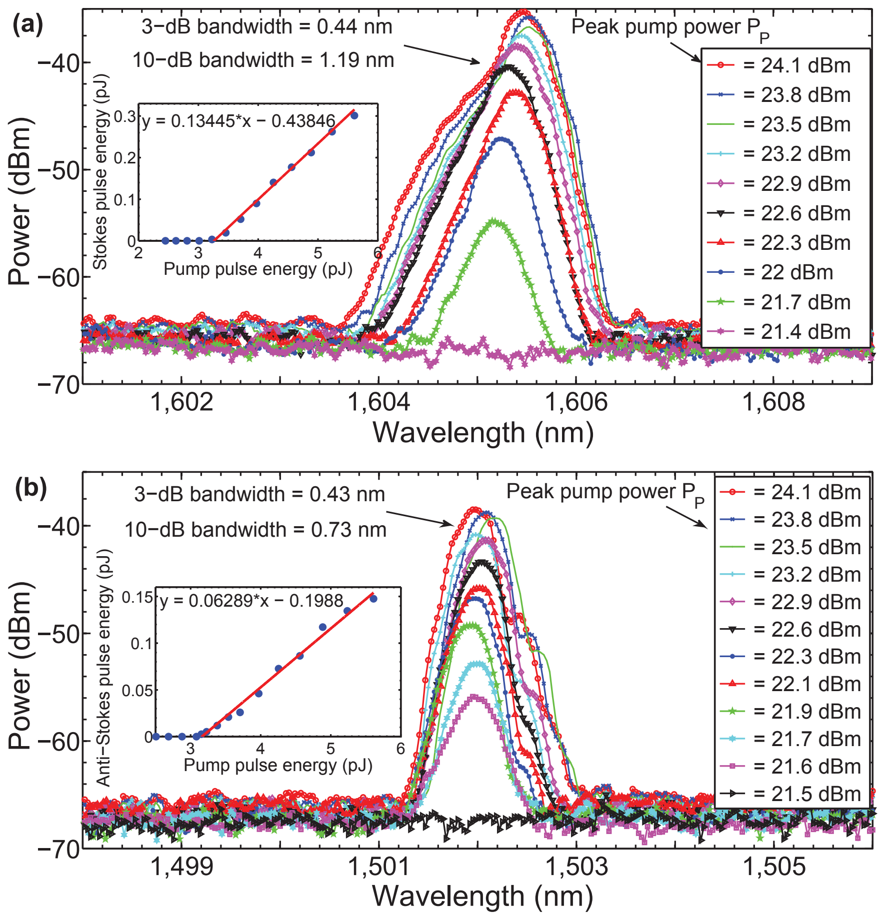

Figure 3.6 Output spectra of the (a) Stokes and (b) anti-Stokes OPO signals for the increasing values of input peak pump power. (Inset) The pulse energy in the Stokes and the anti Stokes output signals are plotted against the input pump pulse energies and are included as inset in (a) and (b) respectively.

When the total single pass parametric gain exceeds the round trip cavity loss of 8dB, the OPO oscillates at Stokes and anti Stokes wavelengths of 1605nm and 1502nm respectively. This represents the conversion of a C-band pump laser to L-band (Stokes) and S-band (anti-

Stokes) OPOs. Figures 3.6(a) and (b) show the spectra of the output Stokes and anti-Stokes OPO signals with increasing peak pump power. The spectral FWHMs of the two OPO outputs are 0.44nm and 0.43nm for the Stokes and the anti Stokes signals respectively. The Stokes signal carries 3.3dB more energy than the anti Stokes one. This can be explained from the additional Raman gain at the Stokes wavelength that almost coincides with the Raman shift wavelength for the As_2Se_3 microwire [82]. Both the Stokes and the anti Stokes OPO signals have a threshold peak pump power of ~21.6dBm, corresponding to pulse energy of 3.15pJ. The slope efficiency of the Stokes OPO exceeds 13%, with the Stokes output pulses carrying >0.3pJ of energy. The slope efficiency of the anti-Stokes OPO is >6% corresponding to a pulse energy ~0.15pJ, providing a total internal conversion efficiency of >19%. This represents high conversion efficiency OPO considering its compactness and the low power operation.

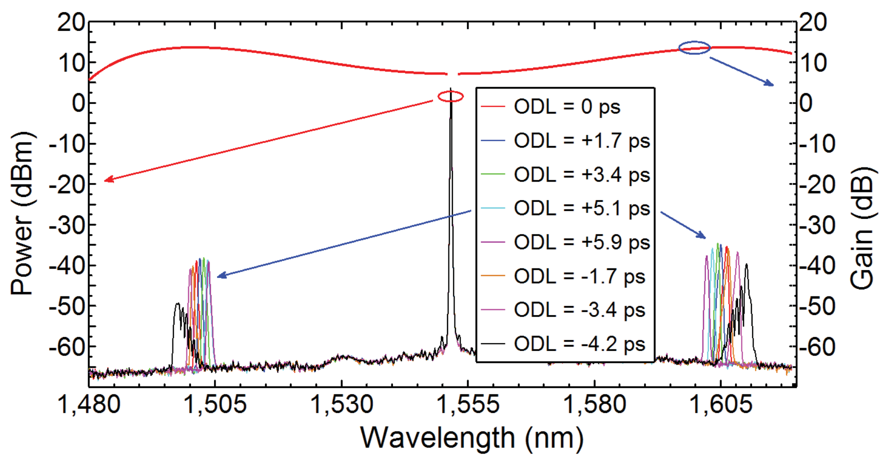

Figure 3.7 Output of the OPO as observed on an OSA for various delay values on the oscillating Stokes and anti Stokes signals. The calculated parametric gain spectrum under the experimental conditions is also included.

Figure 3.7 shows the output spectra of the OPO as recorded on the OSA. The spectra show the simultaneous oscillation of the doubly resonant OPO at the Stokes and anti Stokes wavelengths. After setting up the OPO, we study the effect of adding a delay or advance on the oscillating Stokes and anti-Stokes signals which compromises their precise synchronization with the pump pulse. The OPO continues to operate for a wide temporal detuning of approximately ±5ps beyond which there is no output signal. This temporal detuning allows OPO Stokes and anti-Stokes wavelengths tuning by up to 8nm. The wavelength tuning results from a natural minimization of the group velocity mismatch between the pump wavelength and the Stokes/anti-Stokes oscillating wavelengths. In order to compare the experimental results with theory, the single-pass parametric gain in the microwire of the same dimensions as used in the experiment is calculated for a 24.1dBm peak pump power. The calculated parametric gain profile is included in the Figure 3.7. It is noted that the oscillating wavelengths precisely match the wavelengths where the parametric gain is maximum in agreement with theory.

3.2.3 Summary

In conclusion, we have demonstrated the first optical parametric oscillator in chalcogenide glass. The parametric gain medium is a 1.01μm thick and 10cm long As_2Se_3-PMMA hybrid microwire. The OPO oscillates simultaneously at Stokes and anti-Stokes wavelengths in the L- and the S-telecommunications frequency bands respectively, with the pump lying in the C-band. The OPO has a total internal conversion efficiency of ∼19%, with a threshold peak pump power of 21.6dBm. The wavelength conversion bandwidth of this device can be further extended to the mid-infrared wavelengths region by adjusting the wire diameter to have a net, small value of normal dispersion at the pump wavelength.

Chapter 4

Raman lasing in chalcogenide microwires

[1]In this chapter, we present our work on developing Raman lasers using the As_2Se_3 microwires. We discuss the two different techniques that we employed to realize the As_2Se_3 microwires based Raman lasers. The first half of the chapter explains the fiber loop cavity based Raman laser, while the second half explains the one that was based on a Fabry-Perot type cavity.

4.1 Loop-cavity Raman laser

4.1.1 Introduction

Fiber lasers find many applications where mechanical stability, compactness and integrability into optical systems are the qualities of major importance. One class of fiber lasers, those based on nonlinear optical process of Raman scattering that results from the excitation of optical phonons, are attractive owing to their gain spectrum available over the entire transmission window of the material. This is opposed to the case of rare-earth doped fiber lasers where the gain spectrum is defined by discrete atomic transition band(s). Raman fiber lasers based on silica glass, that is the most widespread material for optical fibers, however

[1]The content of this chapter has been subjected to publication in (1) R. Ahmad and M. Rochette, Chalcogenide microwire based Raman laser, Appl. Phys. Lett. 101, 101110 (2012), and (2) R. Ahmad and M. Rochette, Raman lasing in a chalcogenide microwire-based FabryPerot cavity, Opt. Lett. 37, 4549-4551 (2012).

require lengths of hundreds of meters and/or input pump powers of several tens of Watts for their operation [83–86]. A Raman laser can be realized in an optical cavity when the Raman gain exceeds the round-trip cavity losses. Such lasers have been realized in a variety of optical materials including silicon [87] and other crystals [88] as well as in silica glass, both in fiber, and microresonator geometries [83, 86, 89]. Raman lasers based on crystals are unfortunately bulky, susceptible to misalignment and incompatible with optical fibers while those based on silicon and microresonators are although energy efficient but still lack fiber compatibility. On the other hand, Raman lasers based on silica glass optical fibers require lengths of hundreds of meters and input pump powers of several tens of watts for their operation [83]. In order to facilitate the practical implementation of Raman lasers in fibers, it is of great interest to explore materials with Raman gain coefficients g_R larger than the one of silica [90, 91].

The As_2Se_3 chalcogenide glass is reported to have a Raman gain coefficient $g_{R,As_2Se_3} \sim 780 \times g_{R,Silica}$ [2]. Indeed, a Raman laser based on As_2Se_3 step-index fiber was demonstrated by Jackson et al. in Ref. [91]. However, the laser still required Watt-level threshold pump power and meters long Raman gain medium i.e., the As_2Se_3 single mode fiber. A reduction in the lasing threshold and/or shortening of the laser cavity length can be realized by utilizing the As_2Se_3 microwires where the effective mode area is reduced by more than 150× as compared to that in the regular As_2Se_3 glass optical fibers. This leads to enhanced mode intensity in the microwire and therefore, increased Raman gain for a given amount of pump power. A tremendous effort has been made in the past few years to realize micro- and/or nanowire Raman lasers with successful demonstrations in silicon and other semiconductors [87, 92, 93] but not in a glass medium, such as chalcogenides.

In this section, we report an As_2Se_3-PMMA hybrid microwire based Raman laser that operates in the telecommunications L-band (λ_S =1607-1611nm). The higher nonlinearity in the microwire geometry with respect to the step-index fiber presented in [91] has led to a 5-7× reduced threshold pump power and a 10-40× shortened gain medium. This represents an efficient and compact wavelength conversion device for existing laser sources in the telecommunications wavelengths region.

4.1.2 Theoretical Background

When light travels through a medium, photons interact with the atoms/molecules to create photons of slightly different energy. The energy difference is defined by the properties of the materials phonon energies. In terms of wavelength (frequency), this results in the generation of waves, additional to the pump input, at both shorter (lower) and longer (higher) wavelengths (frequencies). Typically, however, the efficiency of Raman scattering is several orders of magnitude higher for the signal at longer or the so-called Stokes wavelengths. It is found that with a sufficiently high intensity pump source, the spontaneously generated photons can give rise to a stimulated photon emission process, in which the spontaneous photons act as a seed to draw more gain from the pump. This stimulated Raman emission is very efficient and can result in a transfer efficiency reaching up to 100%. Another way to realize the stimulated Raman emission is to inject a seed signal at the Raman wavelength shift together with the pump at the input. This is the principle of Raman amplifiers. In case of Raman lasers, the spontaneously generated photons are typically trapped inside an optical cavity containing the Raman gain medium. As a result, photons are initially generated at the Raman wavelength shift via the spontaneous scattering process, and these photons stimulate the Raman scattering process as they travel alongside the pump to result in more efficient Raman scattering. Raman scattering has found applications in a wide range of fields, ranging from spectroscopy to telecommunications, and is a powerful technique used in carrying out fundamental studies in scientific fields, such as chemistry and nonlinear optics.

The principle of operation of a Raman laser is same as that of any other laser, i.e., it requires a pump source, a gain medium and an optical cavity. The gain in this case is a nonlinear Raman active medium (such as, a chalcogenide microwire), and the pump source is a high intensity laser. The operation of a Raman laser is very similar to that of an OPO; the gain in both cases is provided by a nonlinear optical process. An input signal at a down-shifted frequency from that of the pump laser by the characteristic Raman shift, experiences gain as it propagates through the medium of length L along the pump. The amount of the experienced gain is defined by the Raman gain coefficient g_{Raman} of the medium. Furthermore, the signal also experiences a loss, defined by the loss coefficient α of the medium as it propagates through the medium. The net gain experienced by the signal is given by,

$$G = e^{g_{Raman} P_{pump} L_{eff} - \alpha L}, \tag{4.1}$$

where $L_{eff} = \frac{[1-e^{-\alpha L}]}{\alpha}$ is the effective interaction length calculated by taking into account the loss in the medium and P_{pump} is the peak power of the pump input. The threshold power required for the operation of a Raman laser can be calculated by considering the roundtrip cavity loss R and can be written as [1],

$$R \times e^{g_{Raman} P_{pump} L_{eff} - \alpha L} = 1. \tag{4.2}$$

In the following sections, we discuss our experiments on realizing Raman laser sources using the chalcogenide As_2Se_3 microwires.

4.1.3 Experiment and Results

The hybrid As_2Se_3-PMMA microwire is prepared from an As_2Se_3 fiber (Coractive inc.), following the procedure detailed in Ref. [19]. It has an As_2Se_3 core diameter of 0.55µm and is 12cm long, with a total insertion loss of 8.1dB. The microwire diameter is precisely selected with an aim to (a) reduce the effective mode area so as to maximize the Raman gain and to (b) enable sufficient normal chromatic dispersion and thus avoid parametric amplification [82]. The threshold power for parametric amplification is lower than the Raman scattering process and therefore normal dispersion is required to emphasize the Raman process [1].

Figure 4.1 shows the experimental setup of the Raman laser. A femtosecond mode-locked laser emitting pulses of full-width at half maximum (FWHM) duration ∼450fs, with a repetition rate of 20MHz and spectrally centered at λ =1551nm, is used as the pump laser. The pump is filtered with a ∼0.25nm bandpass filtering (BPF) stage centered at λ =1552nm to lengthen pulses to FWHM duration of ∼22ps. The BPF consists of an assembly including a conventional pigtailed 0.25nm bandpass filter followed by an erbium doped fiber amplifier (EDFA), the output of which is filtered by a combination of optical fiber circulator (CIR) and a fiber Bragg grating (FBG). The EDFA is required to compensate the losses of the double-stage filtering process. The resulting pump pulses are then delivered to the microwire via the 10% output port of a 90/10 fiber coupler (FC). This results into Raman gain at wavelengths in the range of 1605-1613nm. In order to enable a laser operation, the spontaneous Raman emission is fed back to the microwire via the second input port of the FC, thus completing

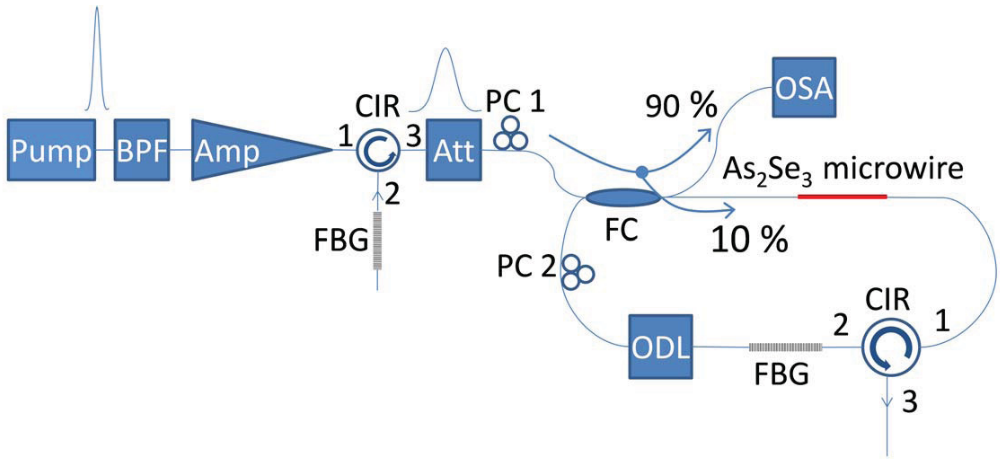

Figure 4.1 Experimental setup of the Raman fiber laser. BPF: band pass filter; Att: optical attenuator; PC: fiber polarization controller; FC: fiber coupler; OSA: optical spectrum analyzer; CIR: optical circulator; FBG: fiber bragg grating; ODL: optical delay line.

the resonant cavity. The residual pump pulse is filtered out from the laser signal with a notch filter centered at λ =1553nm and made out of a second FBG-CIR combination. This eliminates the detrimental self-interference of the pump pulse in the resonant cavity. A fiber coupled variable optical delay line (ODL) is inserted for a precise control of the cavity length so that the amplified Raman signal that resonates in the cavity is precisely synchronized with the incoming pump pulse. The CIR, FBG and ODL in the feedback path contribute to the intra cavity loss by 2dB. A fiber polarization controller (PC) is used to align the polarization state of the lasing signal with that of the incoming pump pulse. The operation of the Raman laser is observed on an optical spectrum analyzer connected to the 90% output port of the fiber coupler. The total round trip cavity loss is 10.1dB.

An effective laser peak is observed at a wavelength of ~1609nm when the total single pass Raman gain exceeds the round trip cavity loss. This represents the conversion of C-band pump laser to L-band output Raman laser. Figure 4.2 shows the laser spectrum (Figure 4.2 (a)) and output power evolution (Figure 4.2 (b)) with increasing peak pump power. As the pump power is increased, the FWHM of the laser spectrum asymptotically increases towards a value of ~6nm. The origin of the relatively broad bandwidth of the laser output is attributed to three possible causes. First, it is observed that pump pulses experience spectrum broadening from self-phase modulation. The inset of Figure 4.2 (b) shows the spectrum of pump pulses after the microwire at two power levels, below and above the lasing threshold.

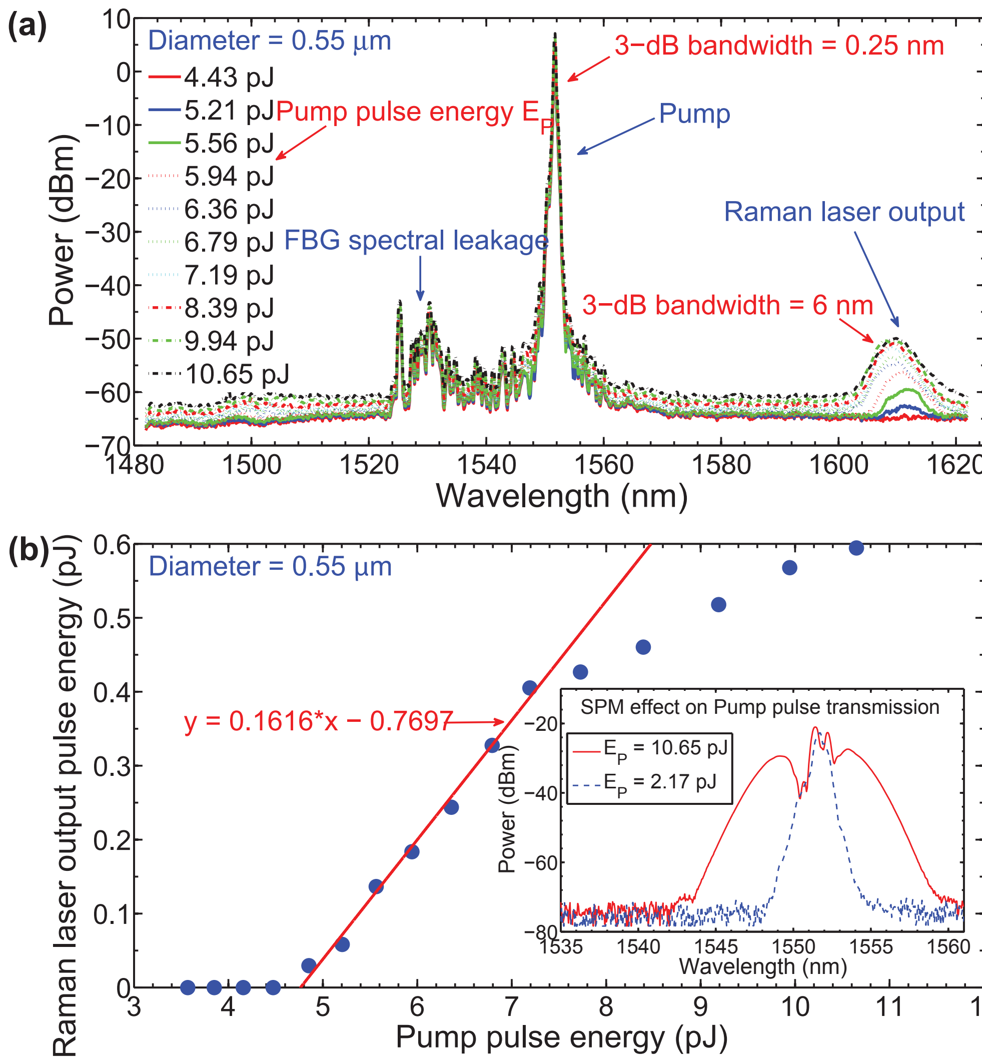

Figure 4.2 (a) Output spectra of the Raman laser for increasing values of input peak pump power. In (b), Raman laser pulse energy as a function of input pump pulse energy. (Inset) The self-phase modulation induced spectral broadening of the pump pulse upon transmission through the microwire is recorded in an open loop.

From this, the signal may broaden from the interplay (i.e. convolution) of the broadened pump and the Raman gain spectrum or by cross-phase modulation between the pump and signal. A second assumption to explain the wide output spectrum of the Raman laser comes from the walk-off and chromatic dispersion in the microwire. With an increasing walk-off effect, pump and Raman lasing pulses become temporally offset from each other in a fewer cavity round-trips and thus the Raman signal at one particular wavelength does not build up sufficiently to extract most of the energy (or gain) from the pump pulse. This is supported by the FWHM of the output Raman signal that could be reduced to ~3nm by proper adjustment of the cavity length, as will be discussed later in more detail. The 3nm FWHM bandwidth of the Raman laser is still relatively broad as compared to the chalcogenide microwire based optical parametric oscillator output [94]. Finally, the third assumption is that the free-carriers generated from two-photon absorption can contribute towards the broadening and the instability of the Raman spectrum. The As_2Se_3 glass is known to suffer from two photon absorption effects when exposed to high intensity telecommunications band pump laser.

The noisy spectral components observed in Figure 4.2 (a) in the wavelength range 1525-1540nm are part of the input pump signal and result from spectral leakage from the EDFA and FBG part of the BPF stage. It may however be noted that these spectral components contain incoherent spontaneous emission from the EDFA that is expected to play no role in the nonlinear process due to the low instantaneous power of the spontaneous emission with respect to the pump pulses.

Figure 4.2 (b) shows the laser pulse energy versus the input pump pulse energy. This reveals the power conversion efficiency of the Raman laser at this wavelength to be more than 16%, with a threshold pump pulse energy of 4.78pJ (peak pump power = 23.4dBm). The maximum power conversion efficiency is $>$ 17% and the threshold pump pulse energy is $<$4.65pJ (peak pump power = 23.2dBm) at a slightly different wavelength when the cavity length is adjusted. This represents high efficiency Raman laser considering its compactness and the low power operation. At a pump pulse energy of $>$7pJ, the laser output saturates as a result of two photon absorption.

Figure 4.3 shows the output spectra of the laser as a function of a relative delay on the lasing signal by adjustment of the ODL. The laser operates over a cavity detuning of $\pm$2.5ps beyond which the output signal fades out. This temporal detuning allows Raman lasing wavelength tuning by up to 5nm. The wavelength tuning results from a natural intra-cavity minimization of the group velocity mismatch between the pump wavelength and the Raman oscillating wavelength.

Also take note that the data shown in Figure 4.2 does not correspond to a precisely zero relative intra cavity delay. Figure 4.4 shows the Raman laser spectrum for a temporal offset of 0ps i.e., when the Raman lasing signal is precisely synchronized with the incoming pump

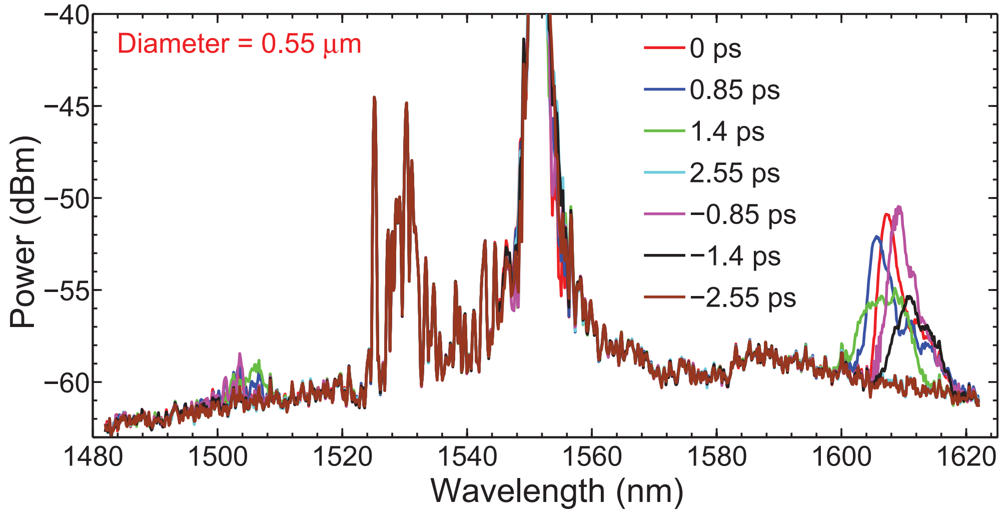

Figure 4.3 Raman laser spectra as a function of the relative intra-cavity delay.

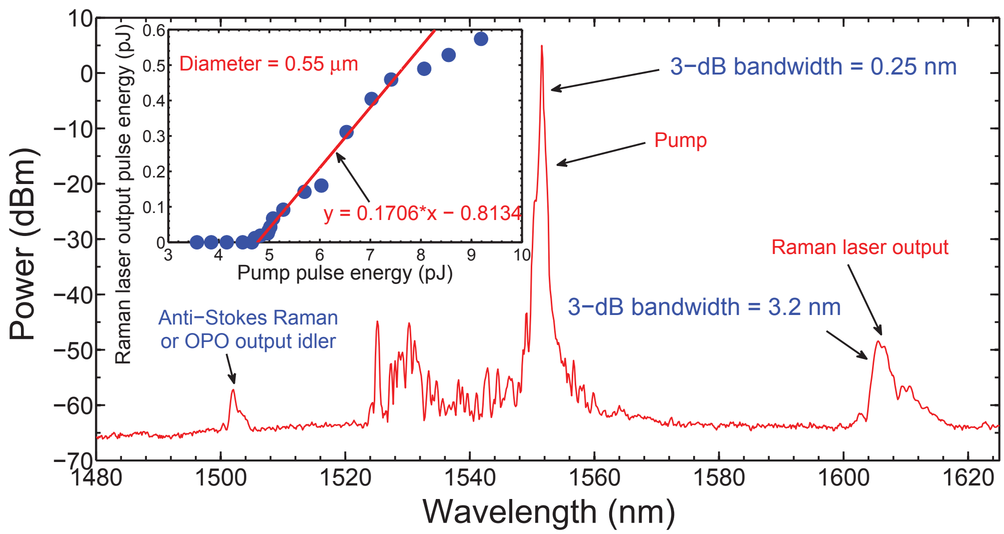

Figure 4.4 Output spectrum of the Raman laser as observed on an OSA for precise synchronization of the lasing signal with the incoming pump pulse i.e., for a delay value of 0ps. (Inset) The Raman laser pulse energy versus the input pump pulse energy with the power conversion efficiency value included as well.

pulse. The FWHM of the Raman laser spectrum in this case reduces to 3.2nm. The inset in Figure 4.4 shows the Raman laser pulse energy as a function of the input pump pulse energy for the case of 0ps intracavity delay. The power conversion efficiency for this case is increased to ∼17% (inset) and the threshold pump pulse energy (peak pump power) is reduced to 4.65pJ (23.2dBm). The saturation pump pulse energy is the same as for the non-zero delay case. In addition, an anti-Stokes output signal is generated at a wavelength offset of -50nm from the pump source, while operating at the same pump power level. The source of this additional anti Stokes output signal is attributed to anti Stokes Raman scattering or a low efficiency optical parametric four wave mixing.

4.1.4 Summary

In summary, we have demonstrated the first chalcogenide glass and microwire based Raman laser operating in the telecommunications band. The Raman gain medium is a 0.55µs thick and 12cm long As_2Se_3-PMMA hybrid microwire. The Raman laser operates in the L-band and is pumped in the C-band. The laser operates with a power conversion efficiency of ~17%, with a threshold peak pump power of 22.3dBm.

4.2 Fabry-Perot cavity Raman laser

4.2.1 Introduction

In this section, we describe the As_2Se_3 microwire based Raman laser in Fabry-Perot cavity configuration. In this work, two Fabry-Perot cavity designs were tested for the lasing operation: (1) a cavity made out of a Fresnel reflection at one end of the microwire and a silver coated, broadband mirror at the other end, and (2) a cavity made out of Fresnel reflections at both ends of the microwire. The microwires are pumped in the C-band and the resulting Raman lasers operate in the L-band.

4.2.2 Experiment and Results

Figure 4.5 shows the Raman laser setup. The output of a DFB laser, centered at a wavelength of λ_P =1549.3nm, is carved from CW to rectangular pulses of 64ns in duration at a repetition rate of 3.8kHz. The pulse carving is carried out by two cascaded Mach-Zenhder modulators driven by an electrical pulse pattern generator and providing an optical extinction ratio of ~40dB. The pulses are amplified using an erbium doped fiber amplifier (EDFA). The unwanted broadband spontaneous emission noise from the EDFA is removed with an optical bandpass filter (BPF) having a full-width at half maximum (FWHM) of 0.2nm. A second EDFA is used to further amplify pulses to the desired power level and is followed by another

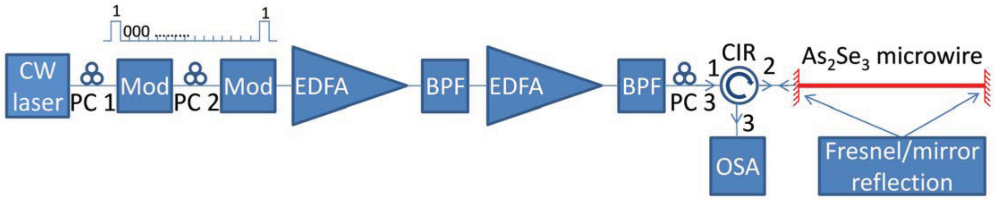

Figure 4.5 Experimental setup of the As_2Se_3 Raman laser. CW laser: continuous wave fiber coupled laser; PCx: polarization controller x; Mod: Mach-Zehnder modulators; EDFA: erbium doped fiber amplifier; BPF: optical band-pass filter; CIR: optical circulator; OSA: optical spectrum analyzer.

BPF having a FWHM of 0.2nm. The quasi-CW pump pulses are then delivered via a fiber polarization controller and a 3-port fiber circulator, to the As_2Se_3 microwire that provides the Raman gain. The duration of the pump pulses is a trade-off between delivering sufficiently long and intense pulses to induce Raman lasing with multiple round-trips in a 13cm long resonant cavity and avoiding the damage of the microwire from two-photon absorption. The microwire used in the experiment is a hybrid structure consisting of an As_2Se_3 fiber core and a PMMA cladding and is prepared following the procedure detailed in Ref. [19]. The diameter of the As_2Se_3 core is 0.95µm and the uniform waist region of the microwire is 13cm long, with 5.5dB loss from single-mode silica fiber-to-chalcogenide microwire-to-single-mode silica fiber. The diameter of the microwire is chosen such that the C-band pump laser provides only the Raman gain the in the L-frequency band without any parametric or four-wave mixing gain. The input end of the microwire is permanently bonded to a standard single mode silica fiber using UV-curing gel so as to efficiently couple light from the fiberized pump laser and avoid free space optics. The refractive index of the curing gel is 1.55 while that of the As_2Se_3 glass is ∼2.81. This refractive index contrast leads to a residual Fresnel reflection coefficient of R≈8%, acting as one mirror of the Fabry-Perot cavity. The output end of the microwire is terminated by a silver mirror with a reflection coefficient R>97.5% reflection over the wavelength range of 0.45-2µm. This completes the resonant cavity required for the laser operation. Considering the optimized reflections at both ends of the laser cavity, the total round trip cavity loss is ∼16.6±1.4dB that includes ∼10.8dB loss due to Fresnel reflection at the As_2Se_3-curing gel interface, and a ∼5.8±1.4dB propagation loss. The third port of the CIR picks up the Raman lasing signal that is then observed with an optical spectrum analyzer.

An effective laser peak is observed at a wavelength of ∼1603.8 nm when the total single

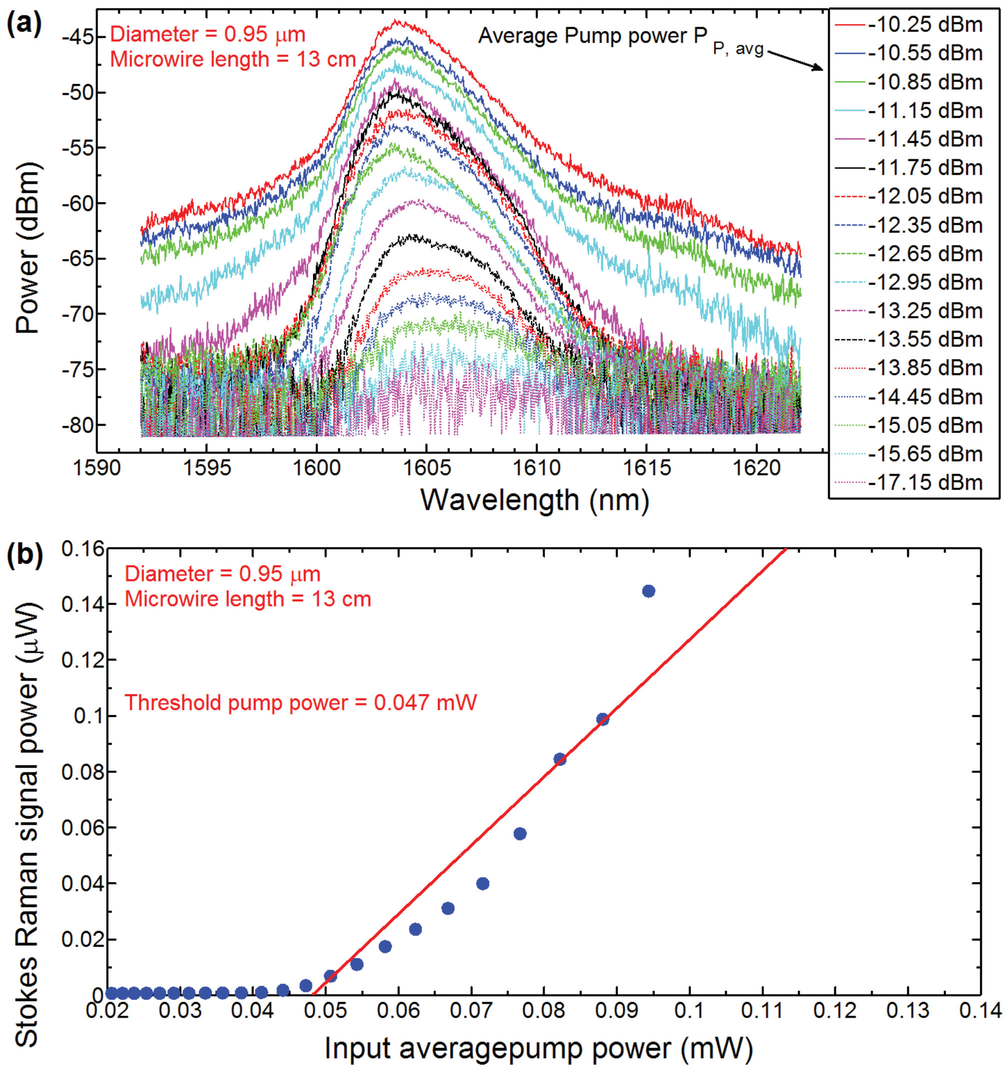

Figure 4.6 (a) Output spectra of the Raman laser for increasing values of input peak pump power. In (b), the Stokes Raman laser average power as a function of input average pump power.

pass gain exceeds the round trip cavity loss. This represents a Raman frequency conversion of ∼6.8THz (54.5nm) from the C-band pump laser to the L-band. Figure 4.6 (a) shows output spectra of the laser with increasing peak pump power. As the pump power is increased, the FWHM of the laser spectrum asymptotically reaches a value of ∼3.4nm. This is comparable to the minimum value obtained in the Raman laser of ref. [95] that was ∼3 nm. The relatively broad FWHM of the laser spectrum is attributed to the short pump duration

(64ns) with respect to the cavity round-trip time (2.4ns), enabling the superposition of spontaneous and stimulated signal with pump only over about 26 round-trips. A second explanation for the relatively broad Raman laser spectrum is the generation of free-carriers in the microwire, which may also reduce the laser extinction ratio as the input pump power is increased. Finally, four-wave mixing between the longitudinal modes of the laser cavity can also broaden the Raman laser spectrum at increasing pump power. Figure 4.6 (b) shows the Raman laser average power versus the input average pump power. This reveals the power conversion efficiency of the Raman laser at this wavelength to be ∼0.25%, with a threshold average pump power of 0.047mW (peak pump power = 0.47W). The kink in the slope of the power transfer curve can be explained from the possible coupling of mirror reflected power to the higher order modes that are supported in the microwire. The threshold pump power could be lowered and the efficiency increased by adjusting the microwire diameter to realize parametric gain as well, at the wavelength of operation. Since, the Raman gain is bidirectional [1], the 13cm long microwire in fact provides a 26cm long Raman gain medium. For the 13cm long and 0.95µm diameter microwire, and the observed lasing threshold peak pump power of 470mW, a Raman gain coefficient of g_R, AsSe≈3.1±0.2cm/GW corresponds to a single-pass Raman gain that exceeds the round trip cavity losses. It is noted from Figure 4.6 (b) that there is no sign of saturation occurring from two photon absorption or other detrimental effects at the power levels used.

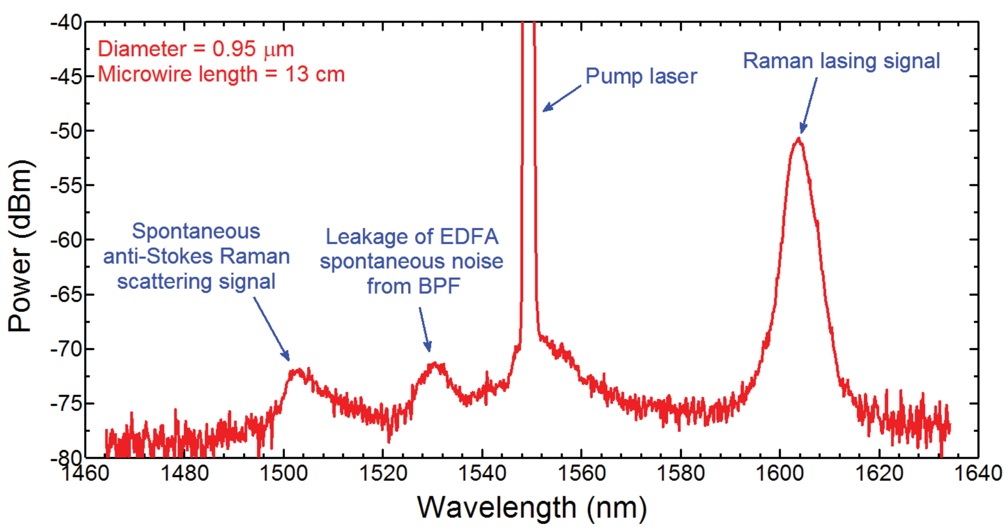

Figure 4.7 Laser output spectrum over a wide spectral range.

Figure 4.7 shows the laser output spectrum over a span of 1464-1634nm with an average input pump power of -12dBm. The spectrum shows Stokes Raman lasing signal as well as spontaneous anti-Stokes Raman scattered signal. The anti-Stokes signal carries ~20dB less power than the Stokes signal. This unbalanced Stokes/anti-Stokes spectrum also confirms that four-wave mixing plays no significant role in this laser operation otherwise the two would have comparable power levels. It may however be noted that the parametric gain is expected to be available at wavelengths offset from the Raman lasing wavelength. However, the bidirectional nature of the Raman amplification draws most of the pump power leading to the Raman lasing and preventing the optical parametric oscillations. The noisy spectral components observed in Figure 4.7 in the wavelength range 1525-1540nm are part of the input pump signal and are the result of spectral leakage from the BPF that follows the EDFA. These spectral components contain incoherent spontaneous emission from the EDFA and are much less powerful than the pump pulses to affect any nonlinear process including the Raman scattering.

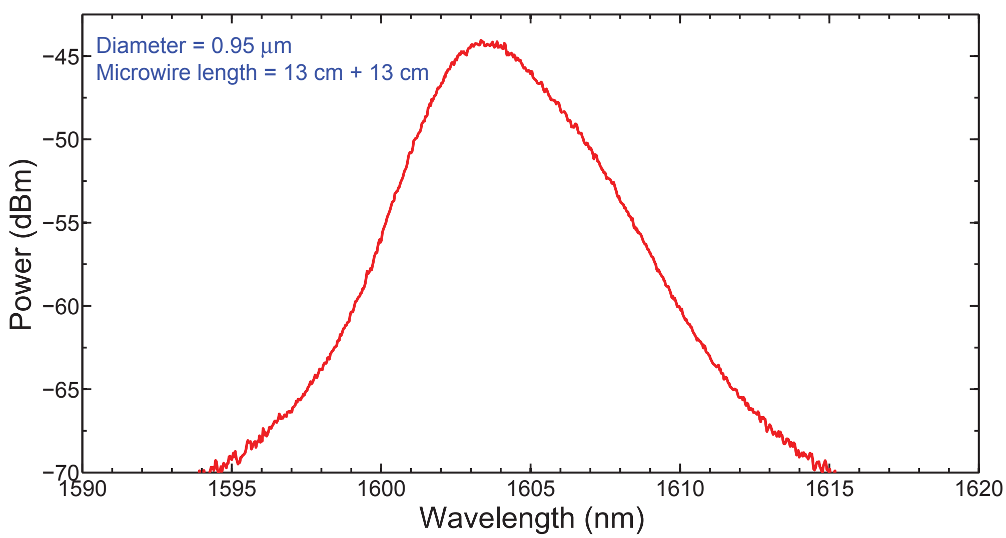

Figure 4.8 Output spectrum of the Raman laser with two cascaded gain sections surrounded by Fresnel reflectors.

Finally, Raman lasing is also observed using two cascaded microwires of 0.95µm in diameter and 13cm in length. This allows the Raman lasing without increasing the reflection coefficient at the far end of the microwires assembly. Instead, the Fresnel reflection (~23%) due to refractive index contrast between the As_2Se_3 and air constitutes the second mirror of the Fabry-Perot cavity whose first mirror is again provided by Fresnel reflection at the microwire/curing gel interface at the input end. Figure 4.8 shows the spectrum of such a Raman laser, where the average input pump power is -11dBm. The average power in the Raman laser output, at the given input pump power, in this case is ~3dB higher than that for the first cavity configuration. This laser configuration eliminates the requirement of a broadband mirror that is used in the first cavity configuration. The mirror in first cavity configuration does not however compromise the all-chalcogenide nature of the Raman laser. Optical waveguides made from glass, semiconductors and polymers are routinely coated with metals including silver, gold and aluminium as well as with dielectric materials for realizing high reflection [96].

4.2.3 Summary

In summary, we demonstrated the first all-chalcogenide and all-fiber Fabry-Perot Raman laser. The high Raman gain in the microwire geometry allows lasing in a short length (13 cm) microwire with a sub-Watt (470mW) peak pump power threshold. This amounts to a reduction in device footprint by more than a factor of 10× and the threshold pump power by up to 2.5× in comparison with the previous demonstration of Raman laser based on As_2Se_3 glass in a step-index fiber geometry. The laser is pumped with a C-band laser source and operates in the L-band. Such an all-chalcogenide fiber laser can potentially operate over the entire transmission window of As_2Se_3 glass given an appropriate pumping source. Further improvements in the threshold pump power and the laser efficiency can be achieved by utilizing highly reflecting Bragg gratings within the As_2Se_3 microwires that will enable the realization of efficient all-chalcogenide DBR and DFB Raman lasers and optical parametric oscillators.

Chapter 5

All-chalcogenide, and combined Raman-parametric laser, wavelength converter and amplifier in a single microwire

[1]In this chapter, we describe our work on developing a combined Raman-parametric laser, wavelength converter and amplifier/supercontinuum generator based on a chalcogenide microwire. A proper choice of microwire diameter for optimizing chromatic dispersion properties, and the fabrication of Bragg gratings in the microwire allows the realization of the multi-functional device.

5.1 Introduction

The future of fiber optic systems lies in the development of all-fiber photonic devices that are compact, power efficient, and can provide novel functionalities. The photonic microwires are attractive owing to their negligible coupling and propagation losses [97], orders of magnitude enhancement in waveguide nonlinear coefficient [98, 99], controllable amount of chromatic dispersion [100] and evanescent optical field propagation [101, 102]. These advantages have

[1]The content of this chapter has been submitted to the IEEE J. Sel. Top. Quantum Electron., and can be seen at the ArXiV website as, (1) R. Ahmad and M. Rochette, All chalcogenide Raman parametric laser, wavelength converter, and amplifier in a single microwire, arXiv:1307.8399, (2013).

driven researchers to use microwires for studying novel low field optical phenomena [103–108], as well as for wide-ranged application in the fields of nonlinear optics [82, 100], sensing [101, 102, 109] and plasmonics [105, 110–112], to name a few.

Optical sources, both coherent and incoherent, are among the basic components of any fiber optic system. The former are narrowband and are usually lasers or their wavelength converted counterparts (via nonlinear wave mixing process), while the latter are broadband, rely on spontaneous emission processes and act as the amplifiers or as broadband light sources. Recently, lasing has been reported in microwires made from rare-earth or dye-doped silica glass [113–116], but these devices required pumping via evanescent coupling to the microwire coiled in a resonator geometry. The evanescent coupling is unfortunately an obstacle to the practical use of such lasers in fiber systems, where the large coupling and/or transmission losses of such devices is a major obstacle towards low power consumption and high power efficiency. Moreover, the gain spectrum following from discrete atomic transitions in doped silica limits the wavelength tunability of these devices.

In contrast with this, the nonlinear optical effects manifest at arbitrary wavelengths. This offers a way to circumvent the issue of wavelength tunability. The As_2Se_3 chalcogenide glass fiber exhibits nonlinear Kerr and Raman gain coefficients that are up to 3 orders of magnitude larger than that of silica fibers [2]. The nonlinear gain, defined as the ratio of output power to the input power, is further enhanced in a microwire geometry, where the optical field intensity is enhanced by more than 2 orders of magnitude due to the correspondingly reduced waveguide modal area. Therefore, As_2Se_3 microwires are excellent candidates for the development of compact and efficient sources based on nonlinear optical effects. The As_2Se_3 glass also brings the advantage of a large photosensitivity [4], enabling the direct inscription of Bragg grating (BG) reflectors within the microwire structure to form the laser cavity [28]. Of great importance also brought by As_2Se_3 is an ultra-wide transmission window that allows the useful operation over the wavelength range of $\lambda \sim$1-10µm [3].

In previous chapters, we described the lasers based on the nonlinear gain in microwires [95, 117], showing the use of microwires within a resonant cavity to generate a laser effect. It appears that the round-trip cavity losses in using the microwires inserted into resonant cavities could be reduced by using a completely integrated solution instead than free-space components or silica glass fiber components. Furthermore, an all-chalcogenide integrated solution would broaden the spectrum of operation of the device, up to the mid-infrared, instead than being limited to the operation spectrum of silica glass.

In this chapter, we describe a distributed Bragg reflector (DBR) type As_2Se_3 microwire Raman parametric laser, wavelength converter, amplifier, and supercontinuum generator in a single chalcogenide microwire. The resonant cavity of the device is made out of two BGs directly written within the As_2Se_3 microwire, exploiting its high photosensitivity. This allows the integration of the nonlinear gain medium and the cavity mirrors in a single microwire, thus minimizing the cavity losses and power threshold of the laser, as well as to improve the slope efficiency. The combination of nonlinear gain and BGs in a single microwire also makes the device compatible with the entire transmission window of As_2Se_3 glass (1-10µm). The sole effect of the microwire as a travelling wave amplifier and supercontinuum generator is also investigated. In addition to providing the functionalities of a laser and wavelength converter, the resulting device thus acts as an ultra broadband multi order, Stokes/anti-Stokes Raman amplifier and/or a supercontinuum source.

5.2 Device fabrication

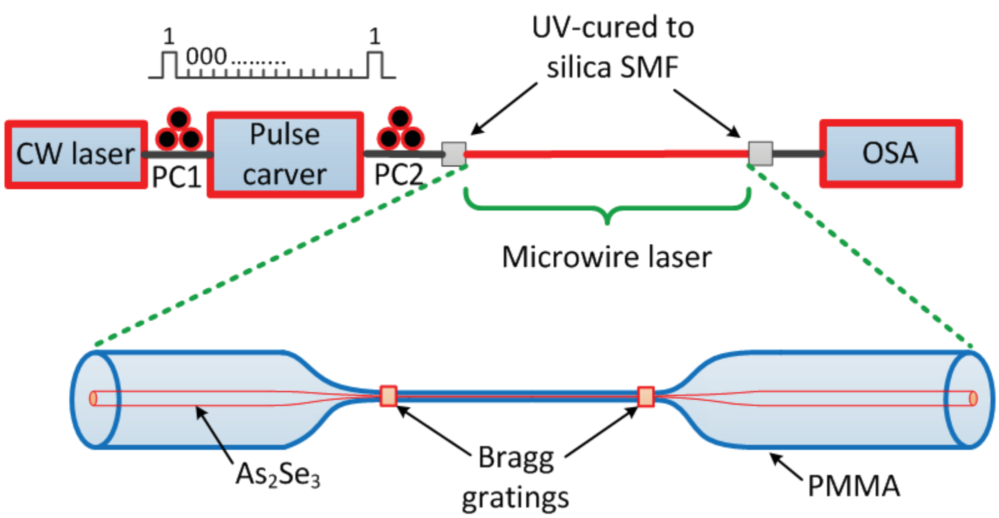

Figure 5.1 Experimental setup and device schematic. The top part shows the experimental setup for the operation of chalcogenide microwire Raman parametric laser, wavelength converter and travelling wave amplifier. A schematic of the micro laser device is also drawn at the bottom. CW laser: continuous wave (CW) tunable laser; PC: fiber polarization controller; SMF: single mode fiber; OSA: optical spectrum analyzer.

Figure 5.1 shows the schematic of the chalcogenide microwire device as well as the setup for the lasing, wavelength conversion and amplification experiments. The fabrication of chalcogenide microwire device is carried out in four steps. In first step, an As_2Se_3-PMMA hybrid fiber preform is fabricated in a home built fiber drawing tower where a heat funnel is mounted at the top and the fiber preform is collected at the bottom. An As_2Se_3 chalcogenide fiber with a diameter of 170µm is inserted into a PMMA tube with an inner diameter of 3.175mm, and the two are introduced into the heat funnel heated to a temperature of 220°C. The resulting hybrid As_2Se_3-PMMA structure is captured at the bottom and is pulled vertically to obtain the hybrid fiber preform. In a second step, the hybrid fiber preform is heated and stretched in the same drawing assembly with a different heating element, to obtain hybrid fibers with the As_2Se_3 core diameter of ~16µm. The PMMA coating diameter of the hybrid fiber is ~18 times greater than that of the As_2Se_3 core and adds physical strength to the final microwire device, in addition to advantageously modifying the dispersion properties for the parametric nonlinear processes [82]. The As_2Se_3 core diameter of 16µm provides optimal mode matching to single mode silica fibers, thus resulting in a predominantly fundamental mode excitation and a low coupling loss [118]. In a third step, a 5.5cm long piece of the hybrid fiber is mechanically polished at the two ends and is stretched in to a microwire of 13cm long uniform core section using the flame brush technique [118]. In the final step, broadband light is coupled through the prepared microwire via the single mode silica fibers (SMF) and the output is observed on a CCD camera and an OSA to optimize coupling towards the fundamental mode of the microwire [61]. The microwire and the silica fibers at both ends are permanently bonded through UV-curing, thus resulting in a fiber coupled microwire device. The microwire device exhibits a total (SMF-microwire-SMF) loss of 5.9dB. The microwire device is then inscribed with the Bragg gratings using a He-Ne laser (λ =633nm) interferometer assisted by a glass prism [28]. The glass prism adjusts the angle in an increased refractive index environment (BK-7 glass) to allow writing the Bragg gratings in As_2Se_3 glass (refractive index ~2.8), which can otherwise not be realized in free space settings with the λ =633nm light. The physical length of the Bragg gratings is ~2mm and is adjustable by controlling the size of the interfering beams with the help of a spherical lens. The diameters of the microwires are carefully selected to control the amount of chromatic dispersion [82], which allows the simultaneous operation of the device as a Raman parametric laser and a FWM wavelength converter. For this purpose, the diameter of microwires used in the current experiment is typically around 1.0µm.

5.3 Experimental setup

The experimental setup consists of the pump pulse formation stage, the microwire device and the OSA for output spectrum characterization. A CW-laser, tunable over the C-band, is passed through a pulse carving stage with an extinction ratio of $\geq$36dB. The pulse carving stage consists of two cascaded 10Gb/s Mach-Zehnder modulators (JDSU OC-192), fed with identical electrical data inputs from a pulse pattern generator (PPG). The power level of the prepared pulses is adjusted to the required levels by using a series of two EDFAs, from PriTel and two bandpass filters with <0.4nm pass-band, followed by an optical attenuator. Depending on the operation of the microwire device as laser or amplifier, the duration and the repetition rate of the pump pulses is adjusted by modifying the bit pattern from the PPG. Finally, the output spectrum from the microwire device is observed and recorded on an OSA (Agilent 86142B).

5.4 Experimental results

5.4.1 Broadband amplification or spontaneous emission

In a first series of experiments, the microwires are being used as travelling wave amplifiers or a broadband source without BGs, and the impact of the microwire diameter is studied. Each microwire is 13cm in length, and is pumped by pulses that are 100ps in duration, have a repetition rate of 1.22MHz and are spectrally centered at a wavelength of λ =1530nm. Figure 5.2 (a) shows the resulting single pass output spectra through a 1.0µm diameter microwire as a function of increasing pump power levels. The zero dispersion wavelength λ_{ZDW} for the 1.0µm diameter microwire lies at λ =1529nm, as shown in the numerically calculated dispersion profile included as the figure inset. This translates to the pump laser lying very close to the zero dispersion wavelength and experiencing anomalous dispersion (β_2 <0), thus setting up the optimal conditions for parametric interactions [1]. As a result, up to five parametrically converted output orders are observed at the anti-Stokes wavelengths, while two such converted orders are observed at the Stokes wavelengths. The next Stokes output signals, if present, are expected to lie beyond the operating wavelength range of the OSA.

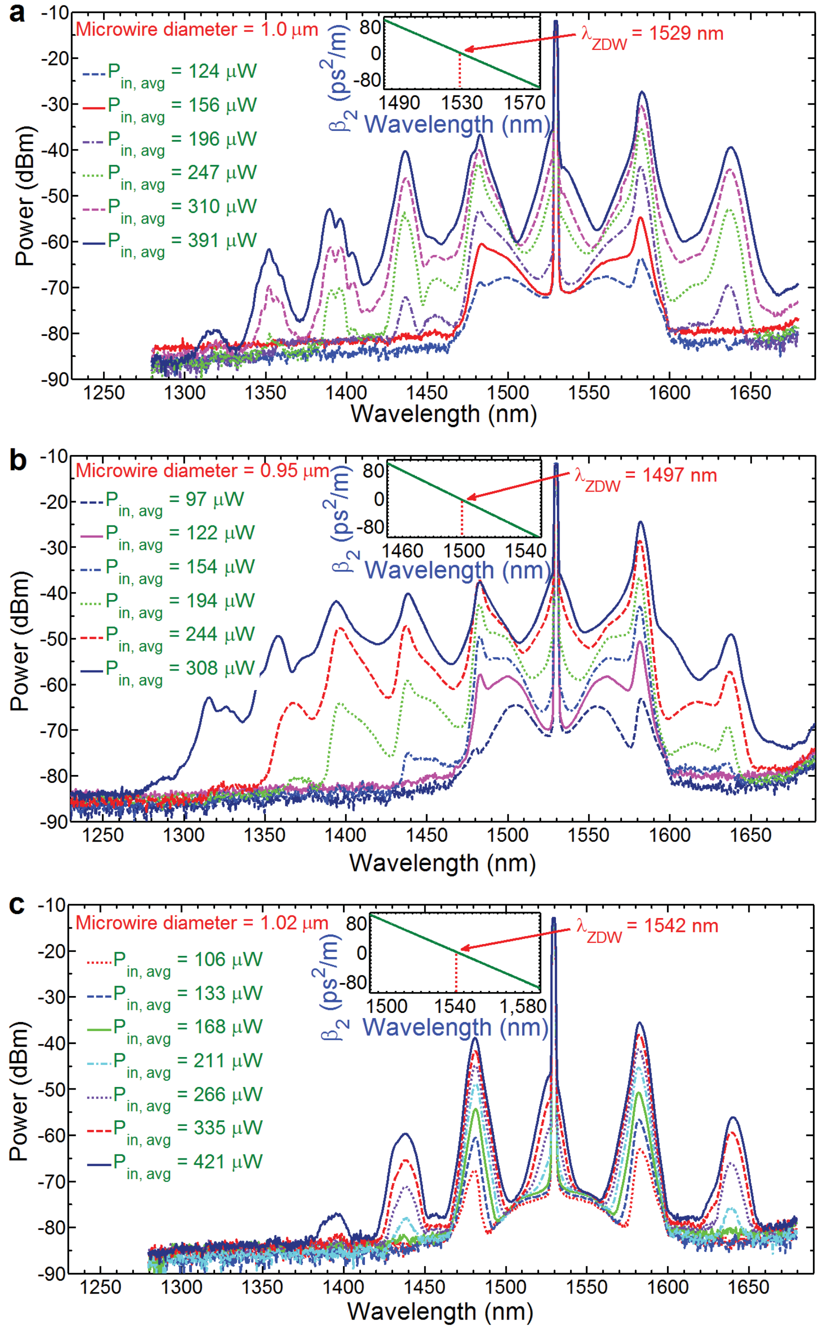

Figure 5.2 Performance as a travelling wave amplifier or a broadband source. Single-pass output spectra as a function of input pump power injected into the wires with diameters of (a) 1.0μm (b) 0.95μm and (c) 1.02μm. Numerically calculated second order dispersion profiles of the corresponding microwires are included as inset in each illustration.

The performance of microwires is also tested when pumped away from λ_{ZDW}, both in anomalous and normal dispersion regions. A microwire of smaller diameter, with 0.95µm, is first used and the spectra obtained at different pump power levels are shown in Figure 5.2 (b). In this case, the λ_{ZDW} is blue shifted and the pump still lies in the anomalous dispersion wavelength region. Almost the same number of total output wavelengths are generated as with the 1.0µm microwire. It is, however, noted that the spectral energy now appears to be shifted towards shorter wavelengths, and the spectrum is relatively flat with respect to the case for 1.0µm diameter microwire. The spectral flatness is due to the observed blue shift of the spectral energy, which leads from the corresponding blue shift of the λ_{ZDW}. The Raman-FWM supercontinuum like spectrum for both 1.0µm and 0.95µm diameter microwires, spans almost the same wavelength (frequency) range of >330nm (47THz). The apparently comparable bandwidth can be explained from the blue shift of energy in the case of 0.95µm microwire. To repeat the experiment on a microwire with >1.0µm diameter, a microwire with 1.02µm is prepared. The spectra for this microwire as a function of the pump power level are provided in Figure 5.2 (c). As expected, fewer, that is up to 3 anti-Stokes outputs are generated in this case, due to the input pump wavelength lying in the normal dispersion (β_2 >0) region.

5.4.2 Raman-parametric lasing and wavelength conversion

To realize a laser, two BGs spatially apart by 11cm are inscribed into a microwire with a diameter of 1.0µm and a length of 13cm. The reflection maxima of the two BGs are centered at λ ~1585nm (L-band) with reflection coefficients of ~90% and 60% at the input and output ends of the microwire, respectively. The pump laser is centered at λ ~1532nm, and the pulse duration and repetition rate are adjusted to 64ns and ~3.8kHz, respectively. The spatial length of the pulses propagating in the microwire is >7.5 meters, which allows the storage and/or amplification of the generated Raman/FWM gain in the microwire resonator for several round-trips (>34, in total) and leads to a quasi-continuous wave operation of the laser. As the device is pumped, Raman lasing is observed at a wavelength of λ ~1585nm that is on the Stokes wavelength side of pump wavelength as shown in Figure 5.3 (a). The precise wavelength of operation of the Raman laser is defined by the central wavelength of the BGs. The FWM led wavelength conversion is also visible at the anti-Stokes wavelength λ ~1482nm. This spectrum represents the simultaneous conversion of a C-band pump laser

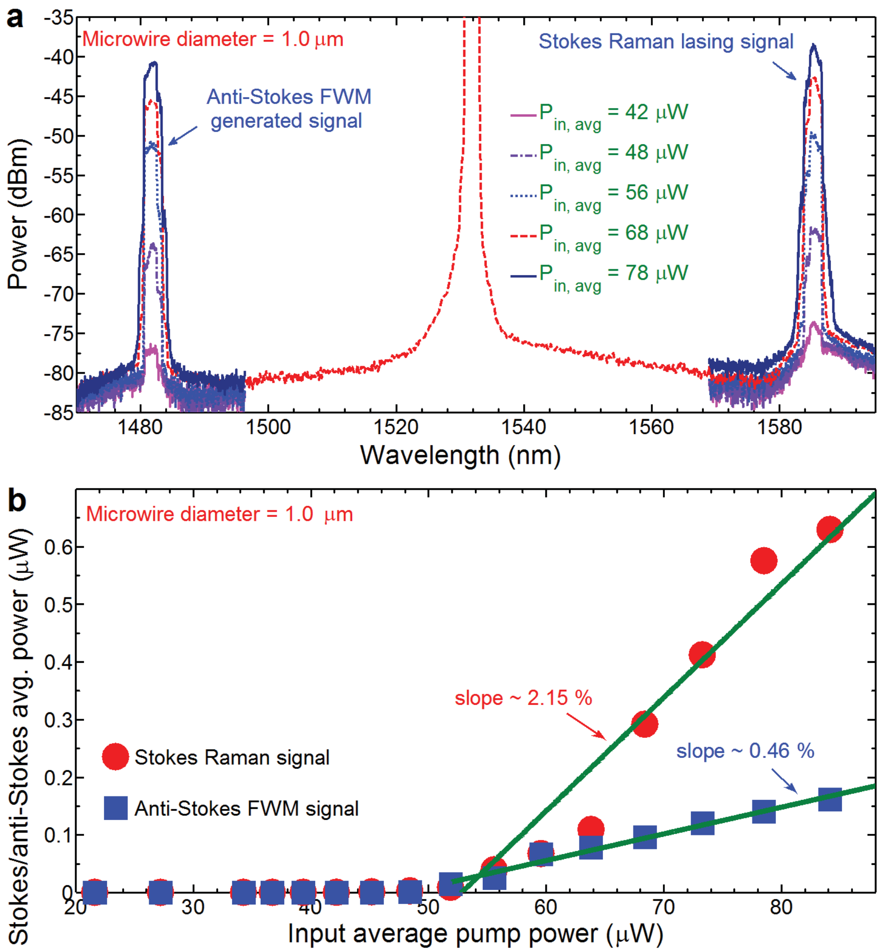

Figure 5.3 Performance as a Raman parametric laser and wavelength converter. (a) Output spectra showing the simultaneous operation of microwire Raman laser and FWM wavelength converter at different input pump power levels (b) Stokes and anti-Stokes slope efficiency curves.

to L-and S-bands frequency spectra. Figure 5.3 (b) plots the evolution of Stokes Raman and anti-Stokes FWM generated signals with increasing input pump power, revealing the respective slope efficiencies of 2.15% and 0.46%, and a threshold average (peak) pump power of ∼52μW (< 207mW). This represents the lowest threshold Raman laser to date in a fiber geometry [117,119], and is also the first demonstration of a fully fiberized microwire laser of any kind. It is emphasized that the laser slope efficiency of >2% is a remarkably high value for such a compact, centimeters long microwire laser, operating at such low power levels. Finally, we test the wavelength tunability of the lasing device. Figure 5.4 (a) summarizes

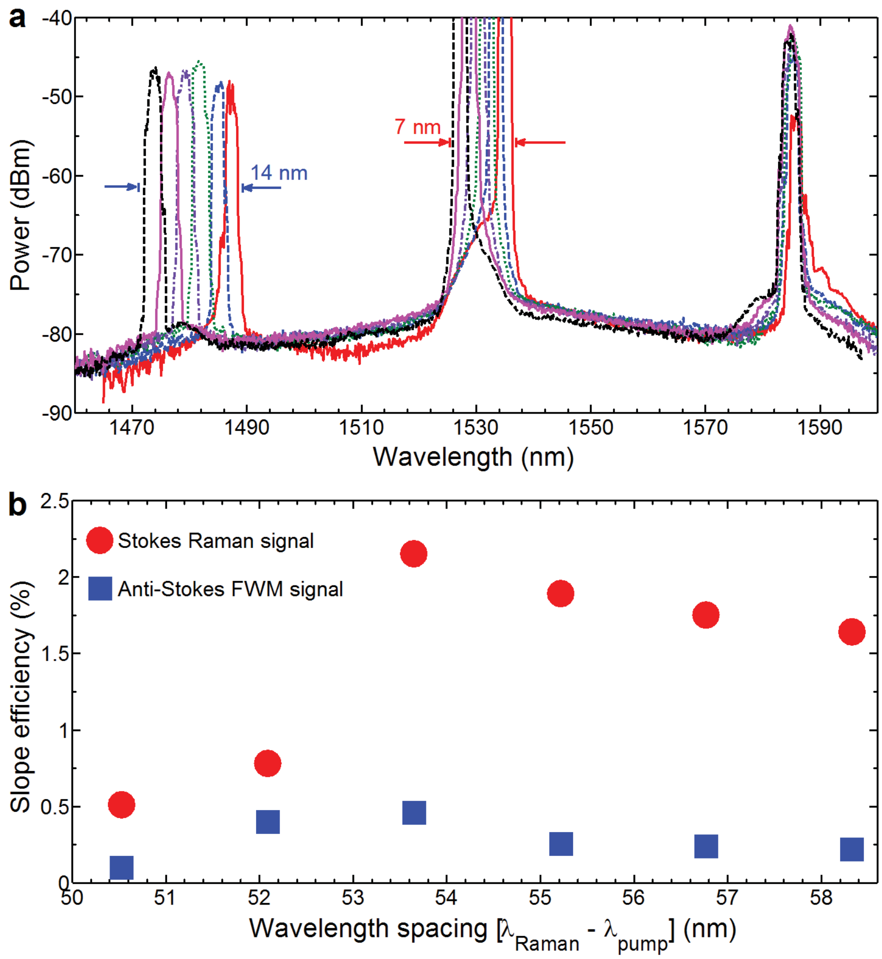

Figure 5.4 Wavelength tunability of the operating device. (a) Spectra of a microwire Raman laser-FWM wavelength converter at different pump wavelengths (b) Slope efficiencies of (Stokes) Raman signal and (anti Stokes) FWM signals for varying wavelength separation between the input pump and the resulting Raman laser.

the results of the wavelength tuning experiment. By tuning the pump wavelength over a range of 8nm (λ =1527-1535nm), the anti-Stokes output is tuned by 14nm (λ =1473-1487nm), while the Stokes Raman wavelength remains fixed, bounded by the fixed resonant wavelengths of the BGs. The laser ceases to operate when the pump laser is tuned beyond the stated wavelength range of ~8nm, which is comparable to the Raman gain bandwidth [2]. The laser can be expected to operate so long as the Raman gain overlaps the reflection spectrum of the BGs. The asymmetric wavelength tuning between the pump laser and the anti-Stokes idler output leads from the phase-matching conditions, naturally satisfied during the FWM process. The slope efficiencies of the Stokes and anti-Stokes outputs are plotted in Figure 5.4 (b), as a function of the wavelength separation between the pump laser and the Stokes Raman laser. The slope efficiencies are maximized for a wavelength separation of ~53.5nm, and decrease in value as the pump laser is detuned to either Stokes or anti-Stokes wavelengths.

5.5 Discussion

The interplay between Raman and parametric processes in nonlinear media has been studied in the past in the context of amplification and wavelength conversion, and is reported to significantly improve the net available gain value and bandwidth in a nonlinear amplifier and wavelength converter [120–123]. The Raman-parametric lasing however has never been reported heretofore. The device presented in this paper utilizes both Raman and parametric gains to operate simultaneously as a laser and an anti-Stokes wavelength converter. It is emphasized that the presented device is different from the reported Raman assisted parametric amplifiers, where the Raman scattering assists in phase matching in an otherwise non phase matched dispersive media [121–123]. Both Raman and parametric gains at the target wavelength are present in the microwire from the beginning, and merely reinforce each other into simultaneous lasing and wavelength conversion.

In order to compare the results with theory, the required threshold pump power is estimated from the roundtrip cavity loss and the other parameters of the microwire laser, including the effective mode area and length of the microwire as well as the gain coefficients of the nonlinear Raman/parametric processes. The roundtrip cavity loss is estimated at ~4.7dB and includes 2.7dB gratings reflectivity loss and a 2dB roundtrip propagation loss. The Stokes Raman signal experiences a bidirectional gain because the spatial length of the pump pulse is much longer than the laser cavity length. The roundtrip gain therefore consists of two components: in forward propagation, the signal co-propagates with the pump and thus Raman parametric gain acts on it, while in counter-propagation the parametric gain is absent and the gain originates solely from the Raman effect. The total roundtrip gain experienced by the signal at Stokes Raman wavelength, trapped within the laser cavity, is written as,

$$G = e^{(g_{Raman-FWM} L_{eff} P_{pump} + g_{Raman} L_{eff} \frac{P_{pump}}{A_{eff}})} \tag{5.1}$$

where P_{pump} is the input peak pump power, L_{eff} is the effective length of the microwire laser that is ~9.7cm corresponding to the propagation loss coefficient α ~10dB/m, and A_{eff} is the effective transverse area of the fundamental mode, and is estimated to be 0.51µm^2 in the 1.0µm diameter microwire. The Raman gain coefficient value for As_2Se_3 glass, as estimated in ref. [124], is g_{Raman} =2.3 × 10^{-11}m/W. The combined Raman-parametric gain coefficient $g_{Raman-FWM}$ is defined as $g_{Raman-FWM} = 2\gamma\Re[\sqrt{K(2q-K)}]$ [123]. Here, the term γ represents the effective waveguide nonlinear coefficient estimated at ~99W^{-1}-m^{-1}. The term $q = 1 - f + f\chi^{(3)}(\Omega)$, where f =0.1 is the fractional contribution of Raman susceptibility to the instantaneous Kerr effect in As_2Se_3 glass [125], Ω is the angular frequency difference between the pump and the Stokes/anti-Stokes signals, and $\chi^{(3)}(\Omega)$ is the Fourier transform of the complex Raman susceptibility function, with its value for Stokes Raman shift of ~6.8THz [$\Omega = 2\Pi \times 6.8 \times 10^{12}$rad/sec], calculated at -4.28i for As_2Se_3 glass. Finally, the term $K = -\Delta k/2\gamma P_{pump} = -\beta_2\Omega^2/2\gamma P_{pump}$ is the linear phase mismatch normalized to the nonlinear contribution to the mismatch, which is from the FWM in present case. The chromatic dispersion parameter β_2 at the pump wavelength λ ~1532nm, is numerically estimated to be -5.6ps^2/km. By using all the available values, the total roundtrip gain G is evaluated from Eq.5.1, as a function of peak pump power P_{pump}. The total roundtrip cavity loss of 4.7dB estimated from the microwire laser parameters can be compensated with a P_{pump} ~76mW. This value is smaller by a factor of more than 2, with respect to the pump peak power value estimated during the experiment. It is hypothesized that this mismatch leads from (1) the possible coupling of power to higher order modes in the microwire, and (2) an uncertainty in the value of pump peak power that is being estimated from the average pump power. The uncertainty in peak power value is due to the asymmetry in temporal profile of the 64 ns duration pulse that is caused by the gain saturation effects in erbium doped fiber amplifiers (EDFAs). Nevertheless, this indicates that in practice, the microwire laser presented here is most likely operating with a sub-100mW threshold pump peak power, and the experimentally estimated threshold value of 207mW, is an over estimate.

5.6 Summary

In summary, the large Raman and parametric gain as well as the photosensitivity available in As_2Se_3 chalcogenide glass is utilized to realize a compact, low threshold, and high efficiency, microwire Raman laser and four-wave mixing wavelength converter in simultaneous operation. A record low threshold average (peak) pump power of 52µW (207mW) and a slope efficiency of >2% is achieved for a ∼11cm long Raman-parametric laser. The generation of combined Raman parametric ultra broadband spectrum is also observed, covering the wavelength (frequency) range of >330nm (47THz). The device is fiber compatible and is ready for immediate use in existing fiber systems. Moreover, the laser, being all-chalcogenide and based on nonlinear optical gain, can also be readily used in the mid-infrared wavelength spectrum to cater for the current high demand of such light sources.

Chapter 6

Conclusion and Future Work

This thesis summarizes the work performed by the author over the past 5 years, towards the realization of photonic devices using highly nonlinear chalcogenide microwires. The ultra high waveguide nonlinear coefficient of chalcogenide microwires (>5 orders of magnitude compared to single-mode silica fibers) is utilized to develop several photonic devices including band-pass filters, lasers, amplifiers, broadband optical (supercontinuum) sources, that are compact, power efficient and compatible with existing fiber-optic systems and networks. In the thesis, first, the fabrication of Bragg gratings in sub-wavelength diameter As_2Se_3 chalcogenide is presented. The first technique uses the interference of visible light (λ =633nm), while the second technique uses the interference of telecommunications-band light (λ =1550nm). The second technique is developed after the photosensitivity of the As_2Se_3 glass in the telecommunications-wavelength range is discovered for the first time in this work. Second, the nonlinear parametric process of four wave mixing is used for realizing an all-optical wavelength converter and a parametric amplifier. The device is 10 cm in length and 0.6-1.0µm in diameter, operates at a (peak) power level as low as 70mW, covers a bandwidth of >190nm and has conversion efficiency that reaches up to 21dB. This parametric gain is then utilized to realize a doubly-resonant optical parametric oscillator that is pumped by a telecommunication C-band pump, and operates simultaneously in the S-and L-bands. Third, the ultra high nonlinear Raman gain coefficient of the As_2Se_3 microwires is used to realize Raman lasers. Two cavity configurations are designed to operate the Raman lasers; one is a fiber loop cavity, while the other is a Fabry Perot cavity. The devices are ~13cm in length, 0.55-0.95µm in diameter, and operate at a threshold average pump power of ~50µW.

Finally, we combine the Bragg grating filters with the parametric and Raman gain to realize a parametric Raman laser (for Stokes Raman wavelength), parametric four-wave mixing based wavelength converter, and a supercontinuum source, all in a single microwire. This device is ~11 cm in length, 1.0µm in diameter, operates as laser and wavelength converter at a threshold average pump power of ~52µW, and covers a wavelength range of >330nm when operated as a supercontinuum generator.

There are still a few remaining challenges, in line with this thesis, that can be further investigated:

– First, a distributed feedback (DFB) type Raman laser and/or parametric oscillator can be realized. Initial calculations show that a 1-2cm long Bragg grating in an As_2Se_3 microwire can act as a DFB parametric-Raman laser. A DFB laser will further reduce the footprint of the laser device by up to an order of magnitude (>10cm to 1cm). Currently, the Bragg gratings fabrication setup is optimized for realizing the gratings that are ~0.5cm long. The work in in progress towards increasing the allowed length of the resulting Bragg gratings. Furthermore, by inscribing multiple Bragg gratings of different resonant wavelengths in a microwire, several lasing devices can be integrated in a single microwire device that is a few centimeters in length. This can lead to compact and power efficient multi-wavelength microwire lasers. Indeed, work towards realizing such a laser is already under way in our group.

– Second, this thesis presents the photonic devices operating in the telecommunications (near-infrared) wavelength range. Recently, there has been a great interest for developing photonic devices for operation in the mid-infrared wavelengths region. The As_2Se_3 glass can transmit light in the wavelength range of 1-10µm, thus covering most of the mid-infrared wavelengths region. A natural next step could be to realize the Bragg gratings, and lasing devices presented in this thesis that can operate over the mid-infrared wavelength region. This can be done by adjusting the angle between the interfering beams in the Bragg gratings fabrication setup. This will result in Bragg gratings that are resonant in the mid infrared region, which can be used to develop the lasing devices operating at the desired mid infrared wavelengths. This work is also under way in our group.

– Third, microwire Bragg gratings based switches can also be realized. For this purpose, a $\lambda/4$ phase-shifted Bragg grating will be ideal. Initial calculations reveal that such an As_2Se_3 microwire Bragg grating switch can operate at sub-Watt peak power levels.

- Four, it was proposed in a series of papers in mid-nineties by Steel and de-Sterke that a Bragg grating can lead to phase matching and thus to the parametric amplification [126–128]. This has, however, never been demonstrated owing mainly to the large amount of power required for silica fiber Bragg gratings. As_2Se_3 microwires have the nonlinear coefficient that is more than 5 orders of magnitude larger than that of silica fibers, and thus the As_2Se_3 microwire Bragg gratings can be used to observe this novel phenomenon. The initial calculations show that <5 Watts of power is sufficient for operating an As_2Se_3 microwire Bragg grating optical parametric amplifier.
- Finally, the ultra-high nonlinear coefficient of As_2Se_3 microwires can be utilized for the generation of correlated photon pairs, as proposed in our paper on the observation of high efficiency and ultrabroadband four-wave mixing in these microwires [82]. Indeed, correlated photon pairs generation have been produced in As_2S_3 chalcogenide waveguides [129], where the nonlinear coefficient was at least an order of magnitude lower than in the presented As_2Se_3 chalcogenide microwires. Indeed, a collaboration has been initiated with the Quantum Photonics group led by Prof. Thomas Jennewein at the Institute for Quantum Computing at University of Waterloo, for the development of correlated photons sources in these microwires.

Bibliography

[1] G. P. Agrawal, *Nonlinear fiber optics.* Springer, 2000.

[2] R. E. Slusher, G. Lenz, J. Hodelin, J. Sanghera, L. B. Shaw, and I. D. Aggarwal, "Large raman gain and nonlinear phase shifts in high-purity as_2se_3 chalcogenide fibers," *Journal of Optical Society of America B*, vol. 21, no. 6, pp. 1146–1155, 2004.

[3] I. D. Aggarwal and J. S. Sanghera, "Development and applications of chalcogenide glass optical fibers at nrl," *J. Optoelectron. Adv. Mater*, vol. 4, no. 3, pp. 665–678, 2002.

[4] B. J. Eggleton, B. Luther-Davies, and K. Richardson, "Chalcogenide photonics," *Nature Photonics*, vol. 5, no. 3, pp. 141–148, 2011.

[5] W. Liang, Y. Huang, Y. Xu, R. K. Lee, and A. Yariv, "Highly sensitive fiber bragg grating refractive index sensors," *Applied Physics Letters*, vol. 86, no. 15, pp. 151122–151122, 2005.

[6] A. D. Kersey, M. A. Davis, H. J. Patrick, M. LeBlanc, K. Koo, C. Askins, M. Putnam, and E. J. Friebele, "Fiber grating sensors," *Journal of Lightwave Technology*, vol. 15, no. 8, pp. 1442–1463, 1997.

[7] B. J. Eggleton, R. Slusher, C. M. de Sterke, P. A. Krug, and J. Sipe, "Bragg grating solitons," *Physical Review Letters*, vol. 76, no. 10, p. 1627, 1996.

[8] H. G. Winful and V. Perlin, "Raman gap solitons," *Physical Review Letters*, vol. 84, no. 16, p. 3586, 2000.

[9] S. Larochelle, Y. Hibino, V. Mizrahi, and G. Stegeman, "All-optical switching of grating transmission using cross-phase modulation in optical fibres," *Electronics Letters*, vol. 26, no. 18, pp. 1459–1460, 1990.

[10] I. V. Kabakova, D. Grobnic, S. Mihailov, E. C. Mägi, C. M. de Sterke, and B. J. Eggleton, "Bragg grating-based optical switching in a bismuth-oxide fiber with strong $\chi^{(3)}$-nonlinearity," *Optics Express*, vol. 19, no. 7, pp. 5868–5873, 2011.

[11] N. Broderick, D. Taverner, D. Richardson, M. Ibsen, and R. Laming, “Optical pulse compression in fiber bragg gratings,” *Physical Review Letters*, vol. 79, no. 23, p. 4566, 1997.

[12] P. Westbrook, J. Nicholson, K. Feder, Y. Li, and T. Brown, “Supercontinuum generation in a fiber grating,” *Applied Physics Letters*, vol. 85, no. 20, pp. 4600–4602, 2004.

[13] J. T. Mok, C. M. De Sterke, I. C. Littler, and B. J. Eggleton, “Dispersionless slow light using gap solitons,” *Nature Physics*, vol. 2, no. 11, pp. 775–780, 2006.

[14] X. Fang, C. Liao, and D. Wang, “Femtosecond laser fabricated fiber bragg grating in microfiber for refractive index sensing,” *Optics Letters*, vol. 35, no. 7, pp. 1007–1009, 2010.

[15] V. Hodzic, J. Orloff, and C. C. Davis, “Periodic structures on biconically tapered optical fibers using ion beam milling and boron implantation,” *Journal of Lightwave Technology*, vol. 22, no. 6, p. 1610, 2004.

[16] W. Ding, S. Andrews, T. Birks, and S. Maier, “Modal coupling in fiber tapers decorated with metallic surface gratings,” *Optics Letters*, vol. 31, no. 17, pp. 2556–2558, 2006.

[17] W. Ding, S. Andrews, and S. Maier, “Surface corrugation bragg gratings on optical fiber tapers created via plasma etch postprocessing,” *Optics Letters*, vol. 32, no. 17, pp. 2499–2501, 2007.

[18] Y. Zhang, B. Lin, S. C. Tjin, H. Zhang, G. Wang, P. Shum, and X. Zhang, “Refractive index sensing based on higher-order mode reflection of a microfiber bragg grating,” *Optics Express*, vol. 18, no. 25, pp. 26345–26350, 2010.

[19] C. Baker and M. Rochette, “Highly nonlinear hybrid asse-pmma microtapers,” *Optics Express*, vol. 18, no. 12, pp. 12391–12398, 2010.

[20] T. Kaino, K. Jinguji, and S. Nara, “Low loss poly (methylmethacrylate-d8) core optical fibers,” *Applied Physics Letters*, vol. 42, no. 7, pp. 567–569, 1983.

[21] J. De Neufville, S. Moss, and S. Ovshinsky, “Photostructural transformations in amorphous as_2se_3 and as_2s_3 films,” *Journal of Non-Crystalline Solids*, vol. 13, no. 2, pp. 191–223, 1974.

[22] J. Ramirez-Malo, E. Marquez, C. Corrales, P. Villares, and R. Jimenez-Garay, “Optical characterization of as_2s_3 and as_2se_3 semiconducting glass films of non-uniform thickness from transmission measurements,” *Materials science & engineering. B, Solid-state materials for advanced technology*, vol. 25, no. 1, pp. 53–59, 1994.

[23] A. Van Popta, R. DeCorby, C. Haugen, T. Robinson, J. McMullin, D. Tonchev, and S. Kasap, "Photoinduced refractive index change in as_2se_3 by 633nm illumination," *Optics Express*, vol. 10, no. 15, pp. 639–644, 2002.

[24] G. Brawley, V. Ta'eed, J. Bolger, J. Sanghera, I. Aggarwal, and B. Eggleton, "Strong photoinduced bragg gratings in arsenic selenide optical fibre using transverse holographic method," *Electronics Letters*, vol. 44, no. 14, pp. 846–847, 2008.

[25] N. Hô, J. M. Laniel, R. Vallée, and A. Villeneuve, "Photosensitivity of as_2s_3 chalcogenide thin films at 1.5 μm," *Optics Letters*, vol. 28, no. 12, pp. 965–967, 2003.

[26] J. Hu, M. Torregiani, F. Morichetti, N. Carlie, A. Agarwal, K. Richardson, L. C. Kimerling, and A. Melloni, "Resonant cavity-enhanced photosensitivity in as_2s_3 chalcogenide glass at 1550 nm telecommunication wavelength," *Optics Letters*, vol. 35, no. 6, pp. 874–876, 2010.

[27] K. Hill, Y. Fujii, D. Johnson, and B. Kawasaki, "Photosensitivity in optical fiber waveguides: Application to reflection filter fabrication," *Applied Physics Letters*, vol. 32, p. 647, 1978.

[28] R. Ahmad, M. Rochette, and C. Baker, "Fabrication of bragg gratings in subwavelength diameter as_2se_3 chalcogenide wires," *Optics Letters*, vol. 36, no. 15, pp. 2886–2888, 2011.

[29] A. Zakery and S. Elliott, *Optical nonlinearities in chalcogenide glasses and their applications*, vol. 135. Springer, 2007.

[30] D. Zhao, *Atomistic Mechanisms and Kinetics of Photoinduced Changes in Chalcogenide Glasses*. Lehigh University, 2011.

[31] Y. Ohmachi and N. Uchida, "Vitreous as_2se_3; investigation of acousto-optical properties and application to infrared modulator," *Journal of Applied Physics*, vol. 43, no. 4, pp. 1709–1712, 1972.

[32] N. Soga, M. Kunugi, and R. Ota, "Elastic properties of se and as_2se_3 glasses under pressure and temperature," *Journal of Physics and Chemistry of Solids*, vol. 34, no. 12, pp. 2143–2148, 1973.

[33] See, for example,
$http://www.smartfibres.com/docs/SmartFBG.pdf$.

[34] J. Leuthold, C. Koos, and W. Freude, "Nonlinear silicon photonics," *Nature Photonics*, vol. 4, no. 8, pp. 535–544, 2010.

[35] D. Cotter, R. Manning, K. Blow, A. Ellis, A. Kelly, D. Nesset, I. Phillips, A. Poustie, and D. Rogers, "Nonlinear optics for high-speed digital information processing," *Science*, vol. 286, no. 5444, pp. 1523–1528, 1999.

[36] K. Inoue and H. Toba, "Wavelength conversion experiment using fiber four-wave mixing," *IEEE Photonics Technology Letters*, vol. 4, no. 1, pp. 69–72, 1992.

[37] E. Ciaramella and S. Trillo, "All-optical signal reshaping via four-wave mixing in optical fibers," *IEEE Photonics Technology Letters*, vol. 12, no. 7, pp. 849–851, 2000.

[38] R. Salem, M. A. Foster, A. C. Turner, D. F. Geraghty, M. Lipson, and A. L. Gaeta, "Signal regeneration using low-power four-wave mixing on silicon chip," *Nature photonics*, vol. 2, no. 1, pp. 35–38, 2007.

[39] J. E. Sharping, Y. Okawachi, J. van Howe, C. Xu, Y. Wang, A. E. Willner, and A. L. Gaeta, "All-optical, wavelength and bandwidth preserving, pulse delay based on parametric wavelength conversion and dispersion," *Optics Express*, vol. 13, no. 20, pp. 7872–7877, 2005.

[40] P. O. Hedekvist, M. Karlsson, and P. A. Andrekson, "Fiber four-wave mixing demultiplexing with inherent parametric amplification," *Journal of Lightwave Technology*, vol. 15, no. 11, pp. 2051–2058, 1997.

[41] M. Fridman, A. Farsi, Y. Okawachi, and A. L. Gaeta, "Demonstration of temporal cloaking," *Nature*, vol. 481, no. 7379, pp. 62–65, 2012.

[42] S. Palomba, S. Zhang, Y. Park, G. Bartal, X. Yin, and X. Zhang, "Optical negative refraction by four-wave mixing in thin metallic nanostructures," *Nature Materials*, vol. 11, no. 1, pp. 34–38, 2011.

[43] M. Pelusi, F. Luan, E. Magi, M. Lamont, D. Moss, B. Eggleton, J. Sanghera, L. Shaw, and I. Aggarwal, "High bit rate all-optical signal processing in a fiber photonic wire," *Optics Express*, vol. 16, no. 15, pp. 11506–11512, 2008.

[44] M. R. Lamont, B. Luther-Davies, D.-Y. Choi, S. Madden, X. Gai, and B. J. Eggleton, "Net-gain from a parametric amplifier on a chalcogenide optical chip," *Optics Express*, vol. 16, pp. 20374–20381, Dec 2008.

[45] S. D. Le, D. M. Nguyen, M. Thual, L. Bramerie, M. Costa e Silva, K. Lenglé, M. Gay, T. Chartier, L. Brilland, D. Méchin, *et al.*, "Efficient four-wave mixing in an ultra-highly nonlinear suspended-core chalcogenide as_38se_62 fiber," *Optics Express*, vol. 19, no. 26, pp. B653–B660, 2011.

[46] C.-S. Brès, S. Zlatanovic, A. O. Wiberg, and S. Radic, "Continuous-wave four-wave mixing in cm-long chalcogenide microstructured fiber," *Optics Express*, vol. 19, no. 26, pp. B621–B627, 2011.

[47] H. Fukuda, K. Yamada, T. Shoji, M. Takahashi, T. Tsuchizawa, T. Watanabe, J.-i. Takahashi, S.-i. Itabashi, *et al.*, "Four-wave mixing in silicon wire waveguides," *Optics Express*, vol. 13, no. 12, pp. 4629–4637, 2005.

[48] M. A. Foster, A. C. Turner, J. E. Sharping, B. S. Schmidt, M. Lipson, and A. L. Gaeta, "Broad-band optical parametric gain on a silicon photonic chip," *Nature*, vol. 441, no. 7096, pp. 960–963, 2006.

[49] J. H. Lee, T. Nagashima, T. Hasegawa, S. Ohara, N. Sugimoto, and K. Kikuchi, "Four-wave-mixing-based wavelength conversion of 40-gb/s nonreturn-to-zero signal using 40-cm bismuth oxide nonlinear optical fiber," *IEEE Photonics Technology Letters*, vol. 17, no. 7, pp. 1474–1476, 2005.

[50] R. Stolen, J. Bjorkholm, and A. Ashkin, "Phase-matched three-wave mixing in silica fiber optical waveguides," *Applied Physics Letters*, vol. 24, no. 7, pp. 308–310, 1974.

[51] M. Ferrera, L. Razzari, D. Duchesne, R. Morandotti, Z. Yang, M. Liscidini, J. Sipe, S. Chu, B. Little, and D. Moss, "Low-power continuous-wave nonlinear optics in doped silica glass integrated waveguide structures," *Nature photonics*, vol. 2, no. 12, pp. 737–740, 2008.

[52] A. Pasquazi, R. Ahmad, M. Rochette, M. Lamont, B. E. Little, S. T. Chu, R. Morandotti, and D. J. Moss, "All-optical wavelength conversion in an integrated ring resonator," *Optics Express*, vol. 18, pp. 3858–3863, Feb 2010.

[53] J. Harbold, F. Ilday, F. Wise, J. Sanghera, V. Nguyen, L. Shaw, and I. Aggarwal, "Highly nonlinear as-s-se glasses for all-optical switching," *Optics Letters*, vol. 27, no. 2, pp. 119–121, 2002.

[54] N. Sugimoto, H. Kanbara, S. Fujiwara, K. Tanaka, Y. Shimizugawa, and K. Hirao, "Third-order optical nonlinearities and their ultrafast response in bi_2o_3–b_2o_3–sio_2 glasses," *Journal of Optical Society of America B*, vol. 16, no. 11, pp. 1904–1908, 1999.

[55] G. W. Rieger, K. S. Virk, and J. F. Young, "Nonlinear propagation of ultrafast 1.5 μm pulses in high-index-contrast silicon-on-insulator waveguides," *Applied Physics Letters*, vol. 84, no. 6, pp. 900–902, 2004.

[56] R. Ahmad and M. Rochette, "Photosensitivity at 1550 nm and bragg grating inscription in as_2se_3 chalcogenide microwires," *Applied Physics Letters*, vol. 99, p. 061109, 2011.

[57] J. Hansryd, P. A. Andrekson, M. Westlund, J. Li, and P.-O. Hedekvist, "Fiber-based optical parametric amplifiers and their applications," *IEEE Journal of Selected Topics in Quantum Electronics*, vol. 8, no. 3, pp. 506–520, 2002.

[58] J. A. Buck, *Fundamentals of optical fibers.* Wiley-VCH, 2004.

[59] J. Swalen, R. Santo, M. Tacke, and J. Fischer, "Properties of polymeric thin films by integrated optical techniques," *IBM Journal of Research and Development*, vol. 21, no. 2, pp. 168–175, 1977.

[60] V. P. Tzolov, M. Fontaine, N. Godbout, and S. Lacroix, "Nonlinear modal parameters of optical fibers: a full-vectorial approach," *Journal of Optical Society of America B*, vol. 12, no. 10, pp. 1933–1941, 1995.

[61] C. Baker, R. Ahmad, and M. Rochette, "Simultaneous measurement of the core diameter and the numerical aperture in dual-mode step-index optical fibers," *Journal of Lightwave Technology*, vol. 29, no. 24, pp. 3834–3837, 2011.

[62] R. Ahmad, S. Chatigny, and M. Rochette, "Broadband amplification of high power 40 gb/s channels using multimode er-yb doped fiber," *Optics Express*, vol. 18, no. 19, pp. 19983–19993, 2010.

[63] J. H. Lee, T. Nagashima, T. Hasegawa, S. Ohara, N. Sugimoto, and K. Kikuchi, "Bismuth-oxide-based nonlinear fiber with a high sbs threshold and its application to four-wave-mixing wavelength conversion using a pure continuous-wave pump," *Journal of Lightwave Technology*, vol. 24, no. 1, p. 22, 2006.

[64] M. R. Lamont, B. Luther-Davies, D.-Y. Choi, S. Madden, and B. J. Eggleton, "Supercontinuum generation in dispersion engineered highly nonlinear($\gamma = 10$ /w/m) as2s3 chalcogenide planar waveguide," *Optics Express*, vol. 16, pp. 14938–14944, Sep 2008.

[65] M. A. Foster, A. C. Turner, M. Lipson, and A. L. Gaeta, "Nonlinear optics in photonic nanowires," *Optics Express*, vol. 16, no. 2, pp. 1300–1320, 2008.

[66] M. Ebrahim-Zadeh and I. T. Sorokina, *Mid-infrared coherent sources and applications.* Springer, 2008.

[67] L. Myers, R. Eckardt, M. Fejer, R. Byer, W. Bosenberg, and J. Pierce, "Quasi-phase-matched optical parametric oscillators in bulk periodically poled linbo$_3$," *Journal of Optical Society of America B*, vol. 12, no. 11, pp. 2102–2116, 1995.

[68] L. E. Myers and W. R. Bosenberg, "Periodically poled lithium niobate and quasi-phase-matched optical parametric oscillators," *Quantum Electronics, IEEE Journal of*, vol. 33, no. 10, pp. 1663–1672, 1997.

[69] C. Canalias and V. Pasiskevicius, "Mirrorless optical parametric oscillator," *Nature Photonics*, vol. 1, no. 8, pp. 459–462, 2007.

[70] M. Ghotbi, A. Esteban-Martin, and M. Ebrahim-Zadeh, "Bib$_3$o$_6$ femtosecond optical parametric oscillator," *Optics Letters*, vol. 31, no. 21, pp. 3128–3130, 2006.

[71] G. Samanta, G. Fayaz, and M. Ebrahim-Zadeh, "1.59 w, single-frequency, continuous-wave optical parametric oscillator based on mgo: sppIt," *Optics Letters*, vol. 32, no. 17, pp. 2623–2625, 2007.

[72] K. Hill, B. Kawasaki, Y. Fujii, and D. Johnson, "Efficient sequence-frequency generation in a parametric fiber-optic oscillator," *Applied Physics Letters*, vol. 36, no. 11, pp. 888–890, 1980.

[73] J. E. Sharping, M. Fiorentino, P. Kumar, and R. S. Windeler, "Optical parametric oscillator based on four-wave mixing in microstructure fiber," *Optics Letters*, vol. 27, no. 19, pp. 1675–1677, 2002.

[74] Y. Deng, Q. Lin, F. Lu, G. P. Agrawal, and W. H. Knox, "Broadly tunable femtosecond parametric oscillator using a photonic crystal fiber," *Optics Lfsetters*, vol. 30, no. 10, pp. 1234–1236, 2005.

[75] B. Kuyken, X. Liu, R. M. Osgood, R. Baets, G. Roelkens, and W. M. Green, "Widely tunable silicon mid-infrared optical parametric oscillator," in *Group IV Photonics (GFP), 2011 8th IEEE International Conference on*, pp. 338–340, IEEE, 2011.

[76] T. Kippenberg, S. Spillane, and K. Vahala, "Kerr-nonlinearity optical parametric oscillation in an ultrahigh-q toroid microcavity," *Physical Review Letters*, vol. 93, no. 8, p. 083904, 2004.

[77] A. A. Savchenkov, A. B. Matsko, D. Strekalov, M. Mohageg, V. S. Ilchenko, and L. Maleki, "Low threshold optical oscillations in a whispering gallery mode caf$_2$ resonator," *Physical Review Letters*, vol. 93, no. 24, p. 243905, 2004.

[78] P. DelHaye, A. Schliesser, O. Arcizet, T. Wilken, R. Holzwarth, and T. Kippenberg, "Optical frequency comb generation from a monolithic microresonator," *Nature*, vol. 450, no. 7173, pp. 1214–1217, 2007.

[79] J. S. Levy, A. Gondarenko, M. A. Foster, A. C. Turner-Foster, A. L. Gaeta, and M. Lipson, "Cmos-compatible multiple-wavelength oscillator for on-chip optical interconnects," *Nature Photonics*, vol. 4, no. 1, pp. 37–40, 2009.

[80] I. H. Agha, Y. Okawachi, M. A. Foster, J. E. Sharping, and A. L. Gaeta, "Four-wave-mixing parametric oscillations in dispersion-compensated high-q silica microspheres," *Physical Review. A*, vol. 76, no. 4, 2007.

[81] L. Razzari, D. Duchesne, M. Ferrera, R. Morandotti, S. Chu, B. Little, and D. Moss, "Cmos-compatible integrated optical hyper-parametric oscillator," *Nature Photonics*, vol. 4, no. 1, pp. 41–45, 2009.

[82] R. Ahmad and M. Rochette, "High efficiency and ultra broadband optical parametric four-wave mixing in chalcogenide-pmma hybrid microwires," *Optics Express*, vol. 20, pp. 9572–9580, 2012.

[83] R. H. Stolen, "Fiber raman lasers," *Fiber & Integrated Optics*, vol. 3, no. 1, pp. 21–51, 1980.

[84] E. M. Dianov and A. M. Prokhorov, "Medium-power cw raman fiber lasers," *IEEE Journal of Selected Topics in Quantum Electronics*, vol. 6, no. 6, pp. 1022–1028, 2000.

[85] S. Skubchenko, M. Vyatkin, and D. Gapontsev, "High-power cw linearly polarized all-fiber raman laser," *IEEE Photonics Technology Letters*, vol. 16, no. 4, pp. 1014–1016, 2004.

[86] J. Travers, S. Popov, and J. Taylor, "Efficient continuous-wave holey fiber raman laser," *Applied Physics Letters*, vol. 87, no. 3, pp. 031106–031106, 2005.

[87] O. Boyraz, B. Jalali, *et al.*, "Demonstration of a silicon raman laser," *Optics Express*, vol. 12, no. 21, pp. 5269–5273, 2004.

[88] H. M. Pask, "The design and operation of solid-state raman lasers," *Progress in Quantum Electronics*, vol. 27, no. 1, pp. 3–56, 2003.

[89] T. Kippenberg, S. Spillane, D. Armani, and K. Vahala, "Ultralow-threshold microcavity raman laser on a microelectronic chip," *Optics Letters*, vol. 29, no. 11, pp. 1224–1226, 2004.

[90] G. Qin, M. Liao, T. Suzuki, A. Mori, and Y. Ohishi, "Widely tunable ring-cavity tellurite fiber raman laser," *Optics Letters*, vol. 33, no. 17, pp. 2014–2016, 2008.

[91] S. D. Jackson and G. Anzueto-Sánchez, "Chalcogenide glass raman fiber laser," *Applied Physics Letters*, vol. 88, no. 22, pp. 221106–221106, 2006.

[92] H. Rong, A. Liu, R. Jones, O. Cohen, D. Hak, R. Nicolaescu, A. Fang, and M. Paniccia, "An all-silicon raman laser," *Nature*, vol. 433, no. 7023, pp. 292–294, 2005.

[93] M. H. Huang, S. Mao, H. Feick, H. Yan, Y. Wu, H. Kind, E. Weber, R. Russo, and P. Yang, "Room-temperature ultraviolet nanowire nanolasers," *Science*, vol. 292, no. 5523, pp. 1897–1899, 2001.

[94] R. Ahmad and M. Rochette, "Chalcogenide optical parametric oscillator," *Optics Express*, vol. 20, pp. 10095–10099, Apr 2012.

[95] R. Ahmad and M. Rochette, "Chalcogenide microwire based raman laser," *Applied Physics Letters*, vol. 101, no. 10, pp. 101110–101110, 2012.

[96] See, for example,
$http://www.evaporatedcoatings.com/mirror-coatings$.

[97] L. Tong, R. R. Gattass, J. B. Ashcom, S. He, J. Lou, M. Shen, I. Maxwell, and E. Mazur, "Subwavelength-diameter silica wires for low-loss optical wave guiding," *Nature*, vol. 426, no. 6968, pp. 816–819, 2003.

[98] P. Dumais, F. Gonthier, S. Lacroix, J. Bures, A. Villeneuve, P. Wigley, and G. Stegeman, "Enhanced self-phase modulation in tapered fibers," *Optics Letters*, vol. 18, no. 23, pp. 1996–1998, 1993.

[99] S. Afshar V and T. M. Monro, "A full vectorial model for pulse propagation in emerging waveguides with subwavelength structures part i: Kerr nonlinearity," *Optics Express*, vol. 17, no. 4, pp. 2298–2318, 2009.

[100] T. Birks, W. Wadsworth, and P. S. J. Russell, "Supercontinuum generation in tapered fibers," *Optics Letters*, vol. 25, no. 19, pp. 1415–1417, 2000.

[101] G. Brambilla, "Optical fibre nanotaper sensors," *Optical Fiber Technology*, vol. 16, no. 6, pp. 331–342, 2010.

[102] G. Brambilla, F. Xu, P. Horak, Y. Jung, F. Koizumi, N. P. Sessions, E. Koukharenko, X. Feng, G. S. Murugan, J. S. Wilkinson, *et al.*, "Optical fiber nanowires and microwires: fabrication and applications," *Advances in Optics and Photonics*, vol. 1, no. 1, pp. 107–161, 2009.

[103] W. She, J. Yu, and R. Feng, "Observation of a push force on the end face of a nanometer silica filament exerted by outgoing light," *Physical Review Letters*, vol. 101, no. 24, p. 243601, 2008.

[104] G. Sagué, E. Vetsch, W. Alt, D. Meschede, and A. Rauschenbeutel, "Cold-atom physics using ultrathin optical fibers: light-induced dipole forces and surface interactions," *Physical Review Letters*, vol. 99, no. 16, p. 163602, 2007.

[105] X. Guo, M. Qiu, J. Bao, B. J. Wiley, Q. Yang, X. Zhang, Y. Ma, H. Yu, and L. Tong, "Direct coupling of plasmonic and photonic nanowires for hybrid nanophotonic components and circuits," *Nano Letters*, vol. 9, no. 12, pp. 4515–4519, 2009.

[106] E. Vetsch, D. Reitz, G. Sagué, R. Schmidt, S. Dawkins, and A. Rauschenbeutel, "Optical interface created by laser-cooled atoms trapped in the evanescent field surrounding an optical nanofiber," *Physical Review Letters*, vol. 104, no. 20, p. 203603, 2010.

[107] K. Salit, M. Salit, S. Krishnamurthy, Y. Wang, P. Kumar, and M. Shahriar, "Ultra-low power, zeno effect based optical modulation in a degenerate v-system with a tapered nano fiber in atomic vapor," *Optics Express*, vol. 19, no. 23, pp. 22874–22881, 2011.

[108] G. Brambilla, G. S. Murugan, J. Wilkinson, and D. Richardson, "Optical manipulation of microspheres along a subwavelength optical wire," *Optics Letters*, vol. 32, no. 20, pp. 3041–3043, 2007.

[109] P. Polynkin, A. Polynkin, N. Peyghambarian, and M. Mansuripur, "Evanescent field-based optical fiber sensing device for measuring the refractive index of liquids in microfluidic channels," *Optics Letters*, vol. 30, no. 11, pp. 1273–1275, 2005.

[110] X.-W. Chen, V. Sandoghdar, and M. Agio, "Highly efficient interfacing of guided plasmons and photons in nanowires," *Nano Letters*, vol. 9, no. 11, pp. 3756–3761, 2009.

[111] P. Wang, L. Zhang, Y. Xia, L. Tong, X. Xu, and Y. Ying, "Polymer nanofibers embedded with aligned gold nanorods: a new platform for plasmonic studies and optical sensing," *Nano Letters*, vol. 12, no. 6, pp. 3145–3150, 2012.

[112] C.-H. Dong, C.-L. Zou, X.-F. Ren, G.-C. Guo, and F.-W. Sun, "In-line high efficient fiber polarizer based on surface plasmon," *Applied Physics Letters*, vol. 100, no. 4, pp. 041104–041104, 2012.

[113] X. Jiang, Q. Yang, G. Vienne, Y. Li, L. Tong, J. Zhang, and L. Hu, "Demonstration of microfiber knot laser," *Applied Physics Letters*, vol. 89, no. 14, pp. 143513–143513, 2006.

[114] X. Jiang, Q. Song, L. Xu, J. Fu, and L. Tong, "Microfiber knot dye laser based on the evanescent-wave-coupled gain," *Applied Physics Letters*, vol. 90, no. 23, pp. 233501–233501, 2007.

[115] A. Sulaiman, S. Harun, F. Ahmad, S. Norizan, and H. Ahmad, "Tunable laser generation with erbium-doped microfiber knot resonator," *Laser Physics*, vol. 22, no. 3, pp. 588–591, 2012.

[116] W. Fan, J. Gan, Z. Zhang, X. Wei, S. Xu, and Z. Yang, "Narrow linewidth single frequency microfiber laser," *Optics Letters*, vol. 37, no. 20, pp. 4323–4325, 2012.

[117] R. Ahmad and M. Rochette, "Raman lasing in a chalcogenide microwire-based fabry–perot cavity," *Optics Letters*, vol. 37, no. 21, pp. 4549–4551, 2012.

[118] C. Baker and M. Rochette, "High nonlinearity and single-mode transmission in tapered multimode as_2se_3-pmma fibers," *IEEE Photonics Journal*, vol. 4, no. 3, pp. 960–969, 2012.

[119] J. Shi, S.-u. Alam, and M. Ibsen, "Sub-watt threshold, kilohertz-linewidth raman distributed-feedback fiber laser," *Optics Letters*, vol. 37, no. 9, pp. 1544–1546, 2012.

[120] N. Bloembergen and Y. Shen, "Coupling between vibrations and light waves in raman laser media," *Physical Review Letters*, vol. 12, no. 18, p. 504, 1964.

[121] T. Sylvestre, H. Maillotte, E. Lantz, and P. Tchofo Dinda, "Raman-assisted parametric frequency conversion in a normally dispersive single-mode fiber," *Optics Letters*, vol. 24, no. 22, pp. 1561–1563, 1999.

[122] C. de Matos, D. Chestnut, P. Reeves-Hall, and J. Taylor, "Continuous-wave-pumped raman-assisted fiber optical parametric amplifier and wavelength converter in conventional dispersion-shifted fiber," *Optics Letters*, vol. 26, no. 20, pp. 1583–1585, 2001.

[123] S. Coen, D. A. Wardle, and J. D. Harvey, "Observation of non-phase-matched parametric amplification in resonant nonlinear optics.," *Physical Review Letters*, vol. 89, no. 27, p. 273901, 2002.

[124] A. Tuniz, G. Brawley, D. Moss, and B. Eggleton, "Two-photon absorption effects on raman gain in single mode as_2se_3 chalcogenide glass fiber," *Optics Express*, vol. 16, no. 22, pp. 18524–18534, 2008.

[125] J. Hu, C. R. Menyuk, L. B. Shaw, J. S. Sanghera, and I. D. Aggarwal, "Maximizing the bandwidth of supercontinuum generation in as_2se_3 chalcogenide fibers," *Optics Express*, vol. 18, no. 7, pp. 6722–6739, 2010.

[126] M. Steel and C. Sterke, "Continuous-wave parametric amplification in bragg gratings," *Journal of Optical Society of America B*, vol. 12, no. 12, pp. 2445–2452, 1995.

[127] M. Steel and C. M. de Sterke, "Parametric amplification of short pulses in optical fiber bragg gratings," *Physical Review E*, vol. 54, no. 4, p. 4271, 1996.

[128] M. Steel and C. M. de Sterke, "Bragg-assisted parametric amplification of short optical pulses," *Optics Letters*, vol. 21, no. 6, pp. 420–422, 1996.

[129] C. Xiong, G. Marshall, A. Peruzzo, M. Lobino, A. Clark, D.-Y. Choi, S. Madden, C. Natarajan, M. Tanner, R. Hadfield, *et al.*, "Generation of correlated photon pairs in a chalcogenide as_2s_3 waveguide," *Applied Physics Letters*, vol. 98, no. 5, pp. 051101–051101, 2011.